Master's Thesis 2013

Candidate: Håkon Molland Edvardsen

Title: System dynamics of asynchronous
generators at islanded grid operation

Telemark University College

Faculty of Technology
M.Sc. Programme

Abstract:

It is well known that the phenomenon of self-excitation allows the asynchronous generator to operate as a standalone unit. The robustness and low cost of the asynchronous generator makes it beneficial for small hydro power plants below 1 MW.

Investigation of the self-excitation process shows that significant overvoltages can occur if a generator with sufficient capacitors is suddenly disconnected from the utility grid. The precondition for a successive voltage build-up is that the generator is left with enough capacitive power and a low load after the disconnection.

The Lønnestad radial in Seljord, Norway, is a distribution radial with both asynchronous and synchronous generators connected. In order to investigate the system dynamics in the radial after it is disconnected from the rest of the 22 kV distribution grid, the radial was modeled and simulated in Dymola.

From the simulations it was seen that the cables in the grid represent enough capacitive power to initiate self-excitation of the seven generators in Sagbekken 1, and Sagbekken 2 and 3 momentarily after the radial is brought into islanded operation. Since the amount of load connected to the radial is low, the self-excitation leads to a successive voltage build-up, resulting in a harmful overvoltage. For simulations with a load connected to the radial, the overvoltage reached its peak value of circa 50 kV only 0.4 seconds after the asynchronous generators are left in standalone operation.

To avoid voltage build-ups caused by self-excitation it is essential with proper parameters in the protection relays. It is recommended to have monetarily disconnection when the voltage exceeds a given limit slightly above the nominal voltage.

In addition to the protection relays, a damping load can be installed in Seljord substation to momentarily connect when the radial is disconnected from the rest of the distribution grid.

Table of contents

Preface

This report is the result of the final project in the master program System and Control Engineering at Telemark University College.

The report requires that the reader has some knowledge in the field of modeling and simulation of dynamic systems, as well as understanding of electric machinery and power systems.

For modeling and simulation of the power system, the Modelica based simulation environment Dymola is utilized with the Electric Power Library.

I would like to thank Skagerak Kraft for giving me the opportunity to work with this thesis, and for offering me a desk at their office during the project.

Finally, would I like to thank the people whom helped me during the project period, and given me a memorable master thesis:

- Dietmar Winkler, supervisor
- Ingvar Andreassen, control engineer at Skagerak Kraft
- Gunne John Hegglid, technical director at Skagerak Kraft
- Geir Kristian Holte, electrical engineer at Skagerak Kraft
- Magne Reinstul, owner of the Sagbekken hydro power plants

Porsgrunn, June 3, 2013

Håkon Molland Edvardsen

Nomenclature

Symbol:	Unit:	Definition:
A	[m^2]	Area
AC		Alternating current
B	[T]	Magnetic flux density
B	[S]	Susceptance
C	[F]	Capacitance
D	[m]	Distance
DC		Direct current
emf	[V]	Electomagnetic force
E	[V]	Induced voltage
f	[Hz]	Frequency
F	[N]	Traveling mmf
g	[m]	Length air-gap
G	[S]	Conductance
GCB		Generator circuit breaker
GD^2	[kgm$^{2]}$]	Flywheel effect
H	[s]	H-value
H	[A/m]	Magnetic field intensity
I	[A]	Current
J	[kgm^2]	Moment of inertia
K	[-]	Distribution and chording factor
l	[m]	Length
L	[H]	Inductance
mmf	[A-turns]	Magnemotive force
M	[L]	Mutual inductance
MCB		Main circuit breaker
n	[rpm]	Rotational speed
N	[-]	Number of turns
p	[-]	Pole pairs
P	[W]	Active power
$p.u.$	[-]	Per unit

6

pf	[-]	Power factor
Q	[VAr]	Reactive power
$\mathfrak{R}$	[H^{-1}]	Reluctance
r	[m]	Radius
R	[Ω]	Resistance
s	[-]	Slip
S	[VA]	Apparent power
SEIG		Self-Excited Induction Generator
t	[s]	Time
T	[Nm]	Torque
v	[m/s]	Relative speed
V	[V]	Voltage
W	[-]	Number of turns per phase
X	[Ω]	Reactance
Y	[S]	Admittance
Z	[Ω]	Impedance
γ	[-]	Propagation constant
δ	[m]	Skin depth
ε	[-]	Permittivity
η	[-]	Efficiency
θ	[rad]	Angular displacement
λ	[Wb-turns]	Flux linkage
μ	[-]	Permeability
ρ	[Ω-m]	Resitivity
Φ	[Wb]	Magnetic flux
Ψ	[Wb]	Linked flux
ω	[rad/s]	Angular velocity

1 Introduction

The main share of the electricity produced in Norway is based on utilization of the nation's large potential of hydro power. Today are nearly all the large waterfalls profitable for hydro power production already utilized, or protected against encroachment on nature. Due to this, there has for the last decades been an expansion in the number of small hydro power plants below 10 MW. This is often minor projects where the power plant is located near a small waterfall owned by a local landowner.

These small hydro power plants are often connected to already existing distribution grids, due to the geographical location and installed capacity of these plants. This is often grids constructed for low capacities with purpose to distribute the electricity out to the local consumers. Connection of power plants in these types of grids will therefore often change the situation of power flow in the grid, and lead to challenges regarding voltage stability and requirements for faults detection.

1.1 Project provider

The project was provided by Skagerak Kraft, which is a subsidiary of the energy company Skagerak Energi.

Skagerak Kraft is the 7th largest producer of electric power in Norway, with a yearly production of 5.4 TWh of electricity from 20 fully owned, and 25 partly owned hydro power plants. Their total installed capacity is presently at 1.314 TW [1].

1.2 Background of the thesis

One of Skagerak Kraft's partially owned hydro power plants is Grunnåi, located in Seljord, Norway. The power plant was built in 2006, having an installed capacity of 15.06 MW. The power plant is connected to the Lønnestad radial, which is part of the local distribution grid in Seljord.

In addition to Grunnåi, there are two power plants, Sagbekken 1 and Sagbekken 2 and 3, connected to the Lønnestad radial. This is two small hydro power plants equipped with three and four asynchronous generators of the squirrel cage type, with a total installed capacity of 875 kW.

After the power plants were connected to the Lønnestad radial, there have been some challenges with unstable voltage in the grid. In 2011 there was an earth circuit incident in Grunnåi, which caused the Lønnestad radial to be brought into islanded grid operation. Later, signs of significant overvoltages could be observed by looking at a blown surge arrester and a damaged power supply.

By comparing the damages with damages reported from similar incidents, it is natural to think that the overvoltages were caused by self-excitation of the asynchronous generators in the Sagbekken plants. This is a well known phenomenon that allows an asynchronous generator to operate as a stand-alone unit if a sufficient amount of reactive power is available.

1.3 Motivation for the thesis

Skagerak Kraft took the initiative for this master thesis after the incident where Grunnåi power plant was subjected to significant overvoltages. For them it was desirable to learn from the incident, and better understand how they could prevent such incidents from happening in the future.

1.4 Outline of the report

The theory needed for modeling a power system with synchronous and asynchronous generators is presented in Chapter 2. The chapter proposes a method for steady state analysis of a self-excited asynchronous generator. A manual routine for modeling and simulation of the dynamics in the power system is not proposed in the report. Modeling and simulation of power systems are fairly intricate, and can more sufficiently be performed by usage of simulation tools.

Chapter 3 describes the Lønnestad radial and the parameters for the different components in the radial. For the zero component parameters, the default values in the simulation tools are applied. This is typical per unit values which is adequate since the main focus is simulations with balanced circuits. The chapter includes a further description of the overvoltage phenomena in Grunnåi.

In Chapter 4, the computerized simulation tools and the different simulation models are presented. Four types of simulations are primarily carried out; investigation of the self-excitation process, islanded operation with and without Grunnåi power plant, and islanded operation of the radial with an earth circuit.

In the end of the report are the results from the previous chapters summarized and discussed before a final conclusion is given.

2 Theory

Following chapter presents the theory needed for modeling and simulation of the system dynamics of an electric grid with both asynchronous and synchronous generators that is brought into islanded grid operation.

2.1 Park's transformation

One of the difficulties in describing the dynamics of electric machinery is that the inductances are a function of both the mechanical and the electrical angles of the machine [2]. To overcome this problem Robert H. Park published a paper in 1929 which proposed a transformation that made the analysis of electric machines more straightforward [3].

Today, this transformation is referred to as the Park's or $dq0$ transform, and is a well known three-phase to two-phase transformation in power system analysis.

The Park's transformation transforms the three phase time-domain signals from a stationary phase coordinate system, abc, to a rotating coordinate system, $dq0$. This transformation has the unique property to eliminate all time varying inductances by referring the stator and rotor quantities to a fixed or rotating reference frame [2].

The compact form of the transformation may be expressed as:

$$F_{dq0} = T_{dqo} * F_{abc} \qquad (2\text{-}1)$$

Where F_{dq0} and F_{abc} are vectors with $dq0$ and the abc components, and T_{dq0} is the transformation matrix. The full equation is expressed as:

$$\begin{bmatrix} f_d \\ f_q \\ f_0 \end{bmatrix} = \frac{2}{3} \begin{bmatrix} \cos\theta & \cos(\theta - \frac{2\pi}{3}) & \cos(\theta + \frac{2\pi}{3}) \\ -\sin\theta & -\sin(\theta - \frac{2\pi}{3}) & -\sin(\theta + \frac{2\pi}{3}) \\ \frac{1}{2} & \frac{1}{2} & \frac{1}{2} \end{bmatrix} \begin{bmatrix} f_a \\ f_b \\ f_c \end{bmatrix} \qquad (2\text{-}2)$$

Here, f is the variable to be transformed, such as voltage, current, flux linkage or electric charge. The angular reference position is expressed as the integral:

$$\theta = \int_0^t \omega(t)dt + \theta(0) \qquad (2\text{-}3)$$

Where ω is the angular frequency, and θ_0 is the initial position angle of the coordinate axes.

The quantity can easily be transformed back to the abc coordinate system by using the inverse transform:

$$\begin{bmatrix} f_a \\ f_b \\ f_c \end{bmatrix} = \frac{2}{3} \begin{bmatrix} \cos\theta & -\sin\theta & 1 \\ \cos(\theta - \frac{2\pi}{3}) & -\sin(\theta - \frac{2\pi}{3}) & 1 \\ \cos(\theta + \frac{2\pi}{3}) & -\sin(\theta + \frac{2\pi}{3}) & 1 \end{bmatrix} \begin{bmatrix} f_d \\ f_q \\ f_0 \end{bmatrix}$$

(2-4)

The two axis in the Park's transformation are called the direct, d-axis, and the quadrature, q-axis, where the q-axis is located 90 degrees from the d-axis. In cases where the three phase system is symmetrical, the zero component will be zero [2].

Figure 2-1 shows the trigonometric relationship between the three instantaneous quantities and the d- and q-axis. Where the three instantaneous quantities are considered as variables directed along stationary paths each displaced by 120 degrees, and the d-axis and q-axis which is orthogonal to each other and rotating with angular velocity, ω.
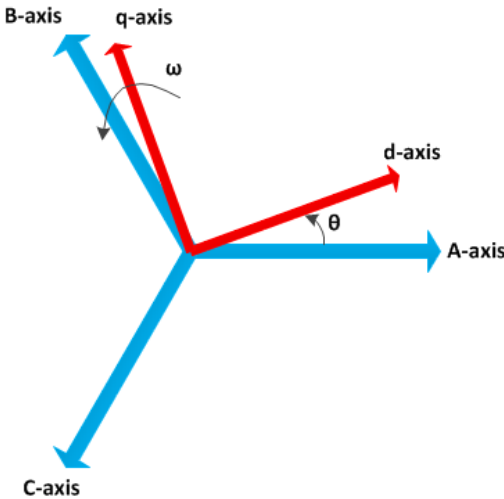
Figure 2-1: Trigonometric relationship between abc and dq0 system

2.2 Electromagnetic concepts

Many of the apparatus used in power systems require a basic understanding of electromagnetic concepts. This sub-chapter will review the different electromagnetic concepts needed for the theory in the following chapters.

2.2.1 Magnetic field intensity and magnetic flux density

Figure 2-2 shows a simple magnetic circuit where the core is composed of a magnetic material whose permeability is much greater than the surrounding air. The cross-section of the core is uniform, and is excited by a winding of N turns carrying a current, which produces a magnetic field in the core, as shown in the figure. The magnetic field can be shown in terms as flux lines, which form closed loops interlinked with the winding [4].
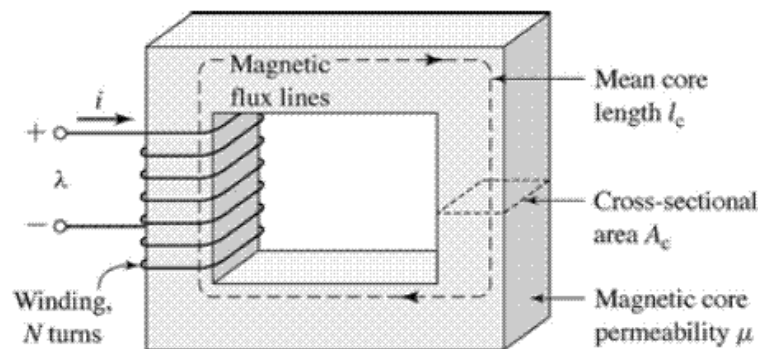
Figure 2-2: Simple magnetic circuit [5]

In magnetic circuit terminology is the source of the magnetic field in the core called the magnetomotive force, mmf, which is the ampere-turn product, Ni, in the winding.

By assuming a uniform magnetic flux density, B, across the cross section of the core, the relationship between the mmf and the magnetic field intensity, H, can be written as [4]:

$$mmf = Ni = H_c l_c \qquad (2\text{-}5)$$

Where l_c is the mean length of the magnetic flux lines.

For every material there is a definite relationship between the magnetic field intensity and the magnetic flux density. This relationship is usually expressed graphically by the *B-H* curve of the material [6].

2.2.2   Magnetic materials

A magnetic circuit consists of a structure composed of a magnetic material with high permeability. This material causes the magnetic flux to be confined to the paths defined by the structure of the circuit, much as currents are confined to the conductors of an electric circuit [4]. Due to the high permeability of the magnetic materials applied in cores, rather small ampere-turns are required to produce the desired flux density.

The permeability of a magnetic material, μ_m, is expressed in the term of the permeability, μ_r, relative to the permeability of vacuum, μ_0:

$$\mu_m = \mu_r \mu_0 \qquad \qquad (2\text{-}6)$$

2.2.2.1 *B-H* curve of vacuum

For vacuum, the magnetic flux density is expressed by:

$$B = \mu_0 H \qquad \qquad (2\text{-}7)$$

Where μ_0 is the permeability of vacuum, which is $4\pi * 10^{-7}$.

Since μ_0 is constant, the magnetic flux density is directly proportional to the magnetic field strength in vacuum. The *B-H* characteristic for vacuum has therefore a straight line since the medium never saturates. Nonmagnetic materials such as paper, rubber, copper, and air have *B-H* curves almost identical to vacuum [6].

2.2.2.2 *B-H* curve of magnetic material

For magnetic materials, the magnetic flux density depends upon the magnetic field intensity to which it is subjected:

$$B = \mu_0 \mu_r H \qquad \qquad (2\text{-}8)$$

Where μ_r is the permeability of the magnetic material relative to vacuum.

The relative permeability is not constant, such as for vacuum, but varies with the magnetic flux density in the material. Consequently, the relationship between *B* and *H* is not linear, which makes Equation 2-8 rather impractical to use. It is therefore more desirable to show the relationship with the *B-H* saturation curve, as shown in Figure 2-3. In the figure are the nonlinear saturation curves for three commonly used materials in electrical machinery shown [6].

13
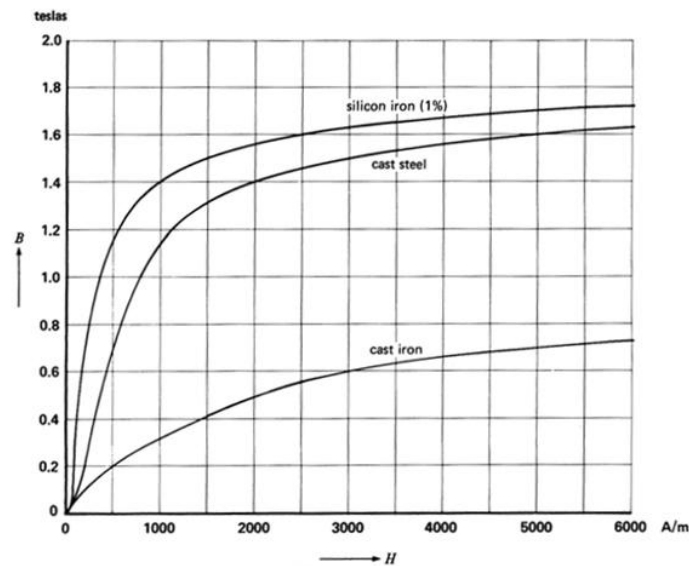
Figure 2-3: B-H saturation curves for three magnetic materials [6]

If an alternating current is applied to the coil, the corresponding magnetic field intensity will cause one of the hysteresis loops shown in Figure 2-4. One cycle of the current completes the loop once, which results in a net dissipation of energy within the material. The energy dissipated per cycle is referred to as the hysteresis loss. By increasing the magnitude of the alternating current and magnetic field intensity, a larger hysteresis loop will be obtained. Of Figure 2-4 it can be seen that the slope of the hysteresis curve tends to diminish as the magnetic field intensity increases below a certain level. At this point, the non-linear region of the magnetic material is reached, and the magnetic material starts to saturate. When the magnetic material has reached the point of full saturation, will a further increase of the magnetic field intensity not lead to a further increase of the magnetic flux density.
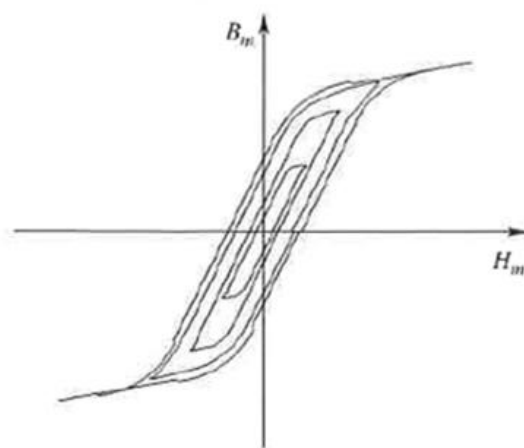
Figure 2-4: Hysteresis loop for a magnetic material [7]

By looking at Figure 2-4, it can be observed that the flux density does not follow the original

14

path when the magnetic flux intensity is reduced, this makes the hysteresis loop. If the magnetic field intensity suddenly is reduced to zero, there will still be a substantial magnetic flux density remaining in the core. This remaining flux is called the residual flux density or the residual induction [6].

2.2.3   Magnetic flux in a core

Dependent on whether the magnetic apparatus is a static or rotational component, the magnetic circuit is a closed core, or a core with an air-gap. For motors and generators there are a rotating and a static part in the magnetic circuit, these two parts are interconnected with an air-gap with permeability, μ_0.

2.2.3.1 Magnetic flux in a closed core

Because of the rather high permeability of materials used in electric machinery, the magnetic flux is confined almost entirely to the core. The field lines follow the path defined by the core, with a essentially uniform flux density over a cross section when the area is uniform. The magnetic flux, Φ, crossing an area is determined by the surface integral [4]:

$$\Phi = \int_S B\ da \qquad\qquad (2\text{-}9)$$

The continuity-of-flux equation states that the net magnetic flux crossing all surfaces of a three-dimensional closed surface is zero. Since magnetic flux lines form closed loops, must all flux entering a surface enclosing a volume leave that volume over some other portion of that surface [4]. As expressed in following equation:

$$\oint_S B\ da = 0 \qquad\qquad (2\text{-}10)$$

By neglecting magnetic flux outside the core, can Equation 2-9 be reduced to following expression:

$$\Phi_c = B_c A_c \qquad\qquad (2\text{-}11)$$

Where Φ_c is the flux in the core, B_c is the flux density in the core and A_c is the cross-sectional area of the core.

2.2.3.2 Magnetic flux in a core with air-gap

Equation 2-11 yields only for transformers which are wound at closed cores. For motors and generators which consist of a rotating and static element, there is an air-gap in the magnetic circuit. Figure 2-5 shows a simple magnetic circuit with an air-gap with length g, where the permeability in the air-gap is assumed to be equal μ_0.
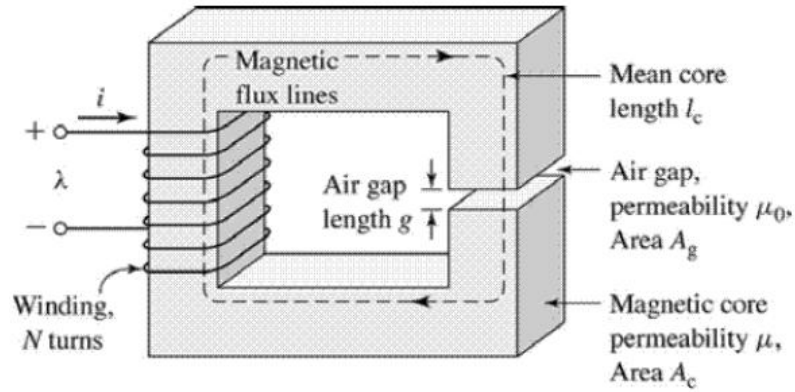
Figure 2-5: Simple magnetic circuit with air-gap [5]

The magnetic circuit in Figure 2-5 can be analyzed as two components in series, a magnetic core of permeability μ_m and mean length l_c, and an air-gap of permeability μ_0 and length g:

$$B_c = \frac{\Phi}{A_c} \qquad (2\text{-}12)$$

$$B_g = \frac{\Phi}{A_g} \qquad (2\text{-}13)$$

Compared to the core, the flux density in the air-gap is not uniform. The reason for this is that there will be a fringing effect in the air-gap where the magnetic field lines bulge outward. This fringing effect results in an increase of the effective cross-sectional area of the air-gap. The fringing effect is usually neglected, which leads us to equally cross-sectional areas for the air-gap and the core. By neglecting the fringing effect, Equation 2-12 and 2-13 can be written as [4]:

$$B_g = B_c = \frac{\Phi}{A_c} \qquad (2\text{-}14)$$

$$mmf = Ni = H_c l_c + H_g g \qquad (2\text{-}15)$$

$$mmf = \frac{B_c}{\mu} l_c + \frac{B_g}{\mu_0} g \qquad (2\text{-}16)$$

Of Equation 2-16 it can be seen that a portion of the mmf is required to excite the magnetic

16

field in the core, while the other part excites the magnetic field in the air-gap. The equation can be rewritten in terms of the total flux:

$$mmf = \Phi \frac{l_c}{\mu A_c} + \Phi \frac{g}{\mu_0 A_c} \qquad (2\text{-}17)$$

The two terms that multiply the flux in Equation 2-17 are known as the total reluctance, $\mathfrak{R}$, of core and air-gap [4]:

$$\mathfrak{R}_c = \frac{l_c}{\mu A_c} \qquad (2\text{-}18)$$

$$\mathfrak{R}_g = \frac{g}{\mu_0 A_c} \qquad (2\text{-}19)$$

Finally, the mmf can be expressed in terms of the reluctances and total flux:

$$mmf = \Phi(\mathfrak{R}_c + \mathfrak{R}_g) \qquad (2\text{-}20)$$

2.2.4   Faraday's law of electromagnetic induction

The relationship between voltage and flux in a circuit is expressed by Faraday's law of electromagnetic induction. This law states that if the flux, Φ, linking a winding with one turn varies as a function of time, a voltage is induced between the terminals of the winding. The magnitude of the induced voltage is then directly proportional to the rate of change in the flux [6]. The term electromotive force, *emf*, is often used instead of induced voltage to represent that component of voltage due to a time-varying flux linkage [4].

If the flux varies inside a coil of *N* turns, the voltage induced is given by:

$$E = N \frac{d\Phi}{dt} \qquad (2\text{-}21)$$

Where $d\Phi$ is the change of flux inside the coil, and dt is the time interval during which the flux change.

For generators, the coils move with respect to a flux that is fixed in space, it is therefore more convenient to calculate the induced voltage with reference to the conductors, rather than with reference to the coil itself. The value of the induced voltage is expressed by the flux cutting equation [6]:

17

$$E = Blv \qquad\qquad (2\text{-}22)$$

Where l is the length of the conductor in the magnetic field and v is the relative speed of the conductor [6].

2.2.5 Inductances

If all turns of a coil are linked by the same flux, Φ, the coil has a flux linkage, λ, where:

$$\lambda = N\Phi \qquad\qquad (2\text{-}23)$$

For a magnetic which is operated in its linear operating region, the flux linkage, λ, is related to the coil current, I, by the coil inductance, L:

$$\lambda = LI \qquad\qquad (2\text{-}24)$$

When the core is in its linear operating region, the inductance is constant, and can be calculated as:

$$L = \frac{NB_cA_c}{I} = \frac{N^2\mu A_c}{l_c} \qquad\qquad (2\text{-}25)$$

Equation 2-25 shows that the inductance of a coil is strictly a property of the magnetic circuit. Provided that the operation of the core is in the linear range of the magnetic material, the slope of the *B-H* characteristic is represented by the permeability, μ [7].

In the same way that conductors guide currents in electric circuits, magnetic cores guide flux in magnetic circuits. However, there is a main difference; the conductivity of copper is approximately 10^{20} times greater than of air, which allows leakage currents to be neglected for electric circuits with low frequencies such as 50 Hz. In magnetic circuits the permeability of magnetic materials are around 10^4 times greater than of air. Due to this relatively low permeability, not all the flux is confined to the core [7].

The total flux, Φ, can be divided into two subparts; the main flux, Φ_m, and the leakage flux, Φ_l. Where the main flux, Φ_m, is confined by the core and links all the *N* turns in the core, and the leakage flux, Φ_l, which is partially or entirely in the air. The leakage flux is represented by an equivalent leakage flux, which also links all *N* turns of the coils, but does not follow the entire magnetic path [7].

$$\Phi = \Phi_m + \Phi_l \qquad (2\text{-}26)$$

The total flux linkage, λ, of the coil can be expressed as:

$$\lambda = N\Phi = N\Phi_m + N\Phi_l = \lambda_m + \lambda_l \qquad (2\text{-}27)$$

The total inductance is often referred to as the self-inductance, and can be obtained by dividing the linkage flux with the current, I:

$$L_{self} = \frac{\lambda}{I} = \frac{\lambda_m}{I} + \frac{\lambda_l}{I} \qquad (2\text{-}28)$$

$$L_{self} = L_m + L_l \qquad (2\text{-}29)$$

Where L_m is the magnetizing inductance due to the main flux, Φ_m, and L_l is the leakage inductance, due to the leakage flux, Φ_l [7].

2.2.6   Lorentz force on a conductor

When a conductor carrying a current is placed in a magnetic field, it is subjected to a force called the electromagnetic force, or the Lorentz force. This force is of great importance since it is the basis of operation of rotating machinery. The force depends upon the orientation of the conductor with respect to the direction of the field, and is at its greatest when the conductor is at right angles to the field, and zero when it is parallel to it. The maximum force, F, acting on a straight conductor is given by:

$$F = BlI \qquad (2\text{-}30)$$

Where l is the length of the conductor in the field [6].

2.3 Transformers

A transformer is a static device with two or more windings that are interlinked by means of a strong magnetic field. In power systems, transformers are used to transfer a certain amount of electric power at a constant frequency, while the voltage is being changed from one level to another with minimally loss of power [8].

Transformers consist essentially of two or more electric circuits on an iron core. As mentioned in Chapter 0, the core increases the magnetic coupling between the two coils, and ensures that as much as possible of the magnetic flux created by one coil links the other one.

The operation of the transformer is based on Faraday's law of induction, which was reviewed in Chapter 2.2.4.

By connecting an alternating-voltage source to the primary side, an alternating flux will be produced whose amplitude will depend upon the magnitude of the voltage and the number of turns in the primary winding. The mutual flux will link the secondary winding, and induce a voltage in it. The magnitude of the induced voltage will then depend upon the number of turns in the windings. In this way, almost every desired voltage can be obtained by selecting the correct ratio of turns [4].

2.3.1   Equivalent circuit of a non-ideal transformer

As mentioned in Chapter 2.2.5, does not only the currents flowing in the primary and secondary winding create a main flux, Φ_m, in the iron core, but also a leakage flux, Φ_l, in the air surrounding the windings. This flux is relatively small compared to the main flux, but need to be taken into account when modeling a non-ideal transformer [9].

The flux linked with the primary and secondary winding can be written as:

$$\Psi_1 = L_{l1}I_1 + L_{m1}I_1 + MI_2 \qquad (2\text{-}31)$$

$$\Psi_2 = L_{l2}I_2 + L_{m2}I_2 + MI_1 \qquad (2\text{-}32)$$

Where L_{m1} and L_{m2} are the coefficients of the self-inductance of the primary and secondary side related to the main flux, and L_{l1} and L_{l2} are the coefficients of the self-inductance of the primary and secondary windings that are related to the primary and secondary leakage flux.

By assuming an ideal magnetic coupling in the transformer, can the mutual inductance, M, can be calculated as the geometric mean of the two self inductances [9]:

$$M = \sqrt{L_{m1}L_{m2}} \qquad (2\text{-}33)$$

The primary and secondary voltage, V_1 and V_2, can then be expressed as:

$$V_1 = I_1R_1 + \frac{d\Psi_1}{dt} \qquad (2\text{-}34)$$

$$V_2 = I_2R_2 + \frac{d\Psi_2}{dt} \qquad (2\text{-}35)$$

Where R_1 and R_2 are the resistance of the primary and secondary winding.

The core losses, which consist of hysteresis and eddy current losses, can by approximation be incorporated in the equivalent circuit shown in Figure 2-6 by putting a resistance R_m in

parallel with the main inductance, L_{m1}. Here, the hysteresis losses represent the energy dissipated in the magnetic material, due to the continuous change of direction of the Weiss particles. While the eddy current losses originate from the eddy currents caused by the time varying magnetic flux in the electrically conductive core [9].
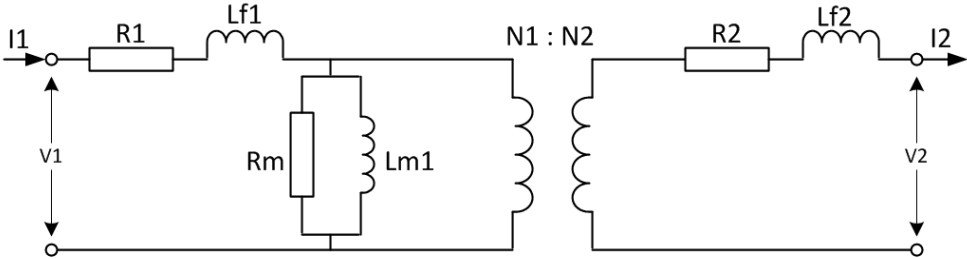
Figure 2-6: Equivalent circuit non-ideal transformer

2.3.2   No-load saturation curve

If the primary voltage, V_1, is increased with the secondary side open-circuited, the mutual flux, Φ_m, will increase in direct proportion to the voltage applied:

$$\Phi_m = \frac{V_1}{4,44fN} \tag{2-36}$$

When operating a transformer in the linear region of the magnetic material, will an increase in voltage and flux lead to an proportional increase in the magnetization current, I_0. This is not valid if the voltage is increased such that the flux reaches the non-linear region of operation. At this stage the magnetic material starts to saturate, which means that the exciting current has to increase very steeply to produce the required flux [6].

Power transformers are usually designed to operate at a peak flux density of about 1.5 T, which corresponds roughly to the knee of the saturation curve for the magnetic material in the core [6]. The nominal voltage can be exceeded for about 10% before the *B-H* relationship becomes strongly non-linear. This is not recommended since operation in the saturation region breaks down the transformer over time.

The non-linear relationship between the voltage applied to the transformer and the exciting current shows that the exciting branch (composed of R_m and X_m) is not as constant as it appears. Although R_m is reasonable constant, X_m decreases rapidly with increased saturation. This is normally not a problem, since a transformer usually operates at rated voltage where R_m and X_m remains essentially constant [6].

2.4 Asynchronous generators

In the industry the asynchronous machine, or induction machine, is used in a wide variety of applications with purpose of converting electrical power to mechanical work. The asynchronous machine is very economical, reliable, and easy to control, which are some of the reasons for its popularity. There are two main types of asynchronous machines based on the rotor construction; squirrel cage type, and wound rotor type. The simplicity and low cost, and the fact that they can be driven as a generator as well as a motor, makes these machines very beneficial for wind power generation and small hydro power plants up to 1 MW.

Unlike for wind power applications, the wound generator is seldom used in small hydro power plants. The reason for this is that generators used in small hydro power plants generally is operated on the principle of self-excitation without any rotor excitation. For such applications, generators with the squirrel cage rotors can with advantage be used instead of generators with wound rotor, since the squirrel cage machine has lower cost.

2.4.1   The principle of the induction generator

The induction machine contains a cylindrical stator and rotor cores with uniform slots separated by a small air-gap, g, (often between 0.3 to 2 mm) [10].

As for all three phase machines, the squirrel cage machine contains stator slots which host a three-phase AC winding, meant to produce a traveling magnetomotive force, mmf. This traveling mmf, F, produces a traveling flux density, B_g, in the air-gap, g:

$$B_g = \frac{\mu_0 F}{g} \cos(\omega_{el} t - p\theta_r) \qquad (2\text{-}37)$$

Where ω_{el} is the electrical angular velocity in stator, p, is the pole pairs, F is the traveling mmf, and θ_r is the position of the rotor. The traveling mmf for three phases can be calculates as [10]:

$$F = \frac{3\sqrt{2} I W_1 K_1}{\pi p} \qquad (2\text{-}38)$$

Where I is the current in each phase, W_1 is the number of turns per phase, and K_1 is the product of the distribution and chording factor, dependent upon the design of the stator [10].

The rotor of a induction machine consist of either aluminum, copper, or brass bars in the slots, where the slots are short-circuited by end-rings with a resistance lower than of the bars. A simple sketch of a squirrel cage rotor is shown in Figure 2-7.
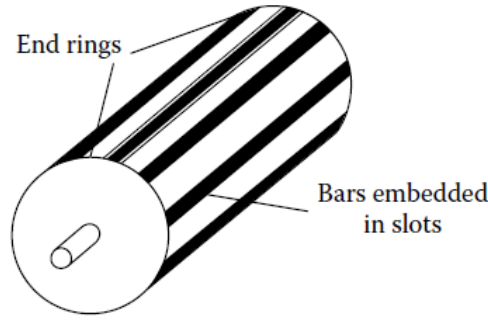
Figure 2-7: Squirrel cage rotor [10]

The angular velocity of the traveling field is obtained by:

$$\omega_{el}t - p\theta_r = constant \tag{2-39}$$

That is, for:

$$\frac{d\theta_r}{dt} = \frac{\omega_{el}}{p} \tag{2-40}$$

$$n_s = \frac{f_1}{p} \tag{2-41}$$

Where n_s is the synchronous speed in revolutions per second, which is proportional to the electrical frequency in the stator, f_1, and inversely proportional to the number of pole pairs, p. The traveling field in the air-gap between the stator and rotor induces an emf in the rotor that rotate at the speed, n, with frequency, f_2 [10]:

$$f_2 = \frac{f_1(n_s - n)}{n_s} = sf_1 \tag{2-42}$$

$$s = \frac{n_s - n}{n_s} \tag{2-43}$$

Where s is the slip of the machine.

By assuming a symmetric squirrel cage rotor, the squirrel cage can be replaced by an equivalent (fictitious) three-phase symmetrical winding that is short-circuited. By doing this, the symmetrical emf is produced in the fictitious three-phase rotor by the traveling air-gap field [10]:

$$E_2 = sE_1 = s\omega_{el}L_m I_m \tag{2-44}$$

23

Here, E_1 is the self-induced emf in each stator phase, L_m is the magnetizing inductance, and I_m is the magnetizing current required to create the resultant air-gap flux.

The rotor may be represented by a leakage inductance, L_{2l}, and a resistance, R_2. The rotor current, I_2, can expressed as:

$$I_2 = \frac{sE_1}{\sqrt{R_2{}^2 + (s\omega_{el}L_{2l})^2}}$$

(2-45)

As for the rotor, the stator is also characterized by leakage inductance, L_{1l}, and a resistance, R_1 [10].

Figure 2-8 shows the equivalent circuit for the squirrel cage induction machine.
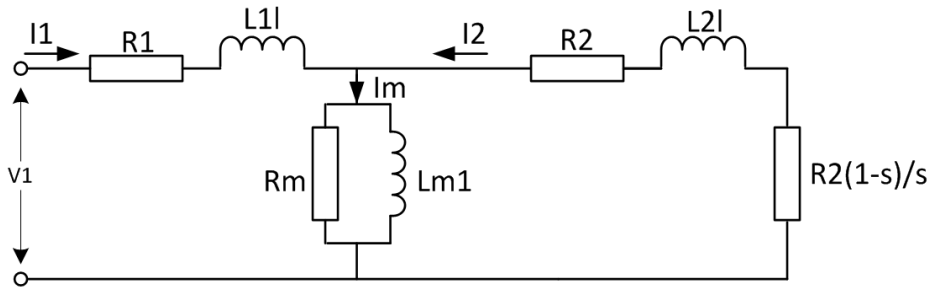
Figure 2-8: The squirrel cage induction machine equivalent circuit

The stator terminal voltage, V_1, can be expressed as:

$$V_1 = E_1 - I_1(R_1 + j\omega_{el}L_{1l})$$

(2-46)

Where the self-induced emf in the stator, E_1, can be written in term of the slip, s:

$$E_1 = I_2(R_2 + \frac{R_2(1-s)}{s} + j\omega_{el}L_{2l})$$

(2-47)

By using the equivalent circuit, the total electromagnetic power transferred across the air-gap, P_g, of a three phase machine can be determined as [4]:

$$P_g = 3I_2{}^2\frac{R_2}{s}$$

(2-48)

It can be shown that the internal mechanical power, P, developed by the machine can be expressed as:

$$P = P_g - rotor\ I^2R\ loss = 3{I_2}^2\frac{R_2}{s} - q_1{I_2}^2R_2 = (1-s)P_g \qquad\qquad (2\text{-}49)$$

The electromagnetic torque, T_e, corresponding to the internal power, P, can then be obtained by:

$$P = (1-s)\omega_1 T_e \qquad\qquad (2\text{-}50)$$

In the end, it can be shown that the internal mechanical power, P, developed by the machine can be expressed as:

$$P = P_g - rotor\ I^2R\ loss = 3{I_2}^2\frac{R_2}{s} - q_1{I_2}^2R_2 = (1-s)P_g \qquad\qquad (2\text{-}50)$$

It is important to notice that the electromagnetic torque, T_e, and the internal power, P, in Equation 2-49 and 2-50 are not the output available at the shaft at motoring because friction, windage, and stray losses remains to be accounted for [4].

By looking at Equation 2-48 it can be observed that the electromagnetic power, P_{g1}, is positive for motoring (s > 0), and negative when generating (s < 0). As seen from the equivalent circuit in Figure 2-8, the equivalent reactance of the induction machine is always inductive, irrespective of the slip sign (motor or generator), while the equivalent resistance changes sign dependent of the slip sign. The induction machine takes the reactive power required for magnetization from the utility grid which it is connected, or from a fixed capacitor bank, irrespective of whether it consume or produce active power.

2.4.2 The phenomena of self-excitation

Unlike the synchronous generator which gets its magnetization from an internal magnetizing source, and can be controlled to operate at a given frequency, the induction generator has no independent control over the air-gap field. The induction generator needs lagging reactive power to produce the main air-gap and winding leakage flux [11]. This phenomenon is referred to as self-excitation since the generator achieves its magnetizing from a grid, or capacitors which are connected to the stator terminals. The phenomena permit utilization of an induction generator as a standalone unit without a voltage source connected. Due to this the induction generator is often referred to as a SEIG, which is an abbreviation for Self-Excited Induction Generator.

The phenomenon of self-excitation has been known for a long time, and a great deal of research has been done in the field of describing the phenomena and its transient behavior.

Various types of models have been proposed, but the main part of them is rather complicated models expressed by the Park's transform.

2.4.2.1 Initiation of the self-excitation process

Self-excitation of a standalone generator may take place if a sufficient amount of capacitors is connected to the generator. In order to initiate the self-excitation process, the residual flux in the rotor iron has to be high enough. The residual flux will induce a voltage in the stator when the generator is accelerated to a certain speed. By connecting capacitors to the terminals of the generator, the induced stator voltage will cause a flow of current from the stator. [12].

For a given capacitor, an SEIG running at no load requires only a minimum speed for the self-excitation to initiate [13].

2.4.2.2 Voltage build-up in the generator

Once the process of self-excitation is initiated, the generator voltage builds up. The voltage build up can more easily be understood by looking at the phasor diagram in Figure 2-9. From the figure it can be observed that a current, I_C, starts to flow from the capacitors once the self-excitation is initiated. This current generates a flux, Ψ_{gen}, into the generator, with the same direction as the residual flux, Ψ_{res}. Therefore, the current, I_{gen}, circulating in the stator reinforces the total flux, Ψ_{total}. This reinforced total flux causes an even higher stator voltage leading to successive increase in current and flux [12].
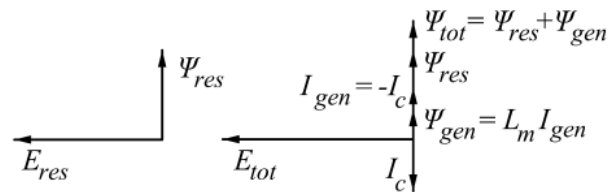
Figure 2-9: Phasor diagram before and after the self-excitation is initiated [12]

Figure 2-10 shows the generator magnetizing characteristic and capacitance for three different frequencies, where the machine magnetizing characteristic is simplified by linear segments with a knee point.

For a given capacitance and generator saturation characteristic, the intersection of the capacitance line and the *V-I*-curve of the generator moves as the frequency increases. The voltage build-up comes to halt when the non-linear magnetization curve for the generator intersects the capacitor voltage curve [11]. This point is the steady state operating point for an induction generator running at no-load with capacitors connected. The no-load steady state operating point is determined by the non-linear magnetization curve of the generator, the value of the capacitors, and the speed of the generator.
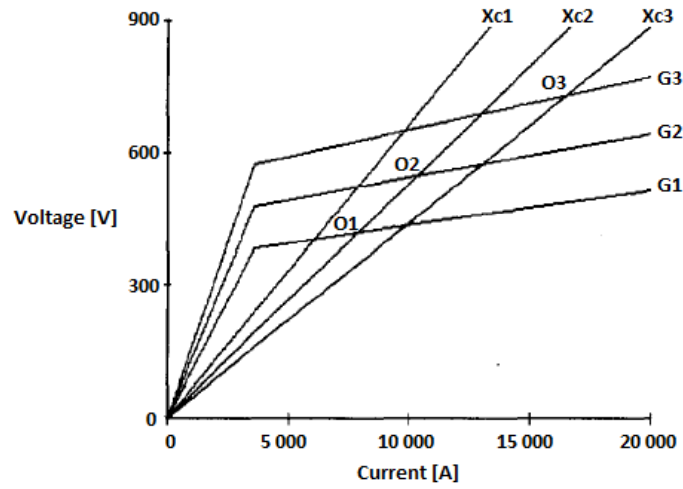
Figure 2-10: V-I curves for induction generator and capacitor at different frequencies [11]

Figure 2-10 shows that by increasing the frequency, the generator curve is moved upwards, while the slope of the capacitor curve decreases, which results in an increase of steady state operation voltage. This states that connection of capacitors supplying a no-loaded induction generator with a larger reactive power than needed may cause overvoltage at the generator terminals [12].

The intersection point between the saturation characteristic and the capacitor line can be defined in terms of the electrical frequency [11]:

$$V(\omega) = \frac{\omega A}{1 - \omega^2 L_d C} \qquad (2\text{-}51)$$

$$I(\omega) = \frac{\omega^2 A C}{1 - \omega^2 L_d C} \qquad (2\text{-}52)$$

Where L_d is the non-linear magnetization inductance defined as $d\psi/dI$ on the saturated portion of the no-load $\psi - I$ curve for the generator, and A is the interception of the dynamic inductance line with the ordinate, defined as $\psi(I) = A + L_d I$ [11].

In order to achieve a steady state operation point at any frequency, the capacitance must satisfy the following expression [11]:

$$\frac{L_a}{\omega^2 L_d} > C > \frac{1}{\omega^2 L_a} \qquad (2\text{-}53)$$

Where L_a is the inductance defined by the air-gap line of the generator [11].

2.4.3 Steady state analysis of SEIG

The steady state analysis gives the opportunity to calculate the correct amount capacitance needed to run an induction generator with a certain load at a desired voltage and frequency.

Several methods have been proposed, and they seem to fall into two main categories [10]:

- Nodal admittance methods
- Loop impedance methods

These two types of methods are based on the equivalent circuit of the SEIG, shown in Figure 2-11, expressed in per unit.

For the frequency, f, and the speed, U, the per unit values can be calculated as:

$$f = \frac{f_1}{f_{1base}} \qquad\qquad (2\text{-}54)$$

$$U = \frac{np}{f_{1base}} \qquad\qquad (2\text{-}55)$$

Where f_{1base} is the base frequency for which the reactances X_{1l}, X_{2l}, $X_m(I_m)$ are calculated, where the magnetizing reactance, X_m, is a non-linear function of the magnetizing current, I_m [10].

This report presents a method for steady state analysis, based on the nodal admittance method.
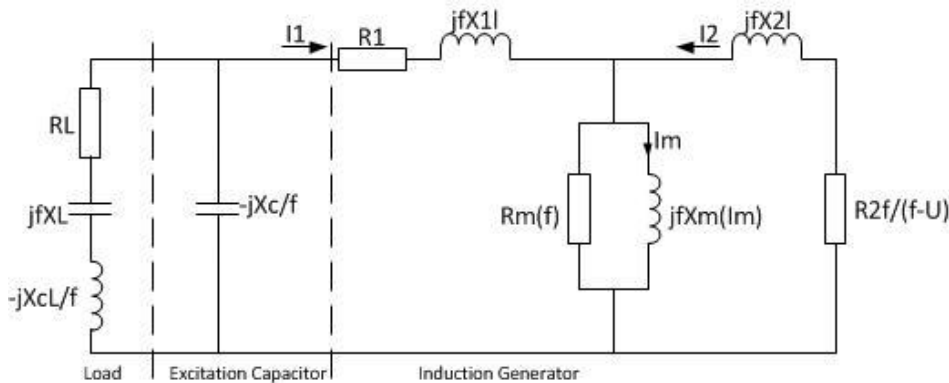
Figure 2-11: SEIG equivalent circuit in per unit for frequency, f, and speed, U

The dependence on core loss resistance, R_m, of frequency, the non-linear dependence on X_m of I_m, and the presence of frequency in the load, makes solving of the equivalent circuit quite difficult. To solve the steady state problem more simply, it can be reduced to two unknowns; frequency, f, and magnetizing reactance, X_m, for a given excitation capacitor, induction generator, load and speed. This method aims to determine the steady state frequency and voltage for a generator with constant rotor speed, and load.

The equivalent circuit shown in Figure 2-11 may be changed by lumping the stator (R_1, jfX_{1l}), the load (R_L, jfX_L, $-jX_{cL}/f$), and the excitation capacitor ($-jX_c/f$) into an equivalent series circuit (R_{1L}, jfX_{1L}) as shown in Figure 2-12. This leaves us to following expression for the lumped equivalent series circuit [10]:

$$R_{1L} + jf\omega_{el}X_{1L} = R_1 + j\omega_{el}L_{1l} + \frac{-j\frac{X_c}{f}(R_l + jfX_L - j\frac{X_{CL}}{f})}{R_L + j(fX_L - \frac{X_c}{f} - \frac{X_{CL}}{f})} \tag{2-56}$$
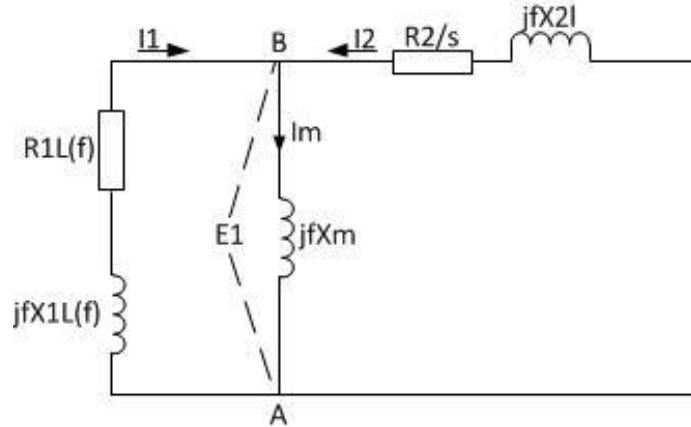
Figure 2-12: Nodal equivalent circuit of the SEIG

For self-excitation to occur, the summation of the currents in node B should be zero:

$$-I_1 + I_m - I_2 = 0 \tag{2-57}$$

Or:

$$fE_1\left(\frac{1}{R_{1L} + jfX_{1L}} + \frac{s}{R_2 + jfsX_{2l}} + \frac{1}{jfX_m}\right) = 0 \tag{2-58}$$

Further, the real and imaginary parts in Equation 2-58 have to be zero for self-excitation:

$$\frac{R_{1L}}{R_{1L}^2 + f^2X_{1L}^2} + \frac{sR_2}{R_2^2 + s^2f^2X_{2l}^2} = 0 \tag{2-59}$$

$$\frac{1}{fX_m} - \frac{sX_{1L}}{R_{1L}^2 + f^2X_{1L}^2} + \frac{sfX_{2l}}{R_2^2s^2f^2X_{2l}^2} = 0 \tag{2-60}$$

With given frequency, f, excitation capacitors, generator parameters, and load, Equation 2-59 remains with only one unknown, the slip, s [10]:

$$as^2 + bs + c = 0 \qquad (2\text{-}61)$$

Where the coefficients a, b and c are defined as:

$$a = f^2 X_{2l}{}^2 R_{1L} \qquad (2\text{-}62)$$

$$b = R_2(R_{1L}{}^2 + f^2 + X_{1L}{}^2 \qquad (2\text{-}63)$$

$$c = R_{1L}R_2^2 \qquad (2\text{-}64)$$

The second order polynomial in Equation 2-61 has two solutions, where the one with smallest absolute value is useful:

$$s_{1,2} = \frac{-b \pm \sqrt{b^2 - 4ac}}{2a} \qquad (2\text{-}65)$$

If solving the Equation 2-65 results in complex solutions, it means that self-excitation is impossible for the given frequency.

When the slip, s, is found for a given frequency, the corresponding per unit speed, U, can be calculated [10]:

$$U = f - s \qquad (2\text{-}66)$$

With s determined, the magnetization reactance, X_m, is calculated as following:

$$X_m = f^{-1} \left[\frac{f X_{1L}}{R_{1L}{}^2 + f^2 X_{1L}{}^2} - \frac{sf X_{2l}}{R_2^2 + s^2 f^2 X_{2l}^2} \right]^2 < X_{max} \qquad (2\text{-}67)$$

Where X_{max} is the maximum unsaturated value of the magnetization reactance at base frequency, f_{1base}.

For self-excitation to be possible, the magnetizing reactance, X_m, has to be smaller than the maximum unsaturated reactance level, X_{max}.

Further on, from design calculations or motor testing, the $X_m(I_m) = E_1/I_m$ characteristic as shown in Figure 2-13 can be determined.

A mathematical expression for the obtained $E_1(X_m)$ characteristic can be found with curve fitting by using following mathematical approximation [10]:

$$E_1 = \omega_{1base} K_1 I_m; \quad I_m < I_0 \tag{2-68}$$

$$E_1 = \omega_{1base} \left[K_1 I_m + \frac{K_2}{d} tan^{-1}(d(I_m - I_0)) \right]; \quad I_m \geq I_0 \tag{2-69}$$

Where I_0 is the highest magnetization current before the magnetization characteristic becomes non-linear, and K_1, K_2, and d are constants which produce the best approximation to the measured magnetization characteristic [10].
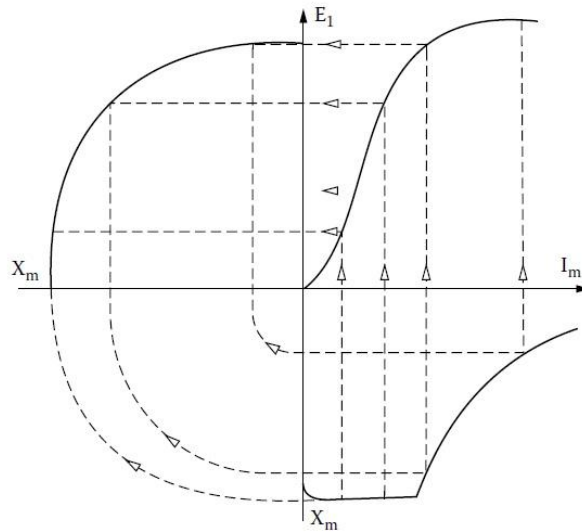
Figure 2-13: Magnetization curve for a given frequency [10]

Here, the magnetization reactance, X_m, is equal the maximum reactance, X_{max}, as long as the magnetization current is in the linear region of the characteristic ($I_m < I_0$):

$$X_m = X_{max} = \frac{E_1}{I_m} = K_1 \omega_{base}; \quad I_m < I_0 \tag{2-70}$$

When the voltage, E_1, is known, all the required variables can be determined by using the equivalent circuit in Figure 2-12 [10]:

$$I_2 = \frac{-fE_1}{\frac{R_2}{S} + jfX_{2l}} \qquad (2\text{-}71)$$

$$I_1 = \frac{-fE_1}{R_{1L} + jfX_{1L}}; \quad X_{1L} < 0 \qquad (2\text{-}72)$$

$$-V_1 = fE_1 + (R_1 + jfX_{1l})I_1 \qquad (2\text{-}73)$$

$$I_C = -V_1 j \frac{1}{fX_c} \qquad (2\text{-}74)$$

$$I_L = I_1 + I_C \qquad (2\text{-}75)$$

$$I_m = I_1 + I_2 \qquad (2\text{-}76)$$

$$I_m = \frac{E_1}{jX_m} \qquad (2\text{-}77)$$

$$X_c = \frac{1}{\omega_1 C} \qquad (2\text{-}78)$$

When all the variables are determined, the phasor diagram can be drawn. Figure 2-14 shows a phasor diagram for a inductive load where the load current, I_L, is lagging behind the terminal voltage, V_1.

Figure 2-14: Phasor diagram SEIG

Once f and E_1 is known, the power loss of the core, P_{iron}, can be calculated [10]:

$$P_{iron} = \frac{3(fE_1)^2}{R_m} \qquad (2\text{-}79)$$

The total efficiency of a SEIG under a certain load is determined by [10]:

$$\eta = \frac{3V_1I_L\cos(\varphi_L)}{3V_1I_L\cos(\varphi_L) + 3R_1I_1{}^2 + 3R_2I_2{}^2 + P_{iron} + P_{mec} + P_{stray} + P_{cap}} \qquad (2\text{-}80)$$
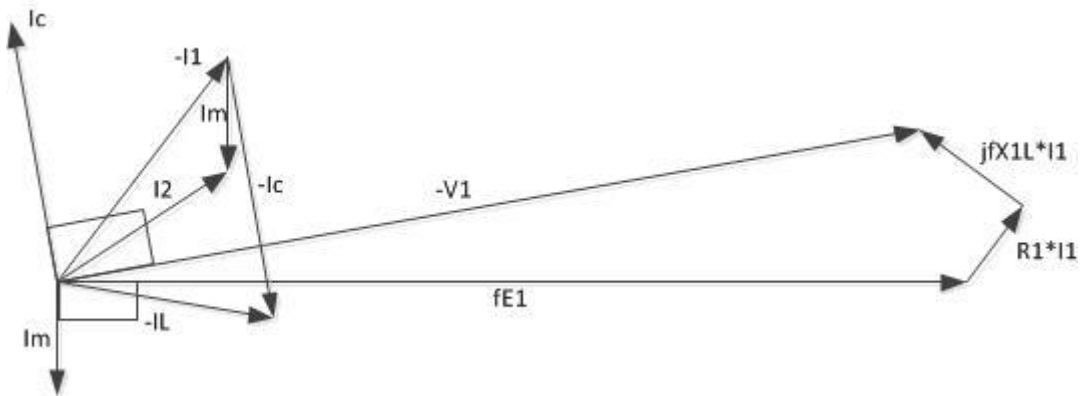
2.5 Synchronous generators

Three phase synchronous generators are the primary source for all the electric energy produced in a power system. One of the reasons is that the synchronous generator gives the opportunity to decide whether it is desirable to produce or consume reactive power, which gives us the ability to regulate the voltage and power flow in an interconnected grid [7].

2.5.1 Rotor with DC excitation

Unlike the asynchronous generator, the rotational speed of the rotor is equal to the synchronous speed of the electrical field at steady state. The rotational speed of the rotor is therefore dependent upon the number of poles in the stator, and the frequency in the grid [6]:

$$n = \frac{120f}{p} \qquad (2\text{-}81)$$

The rotor contains a field winding which is supplied by a DC source. This voltage results in a field current, I_x, which produce the rotor field in the air-gap between the rotor and stator. Controlling the rotor current and hence the rotor produced field, makes it possible to regulate the induced emf and the reactive power of the generator [7].

2.5.2 Induced EMF in stator

By assuming no magnetic saturation, it can be said that the induced emf in the stator depends on two mechanisms. These two mechanisms are the induced emf due to the rotation of the field-flux with the rotor, E_0, and the induced emf due to the rotating magnetic field created by the stator currents, $E_{a,AR}$. Since all the three phases are symmetrical equal, the focus can be on phase-a when discussing the induced emf of the the generator. These two emfs together determines the resultant emf [7]:

$$E_a = E_0 + E_{a,AR} = E_{af} - jX_mI_a \qquad (2\text{-}82)$$

By including the effect of the leakage flux by a voltage drop across the leakage reactance, X_{ls}, and including the voltage drop across the phase winding resistance, R_s, the terminal voltage, E, can be written as [7]:

$$E = E_0 - jX_sI_a - R_sI_a \qquad (2\text{-}83)$$

Where X_s is the synchronous reactance, expressed as the sum of the leakage reactance, X_{ls}, and the magnetizing reactance, X_m:

$$X_s = X_{ls} + X_m \qquad (2\text{-}84)$$

The value of R_s is typically 10 to 100 times lower than X_s, and can therefore be neglected, unless the efficiency or heating effects are of interest [6]. Figure 2-15 shows the simplified equivalent circuit for a synchronous generator.
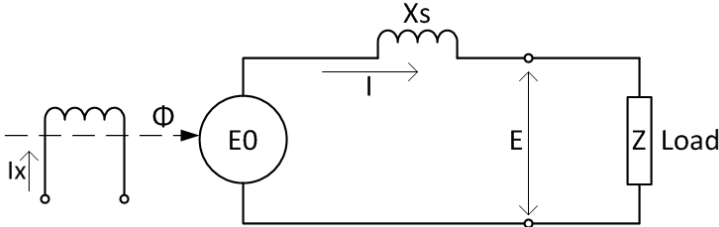
Figure 2-15: Per phase equivalent circuit for a synchronous generator

2.6 Transmission lines

Small hydro power plants are often connected to a local distribution grid. This grid is usually owned by the local utility company, and is normally operated at a voltage level between 11 kV and 22 kV.

A distribution grid is normally composed of a combination of overhead lines and underground cables. The overhead lines are used for long distances and rural areas, while underground cables are used in urban areas and for underwater crossings. An underground cable is 10 to 15 times more expensive than an overhead line, and it is therefore only used in situations where overhead lines are unsuitable [14].

From a mathematical point of view, an underground cable can be modeled in exactly the same way as an overhead line. Here, the values of the electrical parameters are the only difference between them. In a cable, the shunt capacitance is strongly dependent on whether the three-phase conductors are screened or not, and on whether the three conductors constitute separate three-phase cables or one common cable [15].

The typical per unit length series inductance, *L*, of a cable is about half the inductance of a similar rated overhead line. On the other hand, the per unit length charging current is about 30 times more than for a similar rated overhead line. For a critically long cable, the charging current can be equal to the maximum current of the cable, there will then be no capacity left for transmission of power [15].

2.6.1   Electrical transmission parameters

Regardless of whether it is an overhead line or an underground cable, the transmission line is characterized by four basic parameters; series resistance, series inductance, shunt capacitance, and shunt conductance [14].

2.6.1.1 Series resistance, R

In order to minimize the I^2R losses in the transmission line, it is desirable to keep the series resistance, *R*, of the line as small as possible. The resistance depends on the length of the conductor, *l*, the resistivity of the material, ρ, and the effective cross-sectional area, *A*, of the conductor where the current flows:

$$R = \frac{\rho * l}{A} \qquad\qquad (2\text{-}85)$$

Due to the skin effect, the alternating current in a conductor is not uniformly distributed through its cross-section. The skin effect depends upon the frequency, and leads to a higher current density in the periphery of the conductor. The skin depth, δ, of a material at a given frequency, *f*, can be calculated as:

$$\delta = \sqrt{\frac{2 * \rho}{(2 * \pi * f) * \mu}} \qquad\qquad (2\text{-}86)$$

Where μ is the permeability of the material of the conductor.

Figure 2-16 shows the cross section of a conductor and its skin depth. Using a depth of leading material higher than the calculated skin depth is waste of leading material, since it will not result in a lower resistance for alternating currents [7].
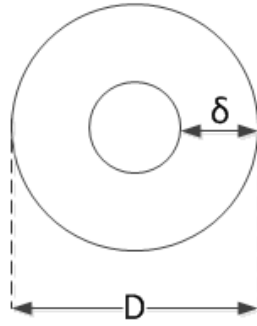
Figure 2-16: Cross-section of a conductor and its skin depth

2.6.1.2 Series inductance, L

The line inductance depends upon the partial flux linkages within the conductor cross-section and the external flux linkages. The inductances for the three phases are equal if the conductors have equilateral spacing. If not, equal inductance can be obtained by transposing the lines in such a way that each phase occupies equally all three possible positions [14].

If the conductors have equilateral spacing, the per phase inductance can be calculated as following:

$$L = \left(\frac{\mu_0}{2\pi}\right) * \ln\frac{D}{r} \qquad (2\text{-}87)$$

Where μ_0 is the permeability of the medium between the conductors, r is the radius of the conductors, and D is the geometric mean distance between the conductors, which can be calculated as [7]:

$$D = \sqrt[3]{D_{ab} * D_{bc} * D_{ca}} \qquad (2\text{-}88)$$

2.6.1.3 Shunt capacitance, C

The potential difference between the conductors causes them to be charged. A charging current flows in the conductors, due to charging and discharging when an alternating voltage is applied to the conductors. The per-phase conductance can be calculated with following equation [14]:

$$C = \frac{2\pi * \varepsilon}{\ln\frac{D}{r}} \qquad (2\text{-}89)$$

Where ε is the dielectric constant of the medium between the charges, q. The dielectric constant is the product of the relative permittivity, ε_0, and the specific permittivity of the medium, ε_s.

For a transposed three phase line without sheath around each conductor, is the equivalent radius, D, calculated by Equation 2-88. A conductor with sheath can be looked at as a concentric cylinder where r is the radius of the conductor, and D is the inner radius between the center of the conductor and the sheath [3].

2.6.1.4 Shunt conductance, G

The conductance accounts for the real power losses between the conductors, and between the conductors and ground. For power system studies are these losses often neglected, since they are usually small compared to the I^2R losses in the conductors [16].

2.6.2   Transmission model, Pi-equivalent circuit

The four electrical transmission parameters are uniformly distributed along the length of a transmission line. In power system analysis is the equivalent circuit suitable for analyzing the line during a three phase symmetrical operation. Figure 2-17 shows an equivalent circuit of a transmission line with distributed parameters. Small letters are used since the parameters are described as per unit length per phase.
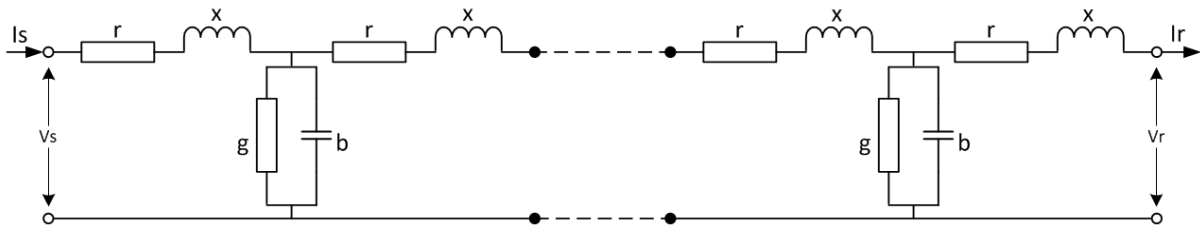
Figure 2-17: Transmission line with distributed parameters

For steady state analysis, the variables of interest are the voltage and current in the sending and receiving end of the line [15]:

$$\begin{bmatrix} V_S \\ I_S \end{bmatrix} = \begin{bmatrix} \cosh \gamma l & Z_c \sinh \gamma l \\ \sinh \gamma l / Z_c & \cosh \gamma l \end{bmatrix} \begin{bmatrix} V_R \\ I_R \end{bmatrix} \qquad (2\text{-}90)$$

Where Z_c is the surge impedance of the line, and γ is the propagation constant, which are both complex quantities that can be calculated as following:

$$Z_c = \sqrt{\frac{z}{y}} \qquad\qquad (2\text{-}91)$$

$$\gamma = \sqrt{zy} \qquad\qquad (2\text{-}92)$$

For analysis purpose it is more convenient to represent the lines as a Pi-equivalent as shown in Figure 2-18.
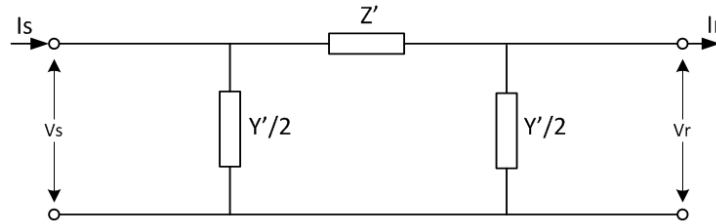
Figure 2-18: Equivalent pi-circuit of a transmission line

The Pi-equivalent parameters Z' and Y' are given by:

$$Z' = Z * \frac{\sinh \gamma l}{\gamma l} \qquad\qquad (2\text{-}93)$$

$$Y' = Y * \frac{\tanh \frac{\gamma l}{2}}{\frac{\gamma l}{2}} \qquad\qquad (2\text{-}94)$$

Where Z is equal to $z * l$, and is the total series impedance per phase, and Y is equal to $y * l$, and is the total shunt admittance per phase. The series impedance and shunt admittance are defined as:

$$Z = R + jX \qquad\qquad (2\text{-}95)$$

$$Y = G + jB \qquad\qquad (2\text{-}96)$$

Figure 2-18 shows that the shunt admittance is lumped with the half of it located in each end of the transmission line [16].

3 Description of the grid

For this investigation, only a small part of the grid in Seljord is of interest, the Lønnestad radial, which radiates from Seljord substation. Seljord substation is located in the center of Seljord, and hosts two transformers which connect the 22 kV distribution grid in Seljord with the 66 kV transmission grid.

An overview of the Lønnestad radial is shown in Figure 3-1, the figure shows the different distribution cables with type and length, the different generator units, and the various busbars with their transformers connected.
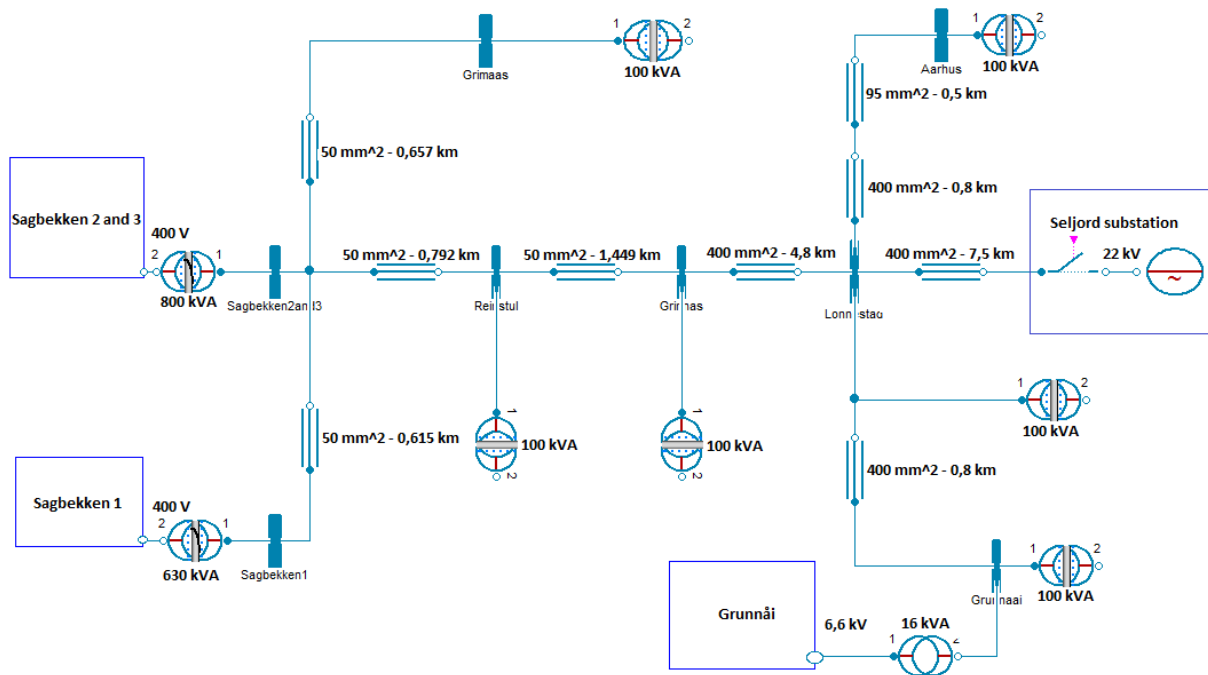
Figure 3-1: Overview of the Lønnestad radial

3.1 Distribution cables in the grid

In total, the Lønnetsad radial consists of 17.91 km with transmission lines, where the main parts of the lengths are cables. These cables are of the TSLE single conductor type, which is a medium voltage cable (12/24 kV) with aluminum conductor, designed for installation in the ground. The four different letters in TSLE explain the structure of the cable, and are shown in Table 3-1. Figure 3-2 shows the structure of a single conductor TSLE cable.

Table 3-1: Explanation of the TSLE cable

Type of Layer:	Letter:	Information:
Insulation	T	Cross-linked polyethylene (PEX)
Metallic screen	S	Wound bare copper wires
Aluminum tape	L	Longitudinal aluminum tape
Sheath	E	Weather resistant polyethylene (PE)

Figure 3-2: Single conductor 12/24 kV TSLE cable [17]

The electric parameters needed for modeling of the different distribution lines are taken from the Norwegian cable manufacturer, Draka Kabel. Since the production of the TSLE cable are replaced with an upgraded version, TSLF, the data sheet for a TSLF cable have been used for parameter calculations. The TSLF cable is basically the same cable, only with a semiconducting outer layer which makes fault diagnostic easier.

Electrical parameters expressed in per unit used for modeling of different dimensions of the TSLE cable are shown in Table 3-2. Calculations of the per unit parameters are shown in Appendix B.

Table 3-2: Per unit values for different dimensions of TSLE

	TSLE 3x1x400 Al	TSLE 3x1x95 Al	TSLE 3x1x50 Al
r [p.u./km]	0,000160	0,000660	0,001321
x [p.u./km]	0,000227	0,000289	0,000309
x0 [p.u./km]	0,000680	0,000866	0,000928
g_pg [p.u./km]	0	0	0
g_pp [p.u./km]	0	0	0
b_pg [p.u./km]	0,060934612	0,035037402	0,02589721
b_pp [p.u./km]	0	0	0
V_nom [V]	22000	22000	22000
S_nom [VA]	1000000	1000000	1000000

For the cable models, the phase to phase susceptance, b_pp, was assumed to be equal to zero since the metallic screen of a TSLE cable is connected to the ground. The shunt conductance, g_pp, and g_pg, were assumed to be negligible, as mentioned in Chapter 2.6.1.4.

3.2 Distributed generation units in the grid

The Lønnestad radial has three different hydro power plants connected; Grunnåi, Sagbekken 1, and the Sagbekken 2 and. In total, these three hydro power plants represent an installed capacity of 15.935 MW.

3.2.1   Grunnåi power plant

Grunnåi hydro power plant has an installed capacity of 15.06 MW. It is owned by several part-owners, where Skagerak Kraft is the main owner. The power plant utilizes a waterhead of 389 meter with a Pelton turbine and synchronous generator. The turbine governor in the plant runs at power control, which means that it runs according to a given power setpoint with an infinity droop.

Figure 3-3 shows a picture of the synchronous generator inside the power plant.

Figure 3-3: Grunnåi Power Station with its generator

3.2.1.1 Synchronous generator parameters

The synchronous generator in Grunnåi is produced by Leroy Somer, and has five pole pairs. Electrical parameters for the generator are presented in Table 3-3.

Table 3-3: Paremeters for Grunnåi generator model

Parameter:	Value:
pp [-]	5
x_d [p.u.]	1.870
x_q [p.u.]	1.170
x_o [p.u.]	0.1
r_s [p.u.]	0.000003131
x_d' [p.u.]	0.42
x_d" [p.u.]	0.22
x_q' [p.u.]	0.44
x_q" [p.u.]	0.27
tc_d' [s]	1.600
tc_d" [s]	0.005
tc_q' [s]	0.25
tc_q" [s]	0.04
xsig_s [p.u.]	0.003
V_nom [V]	6600
S_nom [VA]	15853000

3.2.1.2 Turbine parameters

Due to lack of documentation of the turbine, some assumptions had to be made regarding its mechanical power, P_m, and flywheel effect, GD^2. The mechanical power into the turbine is assumed to be equal to the rated capacity of the generator, and the flywheel effect is assumed to be 10% of the flywheel effect of the rotor.

The parameters for turbine and rotor are shown in Table 3-4. Calculations of these parameters are presented in Appendix C.

Table 3-4: Parameters for Grunnåi turbine and rotor model

Parameter:	Value:
H [s]	1.3
w_nom [rpm]	600
P_nom [W]	15060000

3.2.1.3 Protection relays

In order to protect the equipment in Grunnåi, and components in the grid against unwanted events, the power plant is equipped with several protection relays. Each of these protection relays hosts various functionalities such as protection against over- and underfrequency, and over- and undervoltage. The parameters for voltage and frequency protection for the protection relay operating the generator circuit breaker (GCB) are shown in Table 3-5.

Table 3-5: Protection relay settings Grunnåi

Functionality:	Limit:	Triggering time [s]:
V>	110 %	4 s
V>>	120 %	2 s
V>>>	130 %	0.1 s
U<	90 %	10 s
V<<	80 %	5 s
V<<<	70 %	1 s
f>	51 Hz	5 s
f>>	52 Hz	0.1 s
f<	49 Hz	5 s
f<<	48 Hz	0.1 s

3.2.1.4 Surge arrester

To protect electrical equipment in Grunnåi against unacceptable overvoltage stresses, are surge arresters mounted between each phase and earth at the 22 kV busbar inside the power plant. The surge arresters are of the type ABB MWK, and have a continuous operation voltage, U_c, of 24 kV and a rated voltage, U_r, of 30 kV [18]. This is surge arresters with metal oxide resistors without spark gaps (MO surge arresters), designed for protection of medium voltage equipment such as transformers, cables, and motors [18].

For temporary (short-time) overvoltages, U_{TOV}, the surge arresters are able to withstand an increased operating voltage for a certain period of time. The resistance, T, against such temporary overvoltages is defined as [18]:

$$T = \frac{U_{TOV}}{U_c} \qquad (3\text{-}1)$$

The stability characteristic for the MWK arrester is shown in Figure 3-4. The figure shows how long the arrester can withstand an increased voltage without becoming thermally unstable. Curve *b* and *a* represents the characteristic of the thermal stability, dependent on

whether the surge arrester has been stressed with an energy, W, before the appearance of the temporary overvoltage, or not.
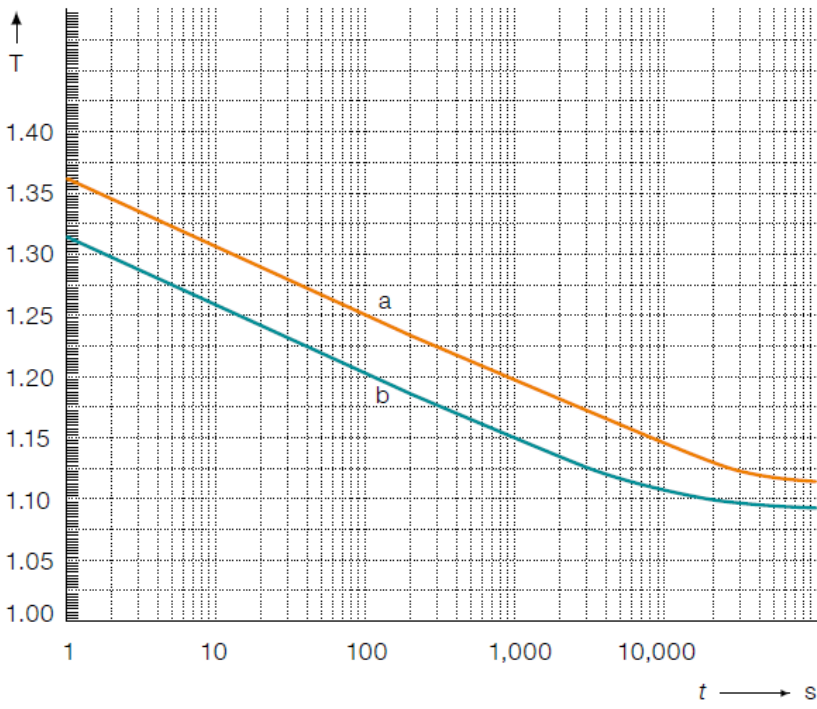

Figure 3-4: Resistance against temporary overvoltages for MWK arresters [18]

3.2.2   Sagbekken power plants

Sagbekken power plants (Sagbekken 1, and Sagbekken 2 and 3) are two power plants owned by a private landowner at Reinstul. These power plants utilize water from the same river, where the outlet from Sagbekken 2 and 3 runs directly into the intake of Sagbekken 1. Due to the rather small installed capacity in these two power plants, the usage of standard equipment has been essential to ensure low costs and good economy in the projects.

Asynchronous machines with squirrel cage rotor have therefore been applied for generators in both of the power plants. This is low cost standard machines with a robust construction, mainly designed for motor applications within the industry.

Standard components have also been applied for the turbines, where all turbines for each power plant are identical independent of the different generator ratings. Here, different types of nozzles have been used to adapt the turbines to the different generators ratings. Since this is low cost machinery, no form for turbine governing is installed. Each turbine is equipped with five nozzles where the opening is adjusted according to the setpoint for production.

3.2.2.1 Asynchronous generator parameters

Parameters needed for the generator models are determined by using the equivalent circuit in Figure 2-8, and results obtained from no-load tests and short-circuit tests performed by the manufacturer. All the machines in the Sagbekken plants are delivered by the manufacturer Lönne, and are within the same model series.

Datasheets for the different machine ratings and calculations of the electrical parameters are presented in Appendix D. It can be observed that the rotor inertia, J, is unspecified for one of the machine ratings. The relationship between the inertia, J, and machine rating, P, was assumed to be linear for the different machine ratings. A linear function of the inertia, J, with respect to the machine rating, P, was therefore obtained with the least square method.

3.2.2.2 Sagbekken 1

Sagbekken 1 consists of three generator units, two with 100 kW rating, and one with 200 kW rating. As seen in Table D-1 in Appendix D, there is no datasheet for the 100 kW machines available. A 110 kW machines are therefore used instead of the 100 kW machines. This machine is only 10 kW larger, and the difference is assumed to be negligible.

3.2.2.2.1 Generator parameters

The per unit generator parameters for Sagbekken 1 are shown in Table 3-6. The per unit values are obtained from the calculations presented in Appendix D.

Table 3-6: Generator parameters for Sagbekken 1

Parameter:	Sagbekken 1 - 110 kW:	Sagbekken 1 - 200 kW:
pp [-]	2	2
x [p.u.]	2.2413	3.7609
x_o [p.u.]	3*x	3*x
r_s [p.u.]	0.0259	0.0276
r_n [p.u.]	1	1
n_r [-]	1	1
xtr [p.u.]	0.0978	0.1240
tc [s]	0.0120	0.0143
xsig_s [p.u.]	0.0494	0.0625
V_nom [V]	400	400
S_nom [VA]	130952	229885

3.2.2.2.2 Turbine parameters

A mentioned in Chapter 3.2.1, the same type of Pelton turbine is mounted at all the three generators, independently of their rating. Table 3-7 presents the parameters used for the turbine and rotor models for Sagbekken 1. Calculation of the parameters is presented in Appendix E.

Table 3-7: Parameters for Sagbekken 1 turbine and rotor

Parameter:	Sagbekken 1 – 100 kW:	Sagbekken 1 -200 kW:
H [s]	0.5322	0.4150
w_nom [rpm]	1500	1500
P_nom [W]	100000	200000

3.2.2.2.3 Protection relays

For fault detection, the Carlo Gavazzi DPC02 multifunction monitoring relay is installed. This is a small and simple unit, which provides monitoring functionalities such; as over- and undervoltage, and over- underfrequency, phase sequence, and phase loss [19]. A picture of the protection relay is shown in Figure 3-5.

Figure 3-5: Carlo Gavazzi DPC02 Monitoring Relay [19]

The protection relay operates the common GCB in the power plant, which means that all the generator units are disconnected if an unwanted event occurs. Parameters used for the protection relay are shown in Table 3-8.

Table 3-8: Protection relay setting Sagbekken 1

Functionality:	Limit:	Triggering time [s]:
V>	107 %	0.7 s
V<	93 %	0.7 s
f>	60 Hz	0.7 s

3.2.2.3 Sagbekken 2 and 3

Sagbekken 2 and 3 utilize the waterhead from two different creeks, and has therefore two different penstocks leading into the power plant. Two generator units are utilizing the waterhead of each penstock. Here, the Sagbekken 2 penstock has a machine of 75 kW, and a machine of 250 kW, while the Sagbekken 3 penstock has two machines with 75 kW rating. The four induction generators inside Sagbekken 2 and 3 are shown in Figure 3-6. The figure gives an impression of the small dimensions for components in this capacity range.

Figure 3-6: The four generator units in Sagbekken 2 and 3

Because of the oversized penstocks in the power plant, the generator units have the opportunity to run at a load higher than their rated capacity. The degree of overload for each generator is limited by the amount of water available, and the temperature rise in the machine. Table 3-9 shows the potential overload for the different generator units in Sagbekken 2 and 3.

Table 3-9: Potential overload for the different generator units in Sagbekken 2 and 3

	Rated capacity:	Potential overload:	Total production:
Sagbekken 2 penstock:			
Generator 1	75	0	75
Generator 2	250	25	275
Sagbekken 3 penstock:			
Generator 1	75	12.5	87.5
Generator 2	75	12.5	87.5

3.2.2.3.1 Generator parameters

The per unit generator parameters for Sagbekken 2 and 3 are shown in Table 3-10. The parameters are obtained from the calculations presented in Appendix F.

Table 3-10: Generator parameters for Sagbekken 2 and 3

Parameter:	Sagbekken 2 and 3 - 75 kW:	Sagbekken 2 and 3 - 250 kW:
pp [-]	2	2
x [p.u.]	2.6446	3.3088
x_o [p.u.]	3*x	3*x
r_s [p.u.]	0.0390	0.0219
r_n [p.u.]	1	1
n_r [-]	1	1
xtr [p.u.]	0.1106	0.1007
tc [s]	0.0090	0.0146
xsig_s [p.u.]	0.0559	0.0507
V_nom [V]	400	400
S_nom [VA]	88235	287356

3.2.2.3.2 Turbine parameters

As for the generators in Sagbekken 1, the generators in Sagbekken 2 and 3 have the same type of Pelton turbine mounted. The calculated turbine and rotor parameters for Sagbekken 2 and 3 are shown in

Table 3-11. Calculations of these parameters are presented in Appendix F.

Table 3-11: Parameters for Sagbekken 2 and 3 turbine and rotor

Parameter:	Sagbekken 2 and 3 – 75 kW:	Sagbekken 2 and 3 -250 kW:
H [s]	0.8500	0.4050
w_nom [rpm]	1500	1500
P_nom [W]	75000	250000

3.2.2.3.3 Protection relays

The four generators in Sagbekken 2 and 3 are protected with two different protection relays, which both operate the main GCB of the power plant.

One of these protection relays is the Carlo Gavazzi DPC02, which is the same protection relay as the one in Sagbekken 1, as mentioned in Chapter 3.2.2.2.3. The other one is the Megacon KCG595 multifunction relay, which is a relay that contains a wide range of functionalities such as over- and underfrequency, over- and undervoltage, voltage imbalance, and rate of change of frequency monitoring [20]. A picture of the Megacon 595 protection relay is shown in Figure 3-7.

Figure 3-7: Megacon KCG595 protection relay [20]

The parameters related to voltage and frequency protection of the power plant are shown Table 3-12. Of the table it can be seen that both the Carlo Gavazzi and Megacon relay provide protection against over- and underfrequency. Because of the triggering time, the Carlo Gavazzi relay will trigger first for overvoltages, and undervoltages below 85 % of nominal voltage.

Table 3-12: Protection relay settings for Sagbekken 2 and 3

Functionality:	Limit:	Triggering time [s]:	Protection relay:
V>	110 %	10 s	Megacon 595
V<	90 %	10 s	Megacon 595
V>	110 %	1.5 s	Carlo Gavazzi DPC01
V<	85 %	1.5 s	Carlo Gavazzi DPC01
f>	55 Hz	10 s	Megacon 595
f<	45 Hz	10 s	Megacon 595

3.3   Transformers in the grid

The transformers connected to the Lønnestad radial are installed to serve two different purposes. Here, the ones installed in the power plants serve the purpose of transforming the generator voltage up to the 22 kV voltage of the Lønnetsad radial. While the small transformers installed in the substations serve the purpose of reducing the 22 kV distribution voltage to a more suitable voltage for the the consumers.

By looking at the overview of the radial in Figure 3-1, it can be seen that nine transformers are connected to the radial. Of these nine transformers, three of them are connected in Sagbekken 1, Sagbekken 2 and 3, and Grunnåi, having a rating of 630 kVA, 800 kVA, and 16 MVA. The six remaining transformers all have a rating of 100 kVA.

For modeling, transformer parameters for the Sagbekken plants and substations were based on the OTW series from Møre Trafo. Parameters for the 16 MVA transformer in Grunnåi are not obtained since the transformer can be modeled as an ideal transformer due to the scenario to be simulated.

Table 3-13 shows the calculated per unit values for the transformers in the grid. The parameters are obtained from the datasheets, which are presented in Appendix G.

Table 3-13: Calculated per unit values for the transformers

Brand:	Møre Trafo	Møre Trafo	Møre Trafo
Model:	OTW 3640	OTW 51170	OTW 6960
Sn [kVA]	100	630	800
r1 [p.u.]	0.0084	0.0041	0.0040
r2 [p.u.]	0.0084	0.0041	0.0040
x1 [p.u.]	0.0177	0.0230	0.0288
x2 [p.u.]	0.0177	0.0230	0.0288
x0 [p.u.]	x1	x1	x1
rm [p.u.]	25243	48402	49893
xm [p.u.]	14327	65485	40778
xm0 [p.u.]	xm	xm	xm
psi_sat [p.u.]	-	1,22	1,22
xm_sat [p.u.]	-	3857	3250
V_nom1 [V]	22000	22000	22000
V_nom2 [V]	400	400	400
S_nom [VA]	100000	630000	800000

3.4 Loads connected to the grid

From correspondence with the local utility company in Seljord, Vest Telemark Kraftlag, it is known that a very small amount of load is connected to the radial. The consumers connected to the grid are mainly private households and some industry. The load is said to be negligible, except some industry related consumption at Århus. This load can vary through the day, but is assumed to be 250 kW with a power factor, pf, equal 0.96 during the working hours.

3.5 Overvoltage phenomena in Grunnåi

The 27th July in 2011, several unwanted events took place in Grunnåi power plant. By looking at the damages it could be seen that significant overvoltages had occurred in the 22 kV busbars of the power plant.

3.5.1 Damages from the events

On the end termination of one of the incoming TSLE cables, a phase to ground fault had occurred. Two pictures of the end termination and its damage are shown in Figure 3-8. From the figure it can be seen that there has been heat generation in the end termination.

Figure 3-8: Phase to ground fault on end termination of TSLE cable

A breakdown of a surge arrester had also occurred under the events. The surge arrester was of the type ABB MWK, as described in Chapter 3.2.1.4.

Figure 3-9 shows the surge arresters with the broken one to the left. By looking at the broken surge arrester and the signs of heat, it is natural to assume that the amount of energy dissipated in the surge arrester was higher than its energy handling capability.

Figure 3-9: Broken surge arrester

Signs of high temperatures and arcs were also seen other places in the rack of the 22 kV busbar, which could be signs of a possible short-circuit due to a high voltage.

Damages did also occur other places in the radial this day, which indicates that the phenomenon didn't only take place locally in Grunnåi.

3.5.2   The sequence of events

By looking into the logs of the protection relays in Grunnåi and Seljord Substation, it was discovered that several functionalities in each of the protection relays had started to count for triggering. Unfortunately weren't the clocks in the protection relays synchronized, so it is impossible to determine which protection relay that triggered first.

Anyway, it is most likely to think that all started with a breakdown in the end termination of the incoming cable in Grunnåi. The breakdown was most likely caused by a weakness in the end termination due an error that was made during the installation. This error may have caused a bad connection or a weakness in the insulation, which led to heat generation, and degradation of the insulation over longer time.

The presumed sequence of events is:

1. Earth circuit fault in Grunnåi due to a breakdown in the end termination of a incoming TSLE cables.
2. The protection relay in Seljord Substations detected the phase to ground fault, and disconnected the Lønnestad radial from the rest of the grid in Seljord momentarily after the fault was detected.
3. The disconnection resulted in heavy imbalance of active power and reactive power in the island.

4. The frequency in the grid increased rapidly since Grunnåi didn't correct for the overproduction in the island.

5. The GCB disconnected Grunnåi from the grid, due to triggering of the overfrequency relay (51 HZ and 0.1 seconds). This left the asynchronous generators in Sagbekken 1 and Sagbekken 2 and 3 alone in the island.

6. Sufficient amount of capacitive power in the grid to initiate self-excitation. The self-excitation led to a successive voltage build-up, which resulted in significant overvoltages in the grid.

7. The high voltage led to a large voltage drop across the surge arresters in Grunnåi. The amount of energy dissipated in the surge arrester was higher than its energy handling capability. This caused one of the surge arresters to breakdown.

8. The high voltage exceeded the dielectric strength of air inside the rack of the busbars. The air became ionized and arcing occurred inside the rack. This arcing led to low impedance in the grid, and the process of self-excitation came to halt.

This is the presumed sequence of events, based on the damages and grid configuration. Following chapter presents simulations from the Lønnestad radial where different scenarios are carried out.

4 Power system model

The power system of the Lønnestad radial was modeled and simulated with the usage of computerized software. Several models were made for the power system to simulate different scenarios. A small project library was made for the power system, containing the different power system models, main components, and subsystems developed for the models.

4.1 Simulation tools

In order to model and simulate the time varying behavior of a large dynamic system, the usage of computer programs is essential. Dynamic systems are often mathematical described by ordinary differential equations (ODE) or by partial differential equations (PDE), which require numerical methods to solve the equations. Even for a rather small dynamic system, the numbers of equations to be solved are often high.

Depending on the type of numerical method applied, and the required accuracy of the simulation, the system often needs to be solved with a small step size (1-2 ms). This makes manual simulation of large dynamic system over a long time period a very inefficient and time consuming process. Therefore, the usage of a computerized tool is crucial for achieving an accurate and time efficient simulation.

A wide range of computer programs exist for simulation of dynamic systems. The different programs offer various toolboxes and functionalities based on the type of system to be simulated. All of the programs have their pros and cons, dependent on the system to be modeled and simulated.

The modeling and simulation of the Lønnestad radial was performed by using Dymola, which is a Modelica simulation environment.

4.1.1 Modelica

Modelica is a non-proprietary, object-oriented, equation based language to conveniently model complex physical systems, e.g., electrical, electronics, thermal, mechanical, hydraulic, control, electric power or process-oriented subcomponents [21]. Figure 4-1 shows some of the physical systems where the Modelica language is applied for modeling and simulation.
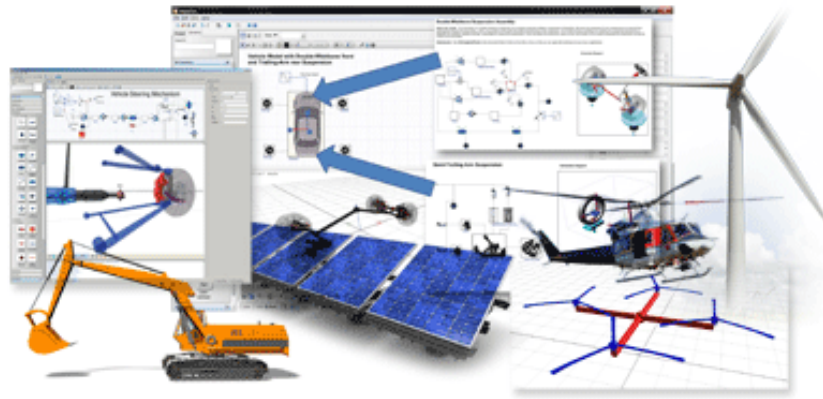
Figure 4-1: Some of the physical system which can be modeled and simulated by the usage of Modelica [21]

Modelica is a language such as Java and C++, and a simulation environment is therefore necessary. The language is developed by the non-profit Modelica Association, which mainly consist of representatives from the various fields of industry and education institutions.

4.1.2   Dymola

Dymola is a complete and powerful tool for modeling and simulation of integrated and complex systems, developed by the French company Dassault Systems. The simulation environment is based on the Modelica open standard, and includes the Modelica Standard Library. The libarary contains about 920 generic model components and 615 functions in different domains. A wide range of add-on libraries are developed to meet the needs of the user, e.g., the Pneumatics Library, PowerTrain Library, Hydro Power Library or the Electric Power Library [22].

The program has a unique multi-engineering capability which gives the user the opportunity to combine components from several engineering domains. All the components are open, and the user is free to modify the ready-made components to better match the unique needs for each model. This allows models of complete systems to better depict reality [22].

4.1.3   Electric Power Library (EPL)

The components and functionalities in the Electric Power Library were used as a basis for the power systems model developed for the Lønnestad radial.

The Electric Power Library is developed by the Swedish company Modelon, which is a company that specializes in providing solutions, services, and technology for research and development of dynamic systems. The library gives the opportunity to model, simulate, and analyze electric power systems, including AC three phase systems, AC one phase systems, and DC systems. The models can be used for both steady state and transient mode for

simulation and initialization. All the components of the library are available for three different reference frame representations (abc, $dq0$, and dq). Also here, the library works in a multi domain, which allows modeling and simulation of power electronics, electricity, mechanics, and thermal dynamics in the same tool [22].

The EPL presents the voltages as the single phase amplitude voltage, V_{samp}, which is expressed as:

$$V_{samp} = \sqrt{\frac{3}{2}} * V_{abc} \qquad\qquad (4\text{-}1)$$

Where V_{abc} is the three phase system voltage.

4.2 Submodels made for simulations

In order to make the different simulation models easier to build, a library with the different components of the grid and its parameters were created in Dymola.

Models for the different power plants were created by gathering all the machines of the plant and the protection relays into submodels.

Since there are no components for protection relays and RMS voltage sensors in the Electric Power Library, these components had to be created. More about these components can be found in Appendix A.

4.2.1   Grunnåi hydro power plant model

Figure 4-2 shows the submodel for Grunnåi power plant. For the generator, a model with electric excitation is used. A simple excitation model with constant excitation voltage is connected to the generator model to excite the rotor. This type of excitation does not match the reality, but is sufficient for the scenario to be simulated. The reason for this is that the exciter has a time delay of 1-2 seconds before it respond to changes in the grid voltage. It is likely to think that the Grunnåi power plant has disconnected due to overfrequency within this time.

For the turbine, a single mass rotor model is utilized. This is a model representing the turbine and rotor with a given inertia, J, speed, n, and torque, T, as output. A governor with constant setpoint is utilized for the model since Gunnåi operates with an infinite droop.

The generator of Grunnåi was running at 11 MW the day when overvoltage phenomena occurred in Grunnåi. This setpoint will therefore be used for all the simulation scenarios.

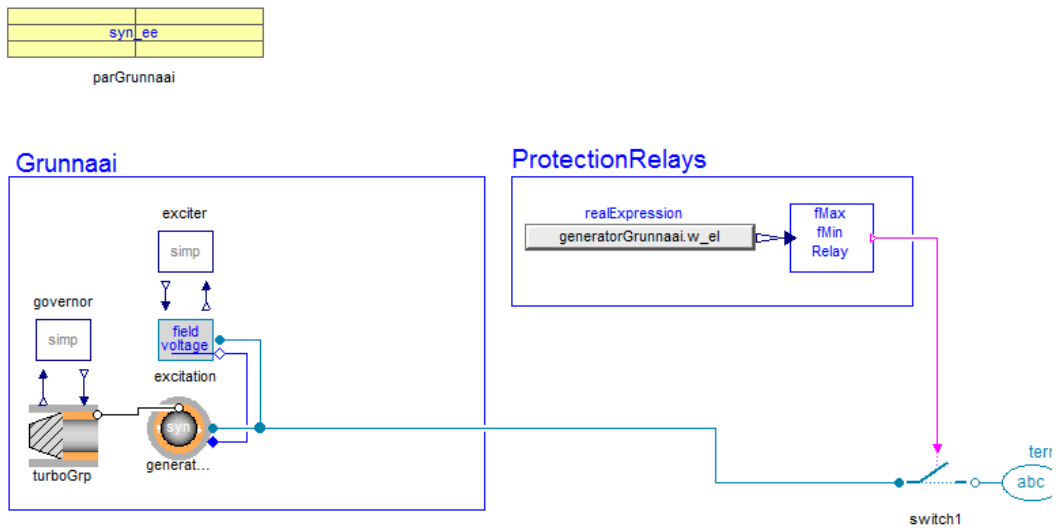Parameters used for the different components in the submodel are presented in Chapter 3.2.1.

Figure 4-2: Submodel Grunnåi

4.2.2   Sagbekken 1 hydro power plant model

The submodel for Sagbekken 1 with its three machines, the common protection relay and GCB are shown in Figure 4-3. The turbines are modeled with a single mass rotor with a constant setpoint. The generators are modeled with an asynchronous machine with squirrel cage rotor. The generators are connected to the output of the submodel via the GCB, which is controlled by the protection relays.

Chapter 3.2.2 presents the parameters used for the submodel of Sagbekken 1.
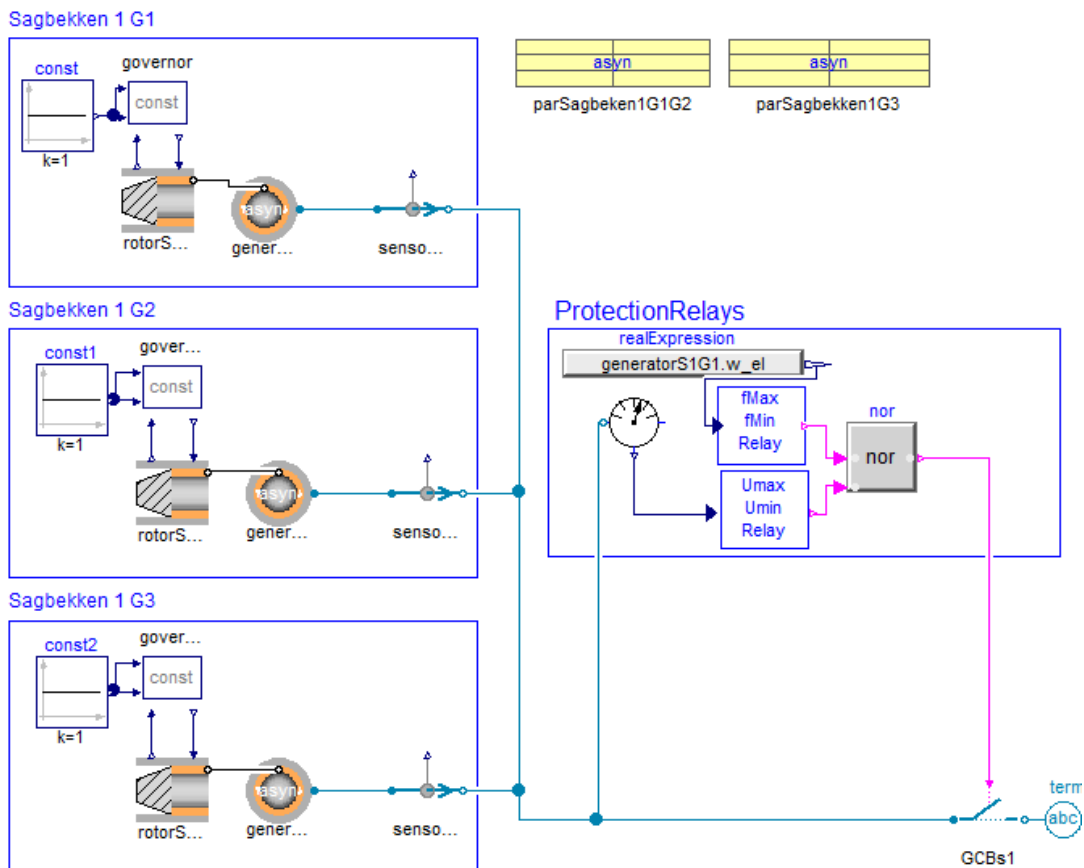
Figure 4-3: Submodel Sagbekken 1

4.2.3 Sagbekken 2 and 3 hydro power plant model

The submodel of Sagbekken 2 and 3 with its four machines, the common protection relay and GCB is shown in Figure 4-4. The submodel is basically constructed in the same way as the submodel for Sagbekken 1, but with an extra machine and different parameters.

Chapter 3.2.2 presents the parameters used for the submodel of Sagbekken 2 and 3.

Since it is known that these four machines have the possibility to run at an overload, the setpoint on the turbine governors are adjusted in terms of the maximum productions mentioned in Chapter 3.2.2.3.
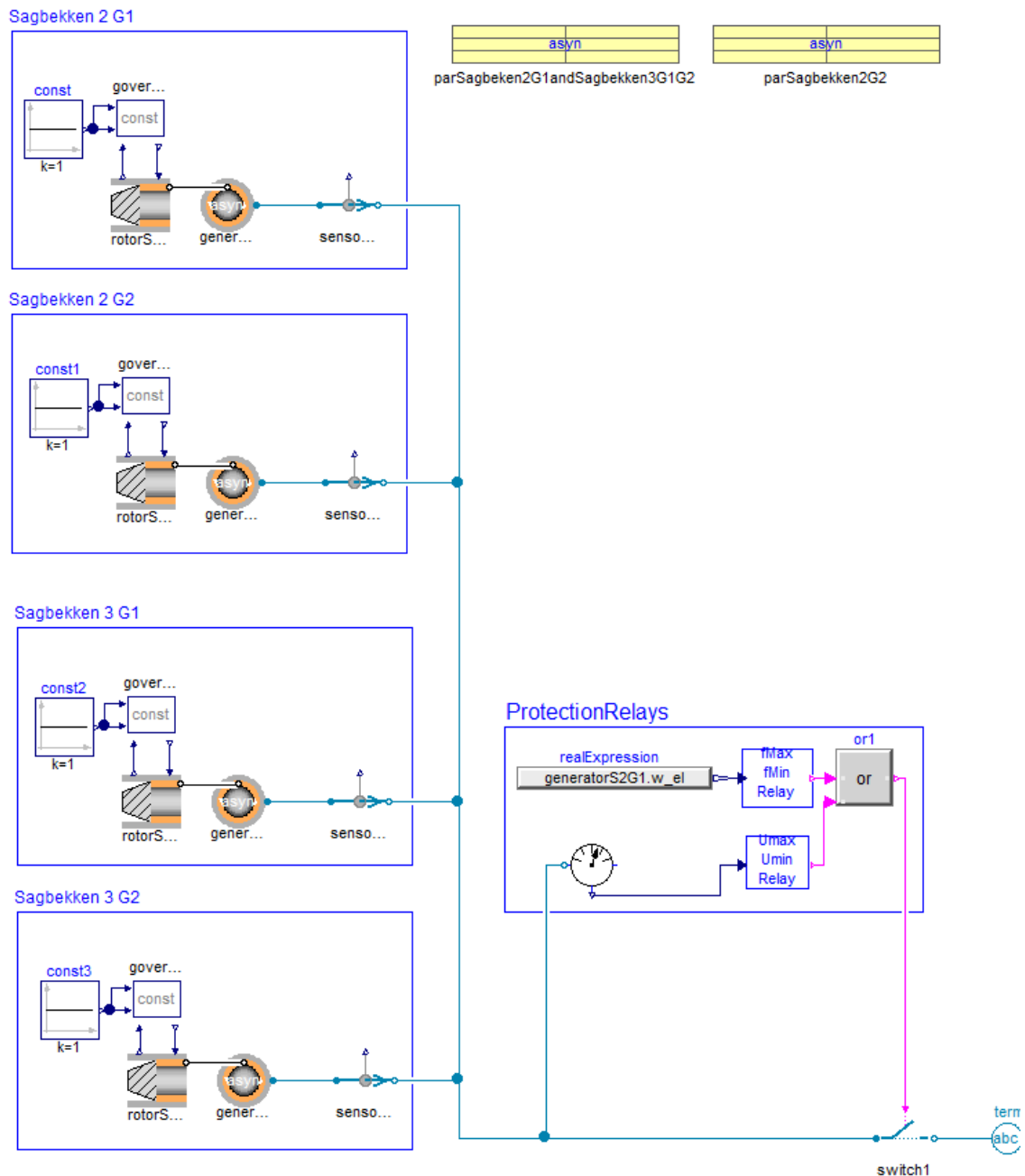
Figure 4-4: Submodel Sagbekken 2 and 3

4.3 Investigation of the self-excitation process

In order to investigate the self-excitation phenomena, the small model shown in Figure 4-5 was made. The model consists of a hydro power plant with asynchronous generator which is connected to an ideal voltage source. For the power plant, the configuration from the 100 kW machine in Sagbekken 1 was applied. Parameters for the turbine and generator can be found in Chapter 3.2.2.2.

To be able to investigate the process with different grid configurations, a capacitor bank and resistive load were connected in shunt with a negligible short line to represent a grid with a

given capacitance and resistive load. The investigation was carried out as sensitivity analysis where different loads and capacitors where compared in order to determine their impact on the system. At t=1 second the circuit breaker was opened, which brought the power plant into islanded grid operation with a given capacitive power and resistive load connected.
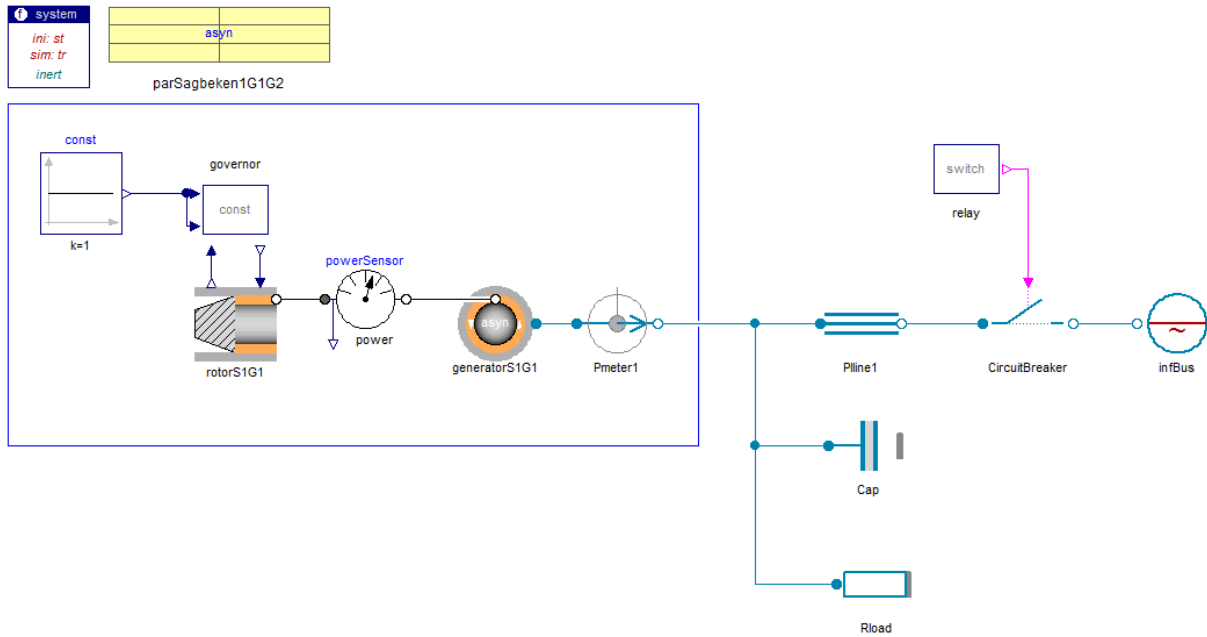

Figure 4-5: Model used for investigation of the self-excitation process

4.3.1 Self-excited induction generator without capacitors

First, the power plant was investigated without any capacitance or load connected at the generator terminals. This represents a situation where the GCB suddenly disconnects the machine from the grid.

Figure 4-6 shows the behavior of the generator after it is disconnected from the voltage source. Before disconnection it can be observed that the generator operates in steady state where it produces 98.4 kW with active power, and consumes 67.1 kVAr with reactive power. Further, it can be noticed that the amount active power produced by the generator is slightly less than the mechanical power at the rotor, due to losses in the generator.

Once the circuit breaker is opened, it can be seen that the voltage decreases rapidly and becomes zero. The reason for this is that the current stops flowing in the stator windings and the generator starts to de-excite. This is not surprising since the induction machine needs supply of lagging reactive power to produce the main air-gap and winding leakage flux.

As the turbine provides the rotor with constant mechanical power, P_m, and the electrical power, P_e, suddenly becomes zero, there is no longer balance in power and torque. The difference in power will then go to accelerate the rotor [9]:

$$P_a = P_m - P_e \qquad (4\text{-}2)$$

By knowing that the active power is the product of the torque, T, and the angular velocity of the rotor, ω_r, the change in acceleration of the rotor can be determined as:

$$\frac{d\omega_r}{dt} = \frac{T_m - T_e}{J} \qquad (4\text{-}3)$$

Where J is the inertia of the turbine and rotor, T_m is the mechanical torque, and T_e is the electromagnetic torque in the air-gap of the generator.

It is important to remember that the model used for the turbine and rotor is a simplified model with constant power output and a given inertia. The efficiency curve of a turbine is therefore not taken into account, and the run-away speed of the turbine is infinite.
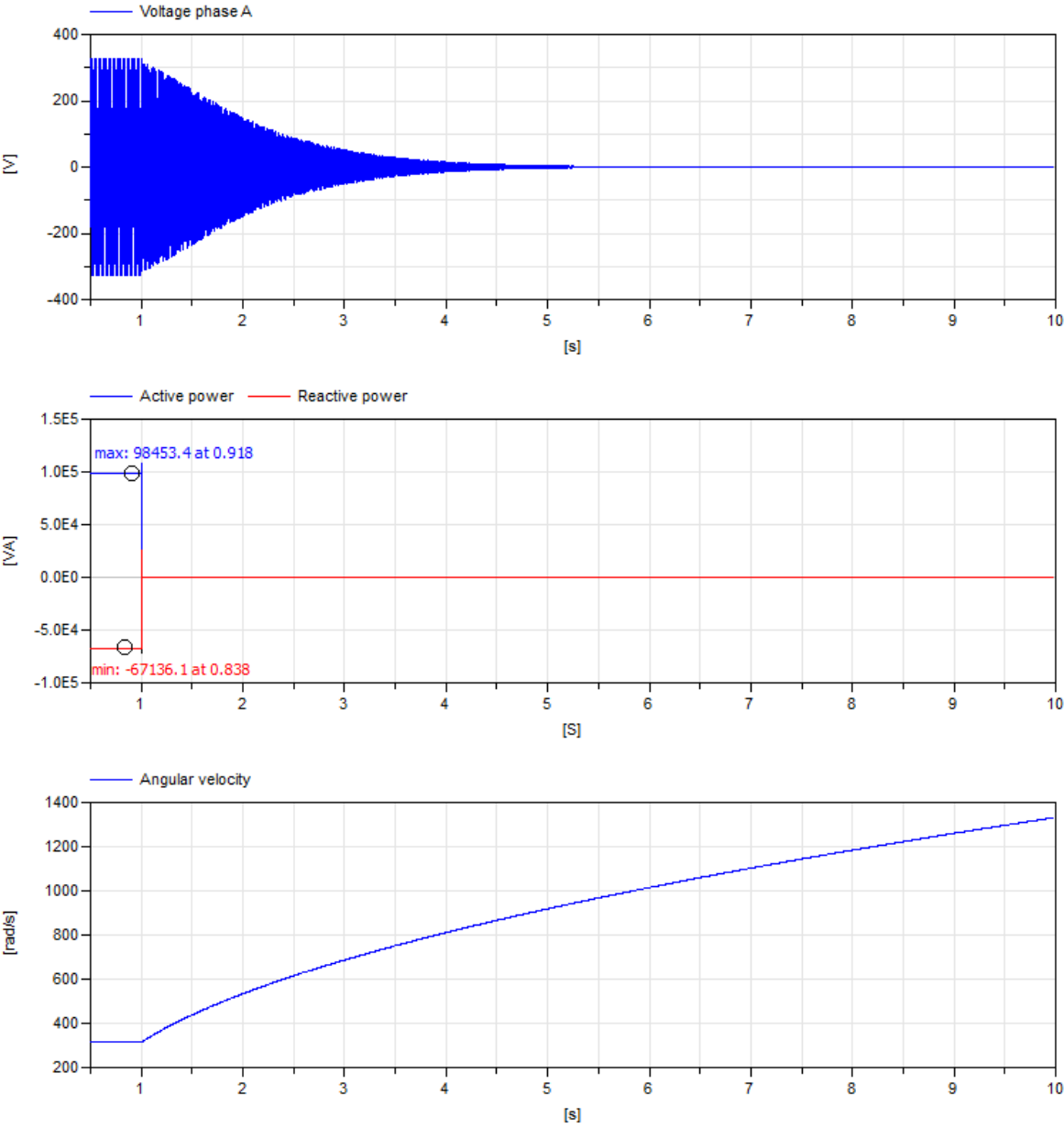
Figure 4-6: SEIG with no capacitor, disconnection at t = 1s

4.3.2 Self-excited induction generator with capacitors

In order to investigate capacitors impact on the unloaded induction generator, the system was simulated with different capacitors connected in shunt with the generator.

Figure 4-7 shows the different generator voltages obtained, and Figure 4-8 shows the electric angular velocity, ω_{el}, reactive power, Q, and electromagnetic torque, T, of the generator.

The first simulation with 2 kVAr of reactive power in shunt with the generator shows that the capacitor does not provide sufficient excitation to initiate the self-excitation process at any speed. It can be seen that the terminal voltage approaches zero as the machine de-excite.

By increasing the capacitive power to 10 kVAr, a successful voltage build-up takes place. The minimum amount of capacitive power needed for self-excitation is therefore between 2 kVAr and 10 kVAr for this system.

From Figure 4-7 it can be observed that a further increase of the capacitive power results in shorter time from the disconnection to the voltage build-up, but a reduced peak voltage.
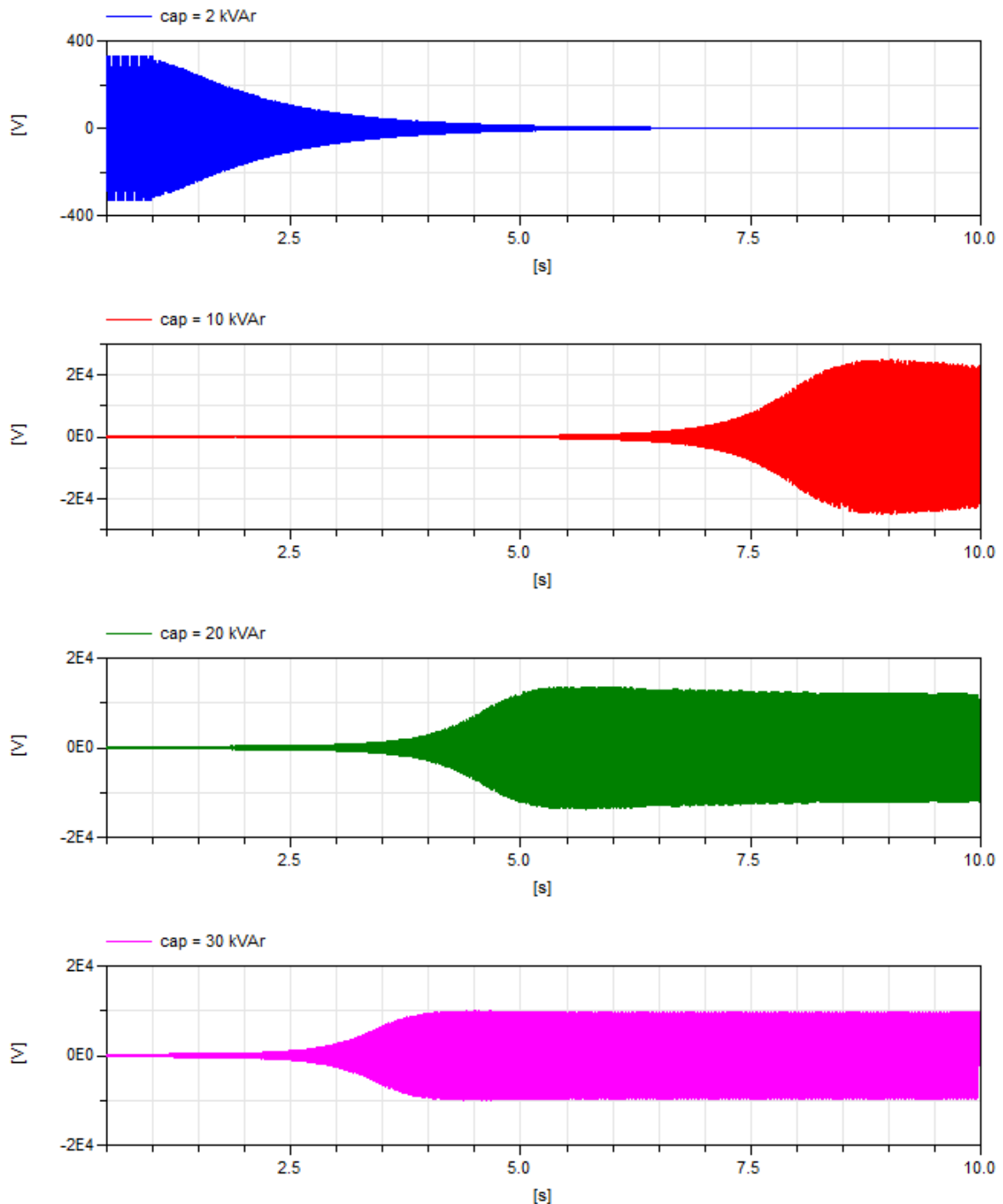
Figure 4-7: SEIG voltage with different capacitors, disconnection at t = 1s

From Figure 4-8 it can be observed how the electric angular velocity, ω_{el}, changes due to the imbalance in power that occur when the circuit breaker is opened.

Further, it can be observed that a higher capacitive power connected to the generator terminals leads to lower angular velocity of the new stable operating point. The voltage build-up does also initiate at a lower angular velocity. This is because a larger capacitor provides the minimum reactive power required for self-excitation at a lower angular velocity than a smaller

one. The reactive power of an capacitor, Q_c, is determined by the voltage, the electric angular velocity, ω_{el}, and the capacitance, C, as shown if Equation 4-3.

$$Q_c = \frac{U^2}{(\omega_{el} * C)^{-1}} \qquad \text{(4-4)}$$

Furthermore, the point where the angular velocity reaches its peak value is the time instant where the electromagnetic torque equals the mechanical torque. From this point, the angular velocity decreases until it reaches its new stable operating point where the balance is obtained again. By looking at the reactive power and voltage, it can be observed that the voltage reaches its peak value when the reactive power is at its greatest.
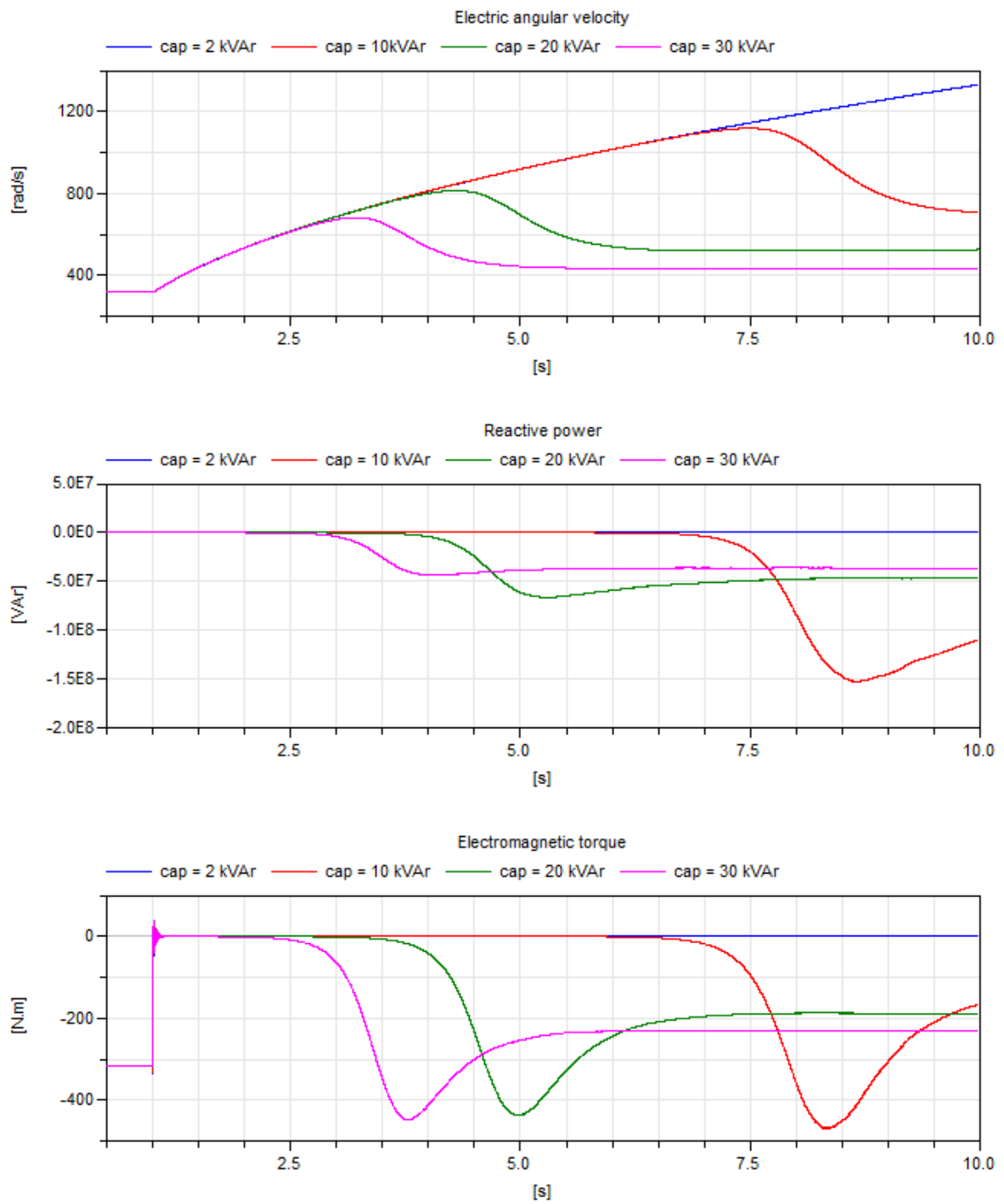
Figure 4-8: SEIG with different capacitors angular velocity, reactive power and electromagnetic torque, disconnection at t = 1s

4.3.3 Self-excited induction generator with capacitors and load

The sensitivity analysis was only performed with a resistive load in the system. Inductive loads in parallel with the capacitors will only reduce the resulting effective load impedance, Z_{eff}, [23]:

$$Z_{eff} = R - j(\frac{1}{\omega_{el}C} - \omega_{el}L) \qquad\qquad (4\text{-}5)$$

Inductive loads will increase the slope of the linear capacitive reactance line, and can more easily be modeled with a smaller capacitor bank.

For all the different loading scenarios, a 30 kVAr capacitor bank was connected in shunt with the generator terminals.

Figure 4-9 shows how the terminal voltage changes when different amounts of resistive loads are connected to the system. From the figure it can be observed that the amount of resistive load connected to the generator has a considerable influence on the new operating point. By comparing the 10 kW simulation in Figure 4-9 with the similar no-load simulation in Figure 4-7, it can be observed that the 10 kW load reduces the maximum overvoltage from 10 kV to 1.4 kV.

For the simulation with 90 kW load, a small decrease in voltage can be observed after the disconnection. This indicates that the load is too large for self-excitation to initiate, and the machine starts to de-excite [10]. At t=2.5 seconds, it can be seen that the angular velocity is high enough to initiate the process of self-excitation, the voltage builds-up again, and the machine starts to demand reactive power, as seen in Figure 4-10.

From Figure 4-10 it can be noticed that an increase of loading results in smaller oscillations in the angular velocity before the new steady state operation point is reached. The reason for this is that an increased loading gives smaller imbalance in power and torque when the circuit breaker is opened.
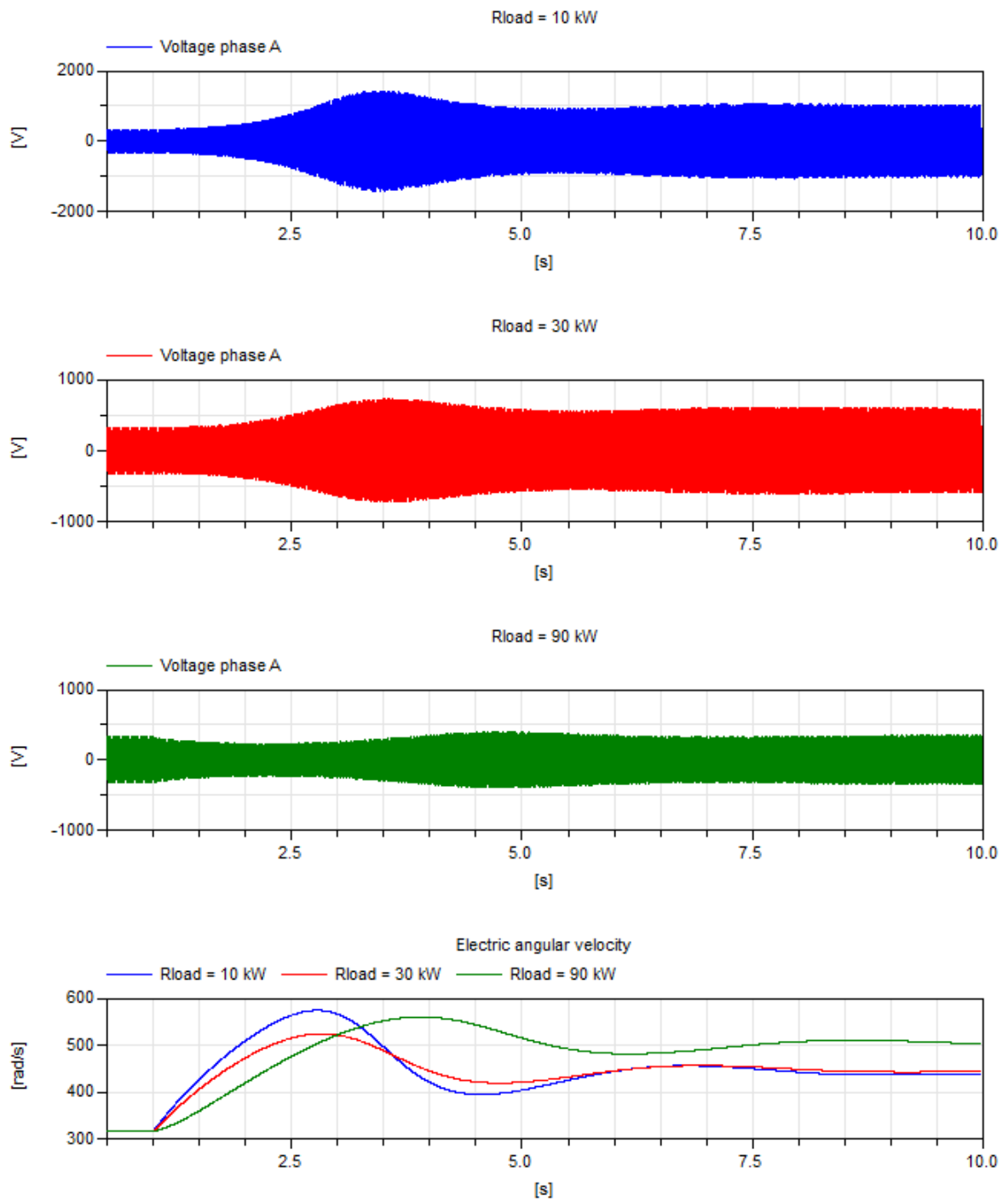
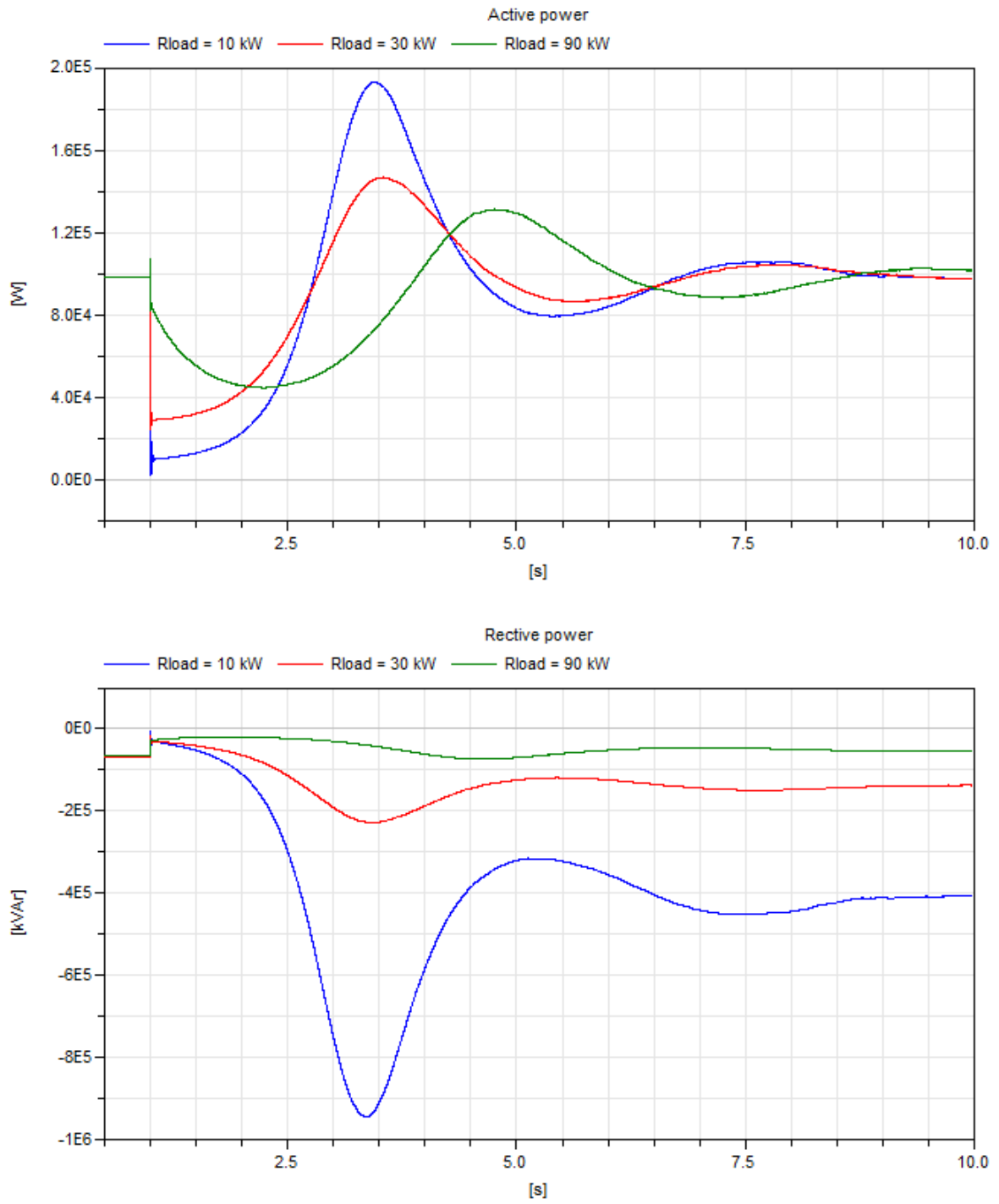*Figure 4-9: SEIG with 30 kVAr capacitors and different loads, disconnection at t = 1s*

Figure 4-10: SEIG with 30 kVAr capacitors, and different loads, active and reactive power, disconnection at t = 1s

4.4 Islanded grid simulations without Grunnåi

For investigation of the scenario where the Lønnestad radial goes into islanded grid operation without Grunnåi power plant connected, the simulation model presented in Figure 4-11 was created.
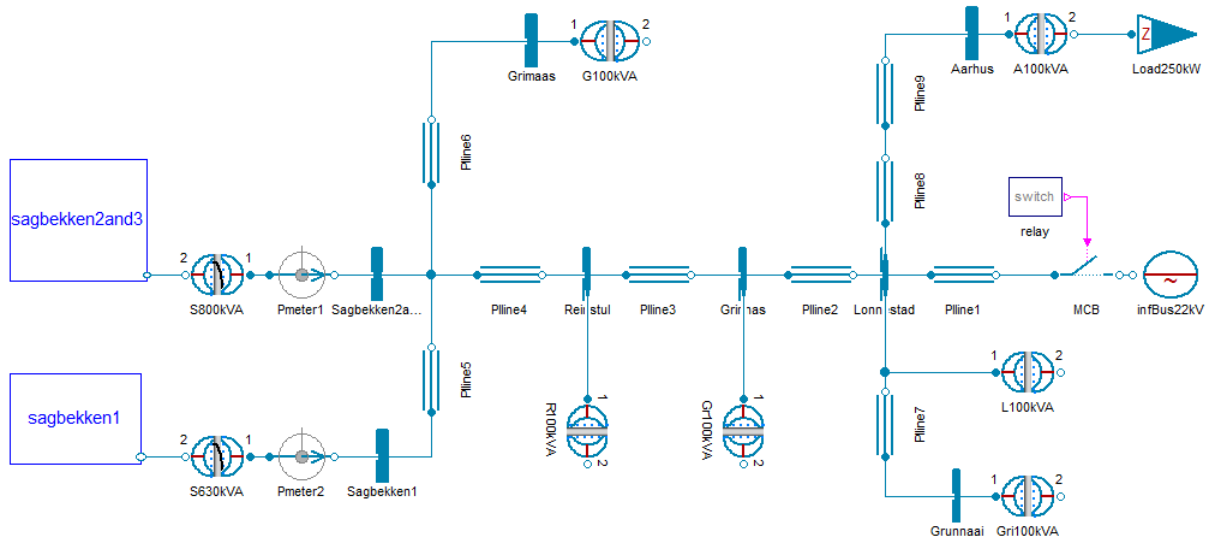

Figure 4-11: Block diagram of the Lønnestad radial without Grunnåi

For the simulation model were cables and transformers modeled with the parameters presented in 3.1 and 3.3, while the submodels presented in 4.2 were used for the power plants.

All the transformers (except Sagbekken 1, and Sagbekken 2 and 3), were modeled with non-ideal transformer models without saturation. For Sagbekken 1, and Sagbekken 2 and 3 were the simulations carried out with non-ideal transformers with and without saturation models.

4.4.1 Transformers without saturation model and no load

The grid was first simulated without load connected, and non-ideal transformers without a saturation model. In reality, there is unlikely that a situation without any load will occur, but the scenario simulates the system dynamics when only transmission and transformer losses are taken into account. The results from the simulation are presented in Figure 4-12, Figure 4-13 and Figure 4-14.

By looking at the plots for Sagbekken 1 and Sagbekken 2 and 3, it can be observed that the self-excitation is initiated immediately after the radial is brought into islanded operation. This indicates that the equivalent capacitance from the cables are higher than minimum capacitance, C_{min}, required to self-excite the 7 generators at nominal speed and no load.

The generator voltage rises quickly, and 0.7 seconds after the self-excitation is initiated, the terminal voltage seems to reach its peak of 2.59 kV. At this point Figure 4-14 shows that the protection relay in Sagbekken 1 trigger and disconnects the power plant from the island.
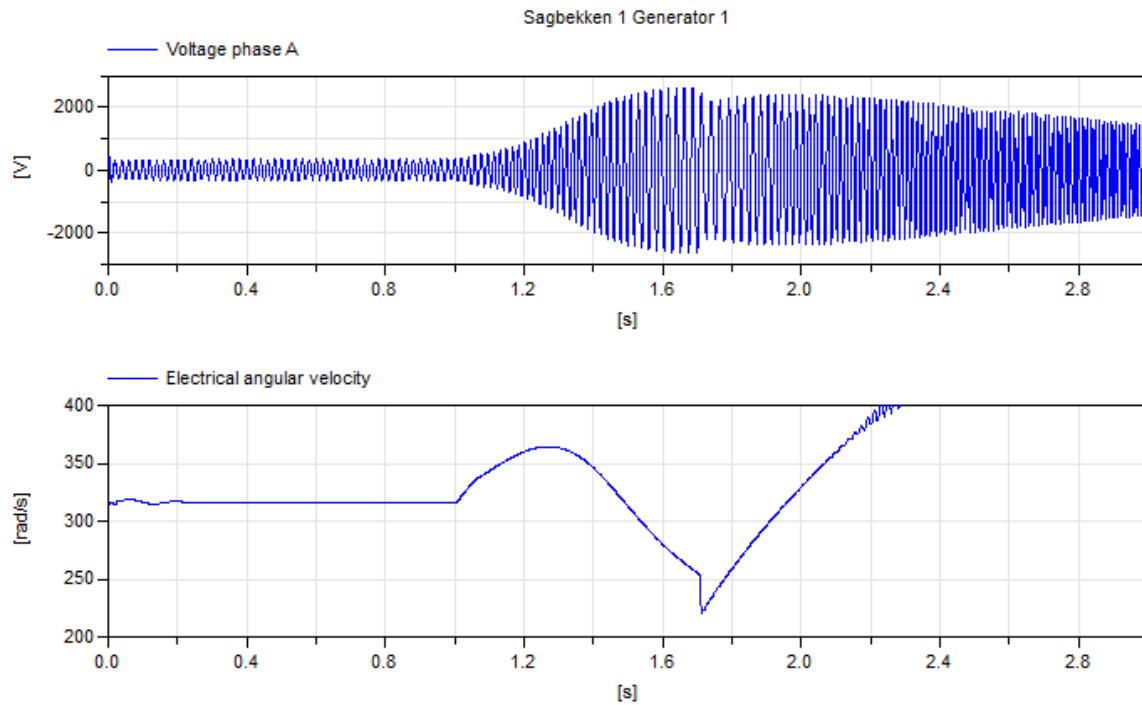
Figure 4-12: Sagbekken 1, transformers without saturation model and no load, disconnection at t = 1s

Figure 4-13 shows that the generator voltage of Sagbekken 2 and 3 decreases to below 2 kV when the contribution from Sagbekken 1 disappears. At t=2.5s the protection relay of Sagbekken 2 and 3 trigger, and overvoltage phenomena in the radial comes to halt.

The voltage at the 22 kV busbar in Grunnåi can be seen in Figure 4-14. Not surprisingly, it can be observed that the voltage build-up in the generator terminals results in significant overvoltages in the entire radial. At Grunnåi busbar the overvoltage reached its maximum value at 144 kV. The overvoltage phenomenon was terminated when both the power plants were disconnected, 2.5 seconds after the grid was brought into islanded grid operations.
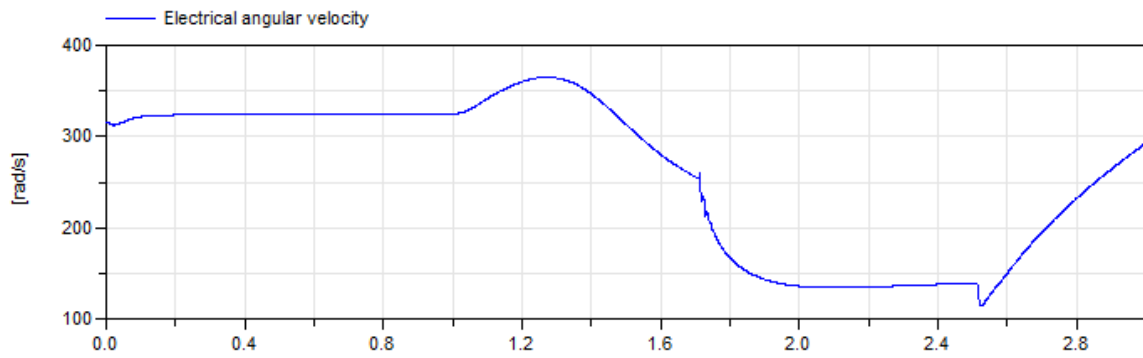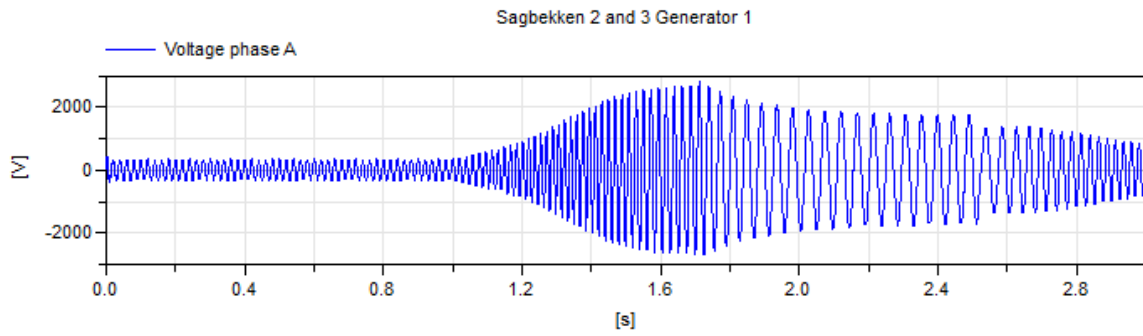
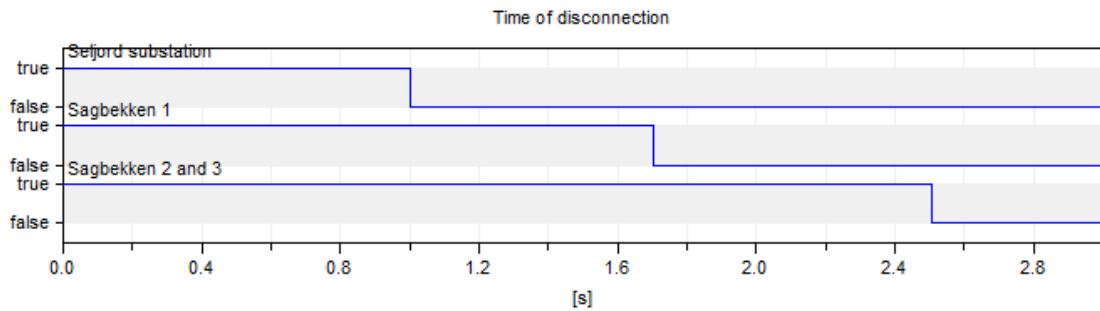*Figure 4-13 - Sagbekken 2 and 3, transformers without saturation model and no load, disconnection at t = 1s*

Figure 4-14: Grunnåi busbar, transformers without saturation model and no load, disconnection at t = 1s

4.4.2   Transformers with saturation model and no load

In order to take the saturation in the transformers into account, the simulation model in Chapter 4.4.1 was upgraded with non-ideal transformers with saturation model for the Sagbekken 1 and Sagbekken 2 and 3 transformers.

The non-ideal transformer model, TrafoSat, from the Electric Power Library was used with the transformer parameters presented in

Table 3-13.

By comparing Figure 4-15 with Figure 4-14, it can be seen that transformer model with saturation gives seemingly the same results as the non-ideal model without saturation.
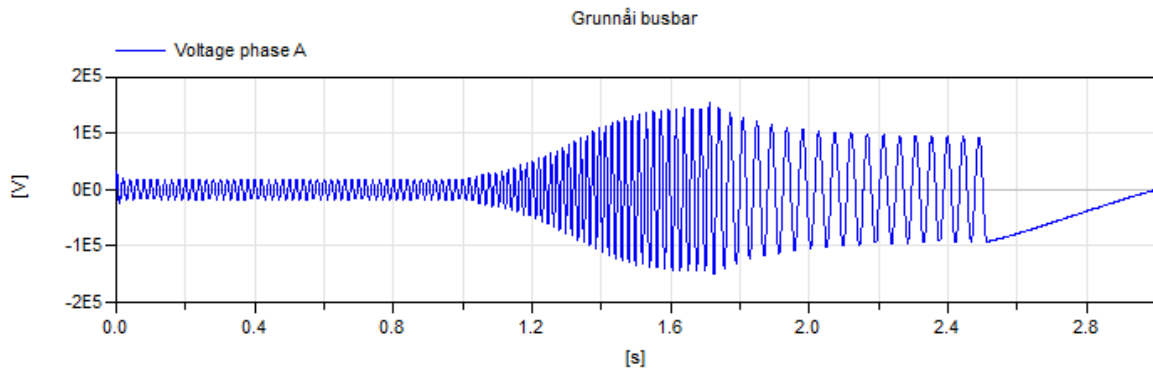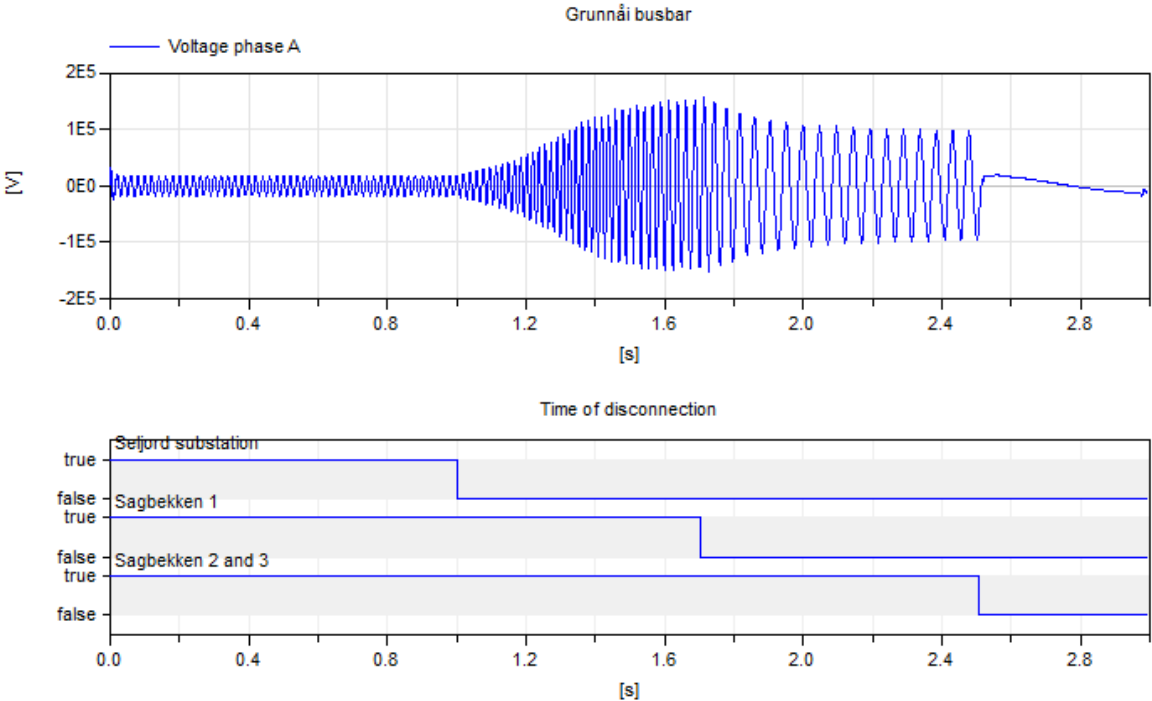

Figure 4-15: Grunnåi busbar, transformers with saturation model and no load, disconnection at t = 1s

4.4.3 Transformers with saturation model and load

In addition to the losses related to transformation and transmission, a 250 kW load with pf equal 0.96 was connected at the Aarhus busbar. The load was connected to represent the consumption from the industry at Aarhus, as mentioned in Chapter 3.4.

By comparing the results in Figure 4-16 and Figure 4-17 with the simulation performed without any load connected, it can be seen that the maximum peak voltage in Sagbekken 1 decreases from 2.59 kV to 0.86 kV by connecting the 250 kW load at Aarhus busbar.

Furthermore, it can be observed that even with the load connected to the grid, the generators seems to initiate the self-excitation immediately after the radial is brought into islanded grid operation.
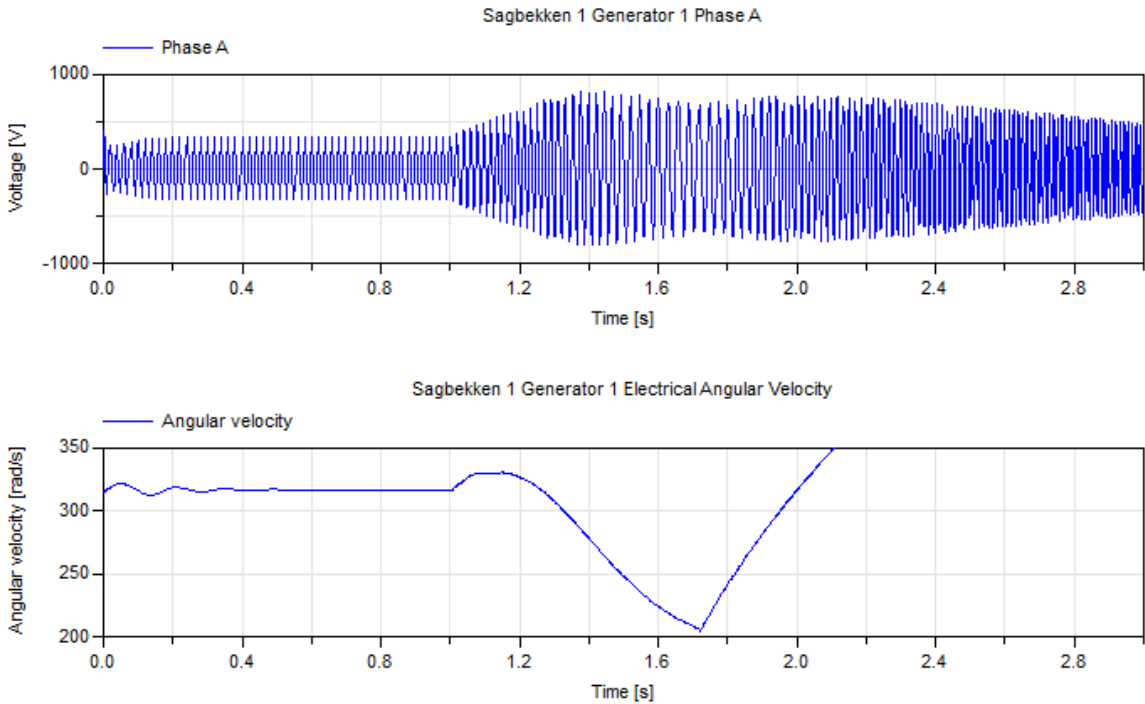

Figure 4-16: Sagbekken 1, transformers with saturation model and load, disconnection at t = 1s
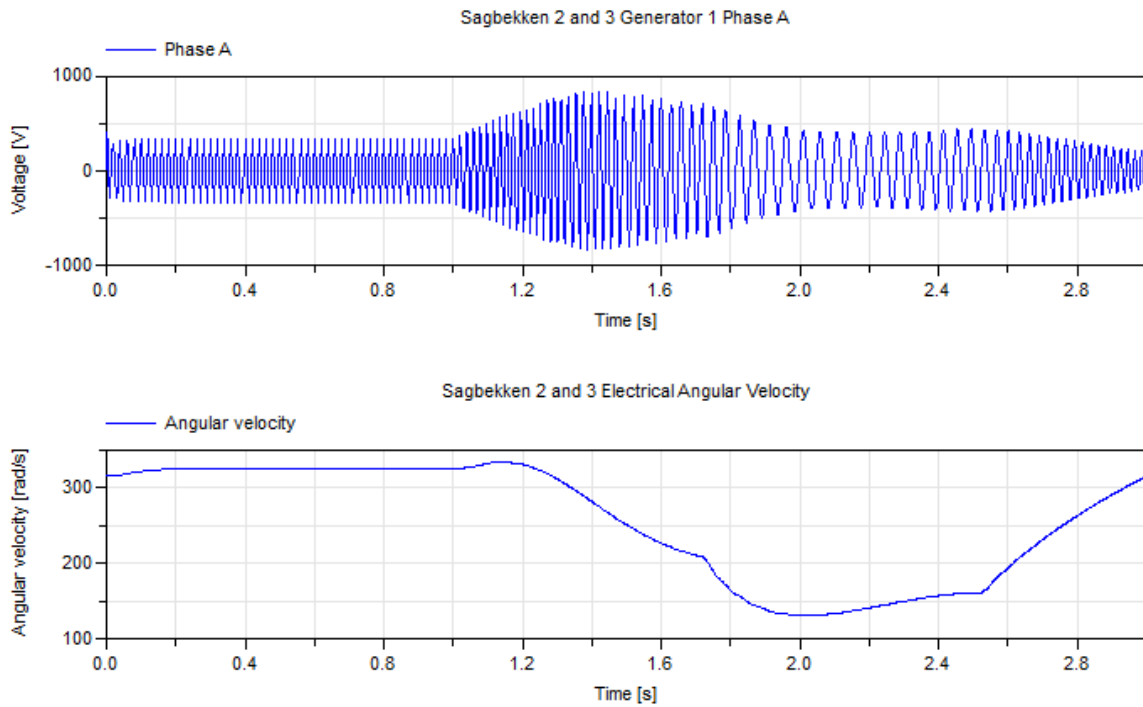
Figure 4-17: Sagbekken 2 and 3, transformers with saturation model and load, disconnection at t = 1s

By looking at Figure 4-18, it can be observed that the overvoltage phenomenon in the radial comes to halt 1.5 seconds after the self-excitation is initiated. At this time the protection relays in both the power plants have triggered and disconnected the generators from the grid. From Figure 4-18 it is shown that the overvoltage at Grunnåi busbar reached its maximum value of 49.6 kV, which is a considerably much lower voltage than the voltage obtained without load connected.
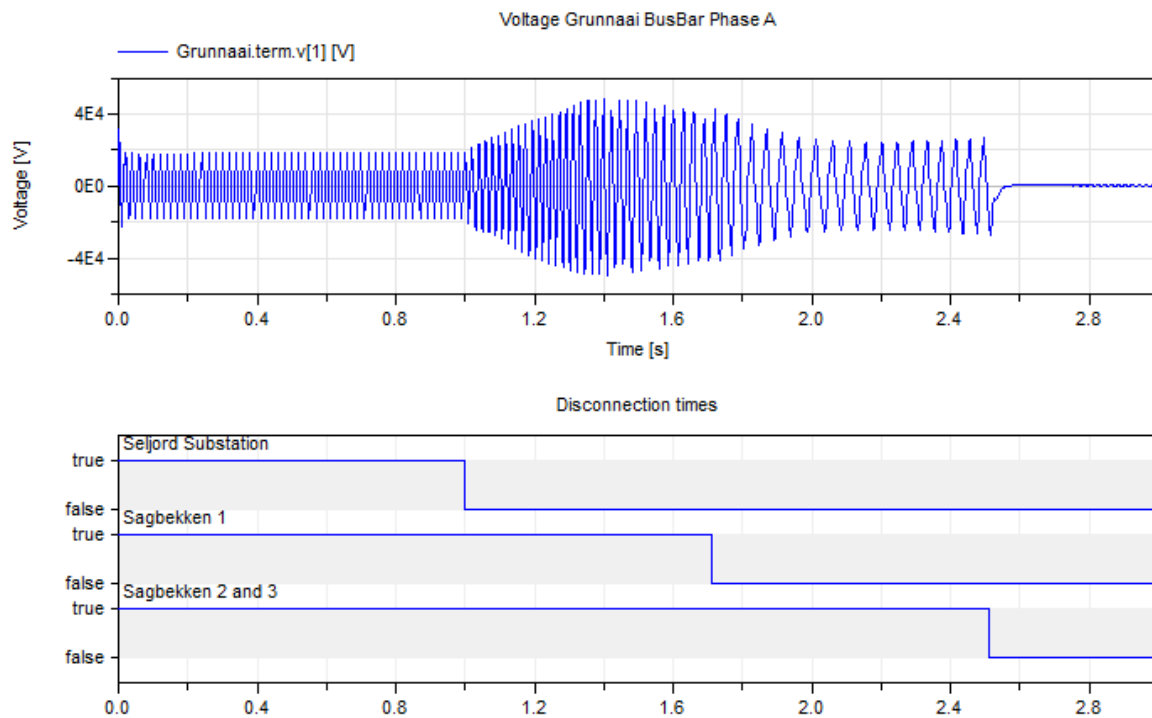
Figure 4-18: Grunnåi busbar, transformers with saturation model and load, disconnection at
t = 1s

4.5 Islanded grid simulations with Grunnåi

To simulate a scenario when the radial is brought into islanded grid operation with both the Sagbekken plants and the Grunnåi plant connected, the submodel for Grunnåi power plant presented in Chapter 4.2.1 was added to the simulation model used in Chapter 0. The power plant was connected to the grid through an ideal transformer. This simplification was made since the droop configuration of the plant will cause disconnection on overfrequency shortly after the radial is disconnected from Seljord substation.

Figure 4-19 shows the block diagram of the radial with Grunnåi power plant and load connected at Århus busbar.
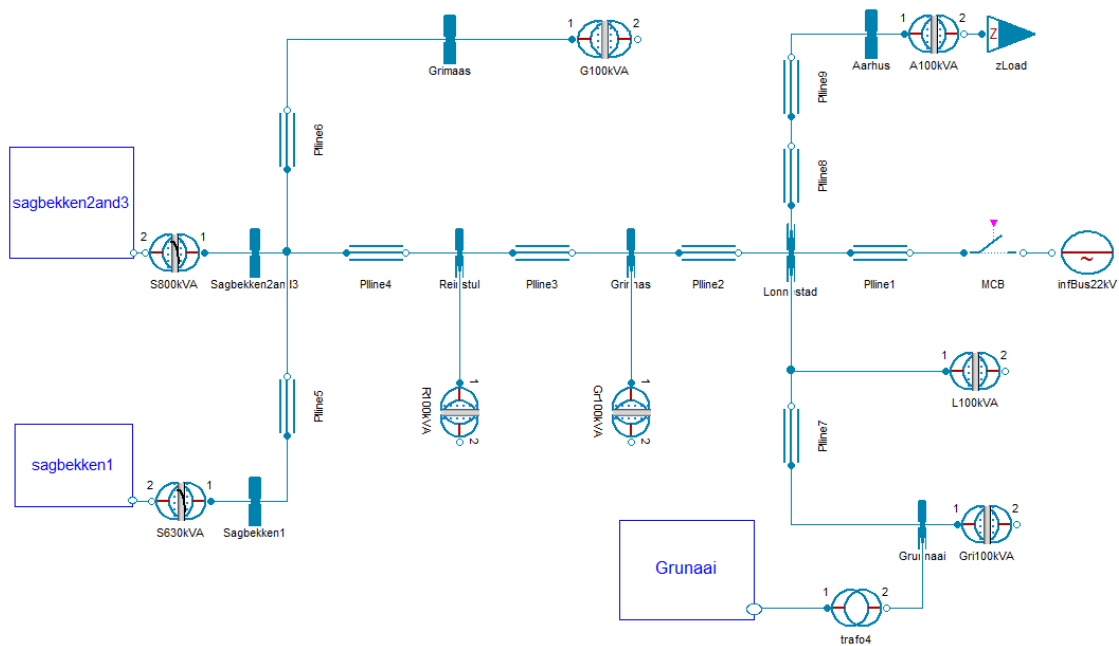
Figure 4-19: Block diagram of the Lønnestad radial with Grunnåi

The generator voltage for the three different power plants in the radial can be seen in Figure 4-20, Figure 4-21, and Figure 4-22. By looking at Figure 4-22 it can be observed that Grunnåi power plant starts to accelerate due to the imbalance in power that occur when the grid is brought into islanded operation.

Since Grunnåi is the largest power plant in the island and has a synchronous generator, it provides the grid with reactive power. This means that the Sagbekken power plants are provided with reactive power until Grunnåi is disconnected from the island at t=1.2 seconds. Figure 4-21 shows that self-excitation is initiated in the Sagbekken plants immediately after the disconnection.
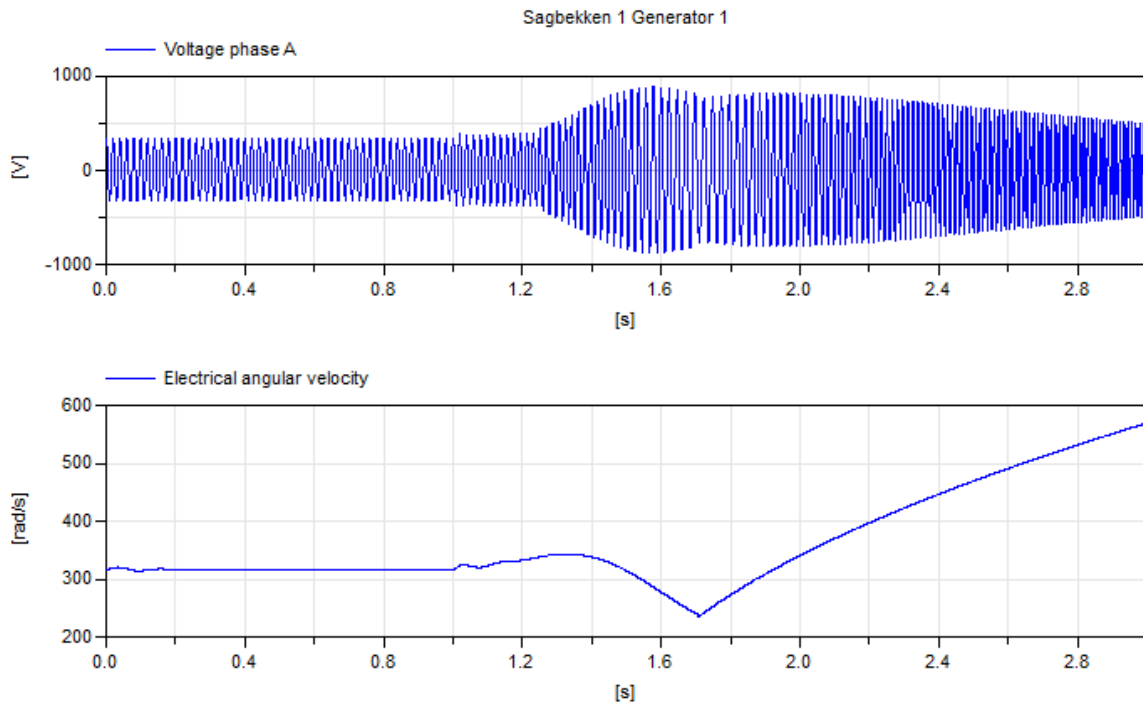
Figure 4-20: Sagbekken 1, voltage and angular velocity, Disconnection at t = 1s
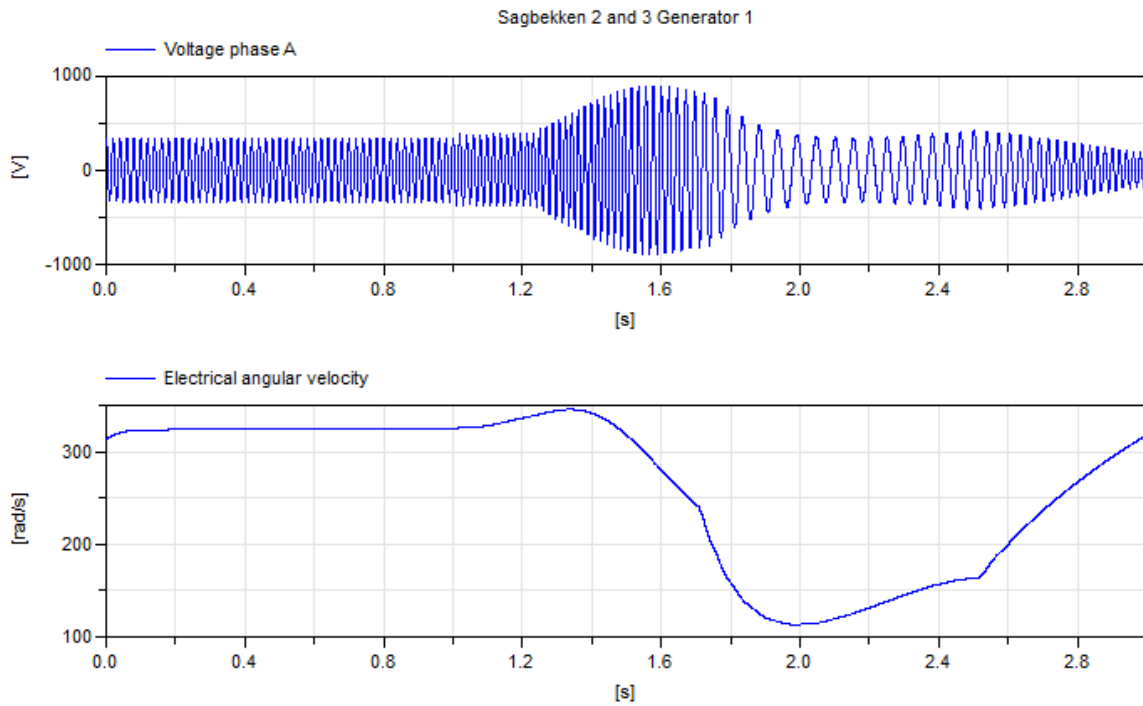
Figure 4-21: Sagbekken 2 and 3, voltage and angular velocity, disconnection at t = 1s
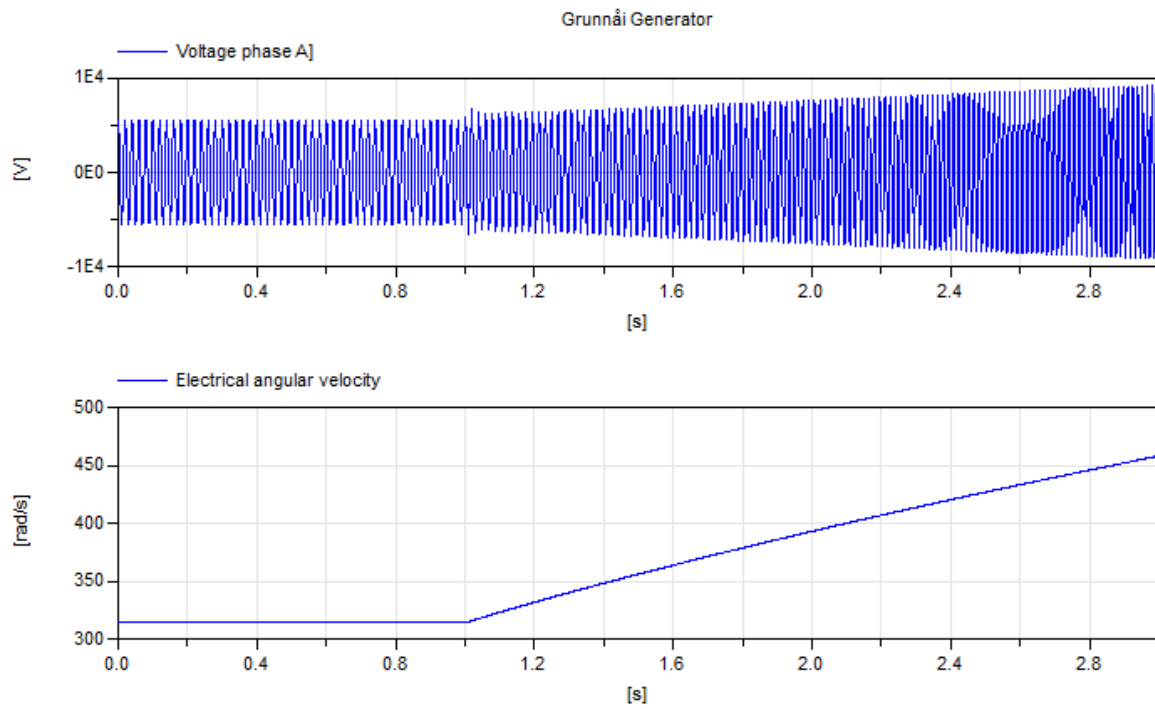
Figure 4-22: Grunnåi, voltage and angular velocity, disconnection at t = 1s

Figure 4-23 shows the overvoltage that occurs at Grunnåi busbar. The overvoltage reaches its peak value of 51.49 kV at t=1.6 seconds, which is 0.4 seconds after the self-excitation was initiated. Also here, the phenomenon of self-excitation comes to halt when the last generator is disconnected.
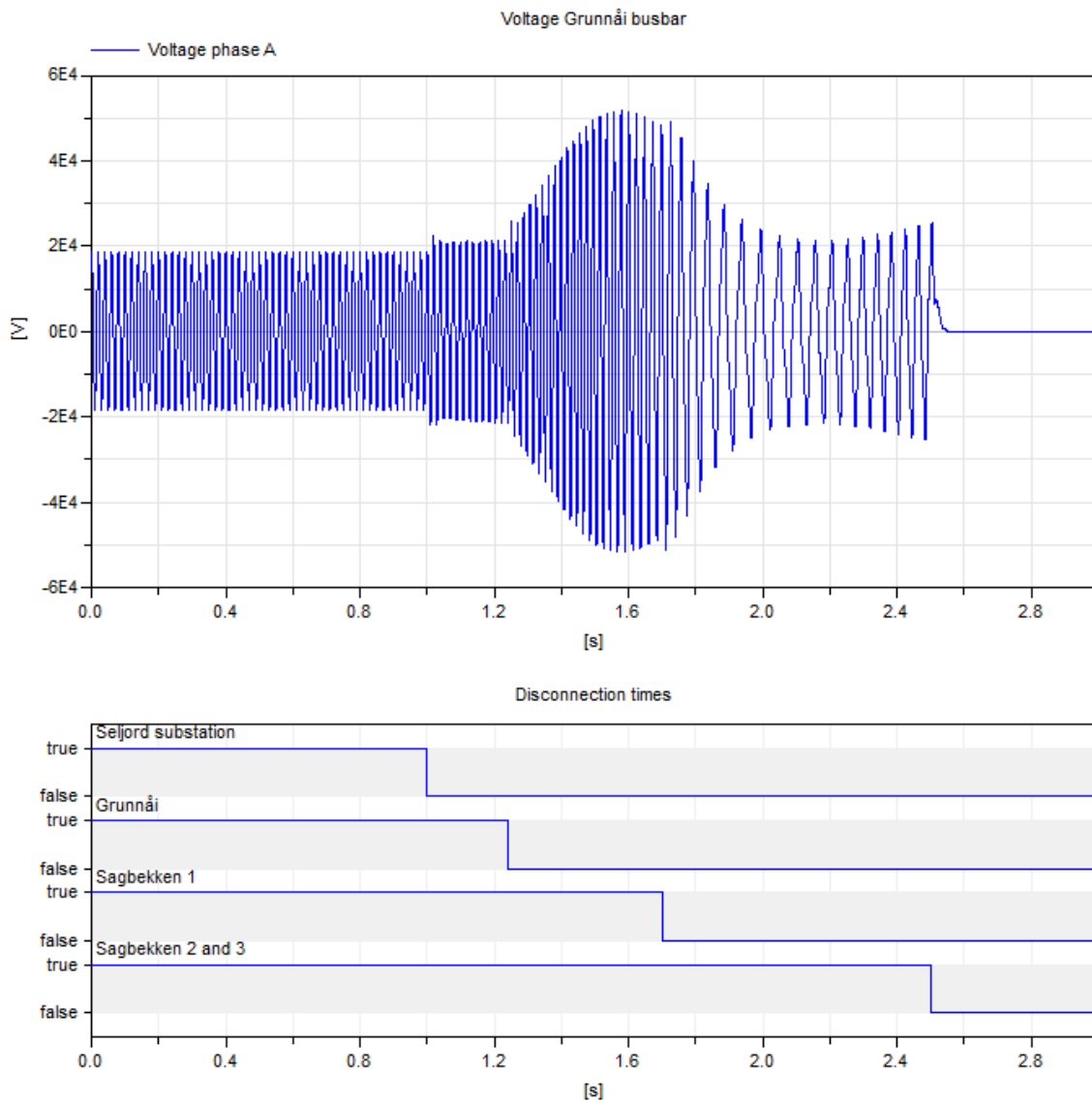
Figure 4-23: Voltage Grunnåi busbar and disconnection times

4.6 Full simulation with phase to ground fault Grunnåi

In order to investigate the overvoltage that occurred at the 22 kV busbar in Grunnåi the 27th July 2011, a scenario with a phase to ground fault at Grunnåi busbar was created. At t=1 second a phase to ground fault occur at phase A. Simultaneously as the phase to ground fault occur, the circuit breaker in Seljord substation disconnects the Lønnestad radial from the rest of the grid, due to momentary triggering settings in the protection relay.

The block diagram for the radial with phase to ground fault is presented in Figure 4-24.
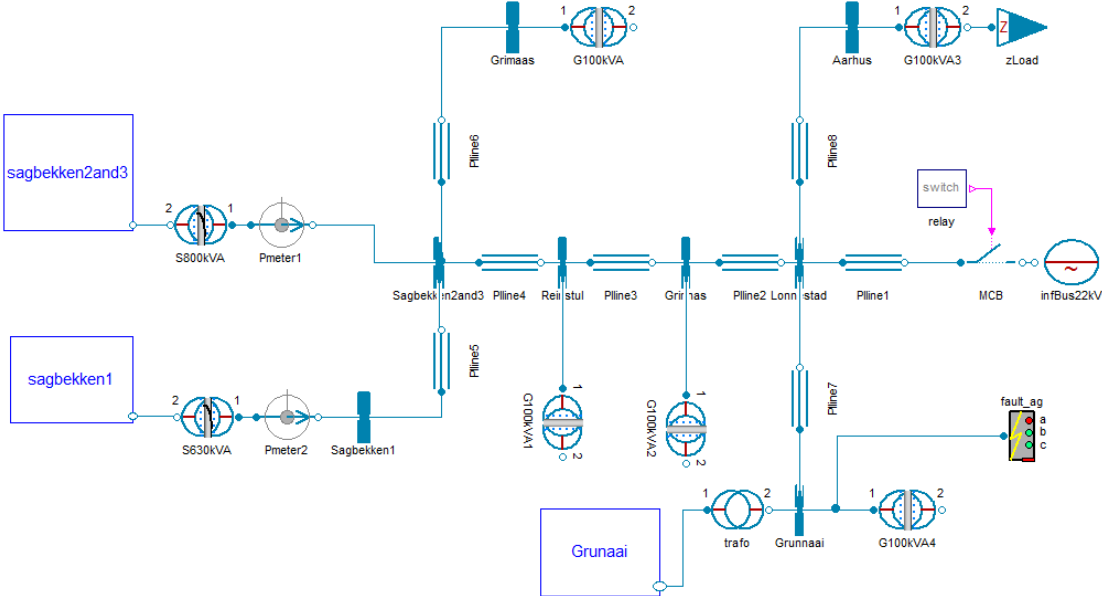
Figure 4-24: Block diagram of the Lønnestad radial with phase to ground fault

Figure 4-25 shows the phase voltages at Grunnåi busbar. From the figure it can be seen how the voltages changes when the phase to ground fault occur at phase A, causing the system to go from a balanced system to an unbalanced system. The phase voltages changes due to the phase imbalance, and the voltage of phase A becomes zero.

By looking at Figure 4-26, it can be observed that it takes 0.3 seconds before the protection relay in Grunnåi disconnects the power plant from the island. Immediately after Grunnåi is disconnected at simulation time equal 1.3 seconds, the induction generators in the Sagbekken plants starts to initiate the self-excitation.
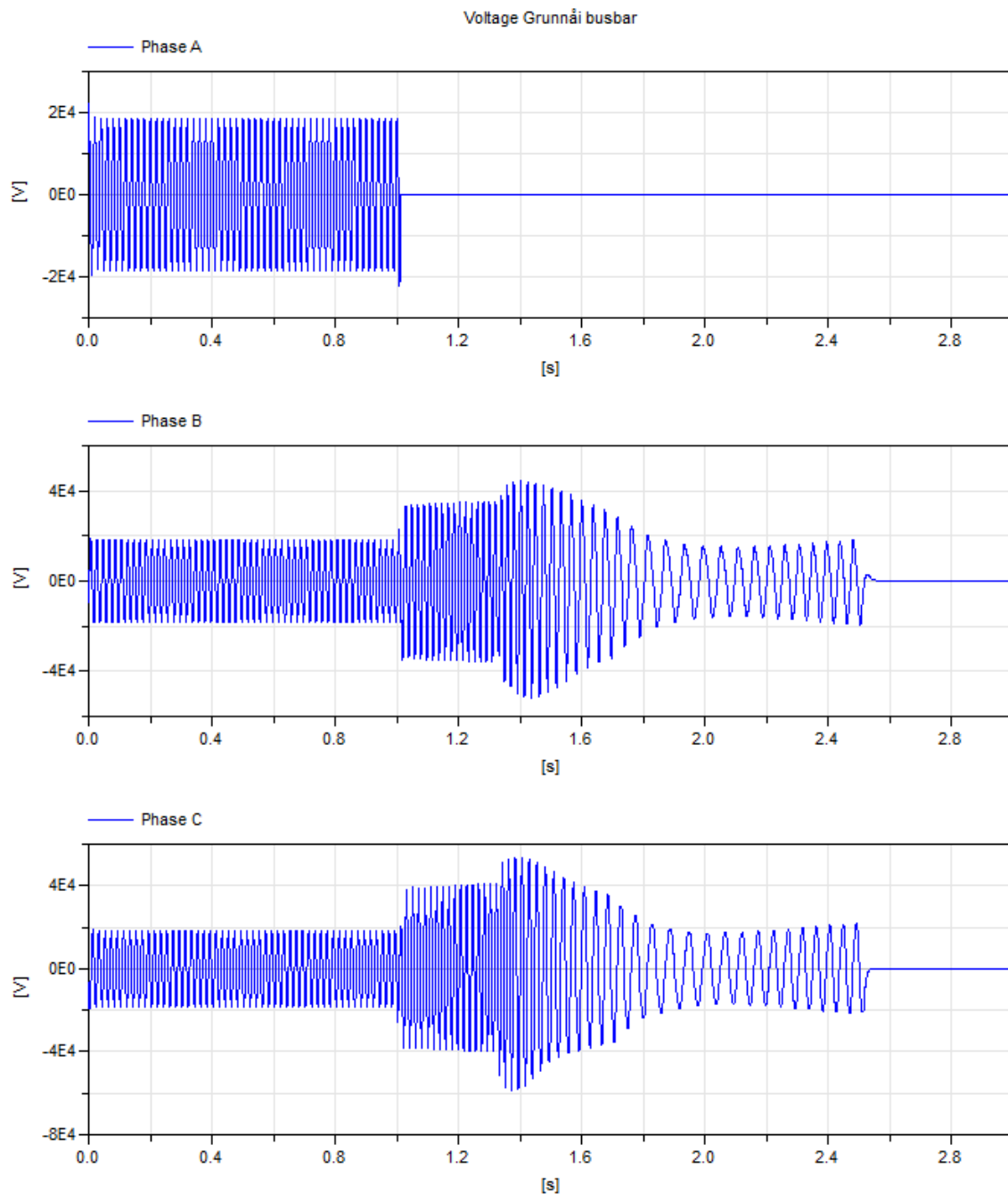
Figure 4-25: Voltage at Grunnåi busbar, phase to ground fault at T = 1s

From Figure 4-25 it can be observed that the process of self-excitation comes to halt at t=2.5 seconds. At this time, Figure 4-26 shows that the last running power plant in the island, Sagbekken 2 and 3 is disconnected from the radial.

During the process of self-excitation, the overvoltage at Grunnåi busbar at reaches its maximum value of 53.36 kV.

Figure 4-25 shows that it took 1.5 seconds from the phase to ground fault occurred at the 22 kV busbars in Grunnåi to all the generators in the radial were disconnected. During this time

the overvoltage was continuously over 30 kV for 0.7 second, and over 40 kV for 0.2 seconds at phase C.
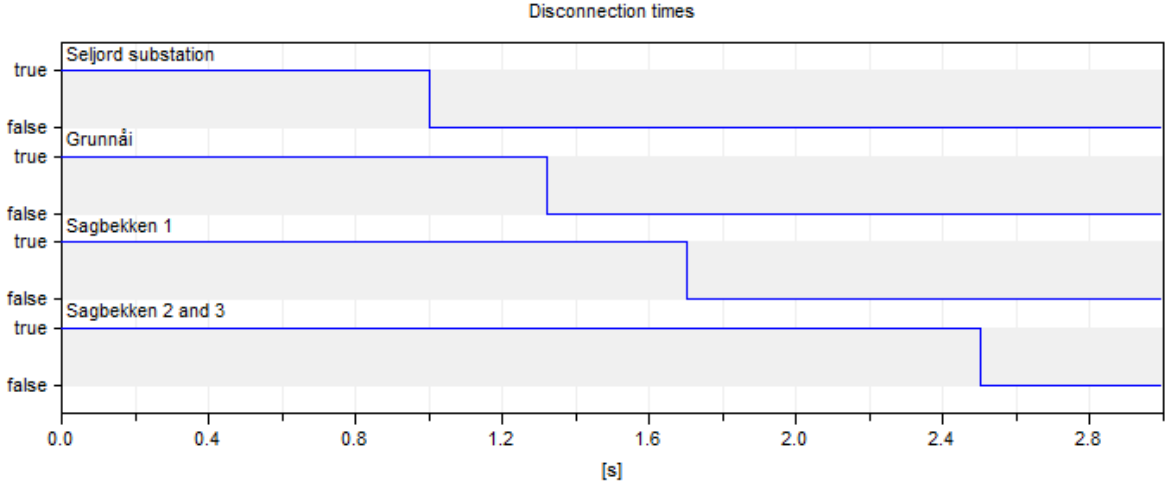
Figure 4-26: Disconnection times, phase to ground fault at T = 1s

5 Discussion

The investigation of the self-excitation process in Chapter 4.3 shows how the dynamics of the generator changes when different capacitors and loads are connected to the generator terminals. For a generator running at no load with capacitors connected to the terminals, there exists a minimum speed for self-excitation to occur. If the capacitors do not provide sufficient excitation to initiate the self-excitation at the given speed, the loss of the utility grid causes a sudden increase in the slope of the equivalent capacitor line seen by the generator [11]. This change may cause a complete or partial loss of the generator excitation. Due to this, the generator fails to produce an electromagnetic torque large enough to overcome the mechanical torque, which results in acceleration of the rotor.

Unless the residual flux is lost, the self-excitation can be initiated when the angular velocity has increased such that the reactive power from the capacitors is sufficient. Once the process of self-excitation is initiated, the terminal voltage starts to build up. The generator reaches its new stable operating point when the dynamic magnetization line of the generator intersects the linear capacitor line.

It was observed that larger capacitors connected to the generator terminals resulted in successive voltage build-up at a lower angular velocity. Larger capacitors do also result in a reduced peak voltage and a lower angular velocity of the new stable operating point. The reason for this is that larger capacitors provide the required reactive power at a lower angular velocity than a smaller one.

For asynchronous generators connected to a utility grid with much reactive power in form of capacitors or cables, it is crucial with quick detection and low trigger time for overfrequencies to avoid unwanted overvoltages.

The amount of load connected to the grid has major influence on the self-excitation. The investigation shows that connection of a rather small load results in a significant reduction of the peak voltage. Connection of load results in smaller imbalance in electric and mechanical torque after disconnection. The balance is therefore obtained at a lower angular velocity, causing a larger magnetization reactance and reduced flux, which implies reduced voltage [24].

From the simulations of the Lønnestad radial it can be seen that reactive power from the cables are large enough to initiate self-excitation at nominal frequency.

The simulations without load connected to the radial, without Grunnåi power plant connected, shows how the voltage build-up takes place in a situation when Grunnåi power plant is not running. It was shown that the simulation with transformers with saturation gives seemingly the same results as simulations without saturation. Several parameters were tested, but the TrafoSat model in Electric Power Library seems to give the same output independent of the voltage.

The overvoltage in the distribution grid reached its maximum value of 144 kV for the unloaded simulation. When the 250 kW load was added to Århus busbar, the peak voltage in the distribution grid dropped to 49.6 kV.

In a situation where Grunnåi power plant is connected, the self-excitation in the Sagbekken plants is not initiated before Grunnåi power plant is disconnected. Since Grunnåi has an infinite droop, the electric angular velocity in the grid will rise as the active load in the island is smaller than the production. Once Gunnåi power plant is disconnected from the grid, the self-excitation is initiated in the Sagbekken plants.

The simulations shows that the reactive power in the grid is great enough initiate self-excitations that results in harmful overvoltages, independently of whether the load is connected or not. It is seen that the voltage build-up happens quickly. It takes below 0.4 seconds from the radial is brought into islanded operation to the voltage reaches its peak value.

Significant overvoltages can also occur when a phase to ground fault arise at Grunnåi busbar. Regardless of whether Grunnåi power plant is connected or a phase to ground fault arise, the self-excitation of the Sagbekken plants will result in harmful overvoltages. For all the simulations, the magnitude and length of the overvoltages are greater than the thermal stability limit of the surge arresters in Grunnåi power plant.

Correct parameters for the protection relays are essential for providing sufficient protection of the grid. This is also the easiest way to protect the Lønnestad radial against harmful overvoltages. Simulations show that the peak value of the angular velocity can vary dependent on the load scenario. Correct parameters for detection of overvoltages are therefore most important for the protection relays.

In addition to the protection relays, it is suggested to install a damping load in Seljord substation. The load can be installed in such a way that it is momentarily connected when the MCB disconnects the radial. This will prevent self-excitation from occurring if the impedance is small enough.

For the modeling and simulation of the power system, Dymola with the Electric Power Library has shown to be a great tool that allows straightforward modeling with block diagrams. The library contains advanced models with different levels of complexities, giving the user the opportunity to choose the desired level of complexity for his model.

One of the drawbacks with the library is that some of the models have a lack of documentation. It would have been convenient if the library contained a spectrum of generator and transformer parameters from known manufacturers. This makes modeling of power systems less time consuming since some design parameters seldom are known.

6 Conclusion

This thesis investigates the system dynamics in the Lønnestad radial when it is brought into islanded operation. Modeling and simulation of the transient behavior of an asynchronous generator is a fairly complex job that requires good knowledge of electric machinery and dynamic systems. Due to this, there is often a lack of knowledge in small utility companies when it comes to the asynchronous generator.

The asynchronous generator has the opportunity to operate as a standalone unit if the amount of reactive power in the cables or capacitors is sufficient. For the Lønnestad radial, it was proven that the amount of reactive power in the grid is large enough to initiate self-excitation of all the seven asynchronous generators in the radial.

The self-excitation leads to fast voltage build-ups that results in a harmful overvoltage in the distribution grid. For the simulations with load connected, it was observed that the overvoltage in the distribution grid reached its maximum voltage of circa 50 kV, only 0.4 seconds after the radial was brought into islanded operation.

This is a type of overvoltage that requires a great deal of knowledge regarding self-excitation to ensure good protection of the grid. Normal protection methods as surge arresters will not be adequate, since these are designed to protect against surge voltages, and not transient overvoltages with several seconds duration.

Simulations performed in this thesis shows that it is crucial with correct protection parameters in the Sagbekken plants to protect equipment in the Lønnestad radial against overvoltages caused by the generators. To avoid unwanted voltage build-ups, correct parameters for overvoltage detection is the most important protection. It is recommended to have momentarily disconnection when the voltage exceeds a given value.

If it is desirable to reduce the risk of self-excitation further, a damping load can be installed in Seljord substation.

References

[1] Skagerak Energi, "Fakta om Skagerak Energi," [Online]. Available: http://www.skagerakenergi.no. [Accessed 19 5 2013].

[2] C. Laughman, S. Leeb, L. Norford and P. Armstrong, "Mitsubishi Electric Research Laboratories," 5 2010. [Online]. Available: www.merl.com. [Accessed 28 2 2013].

[3] Y. Hase, Handbook of Power Systems Engineering, Chichester: Wiley, 2013.

[4] A. Fitzergald, C. Kingsley and S. Umans, Electric Machinety, Tokyo: McGraw-Hill, 1983.

[5] Connxions, "Magnetic Circuits and Magnetic Materials," [Online]. Available: http://cnx.org/content/m28345/latest/?collection=col10767/latest. [Accessed 19 3 2013].

[6] T. Wildi, Electrical Machines, Drives, and Power Systems, New Jersey: Pearson, 2006.

[7] N. Mohan, Electric Power Systems, A First Course, Hoboken: Wiley, 2012.

[8] ABB, Transformer Handbook, Geneva: ABB, 2007.

[9] P. Schavemaker and L. Van der Sluis, Electrical Power Systems Essentials, Chichester: Wiley, 2008.

[10] I. Boldea, Variable Speed Generators, Boca Raton: Taylor & Francis, 2006.

[11] L. Tang and R. Zavadil, "Shunt Capacitor Failures due to Windfarm Induction Generator Self-Excitation Phenomenon," *IEEE,* 1993.

[12] F. Sulla, "Island Operation with Induction Generators," Lund University, Lund, 2009.

[13] D. Seyoum, C. Grantham and F. Rahman, "Analysis of an isolated self-excited induction generator driven by a variable speed prime mover," The University of New South Wales.

[14] P. Kundur, Power System Stability and Control, Palo Alto: McGraw-Hill, 1993.

[15] J. Machowski, J. Bialek and J. Bumby, Power Systems Dynamics and Stability, Chichester: Wiley, 1997.

[16] J. Glover, M. Sarma and T. Overbye, Power System Analysis & Design, Stamford: Cengage, 2012.

[17] Draka Kabel, "TSLF 12/24 kV med yttre halvledende sjikt," [Online]. Available:

http://www.draka.no/draka/Countries/Draka_Norway/Languages/Norsk/Navigation/Pro
dukter/Teknisk_info/tslf.pdf. [Accessed 10 3 2013].

[18] ABB, "Overvoltage protection," 2011. [Online]. Available:
http://www05.abb.com/global/scot/scot245.nsf/veritydisplay/70e9fd6933c8c644c12578
d200333cb5/$file/952_abb_awr_mittelspannung_E_low.pdf. [Accessed 13 5 2013].

[19] Carlo Gavazzi, "HTML Datasheet," [Online]. Available:
http://www.htmldatasheet.com/carlo/dpc02dm48.htm. [Accessed 26 4 2013].

[20] Megacon, "Megacon KCG595," [Online]. Available:
http://www.megacon.com/default.aspx?pageId=96. [Accessed 4 26 2013].

[21] Modelica Association, "Modelica," [Online]. Available: www.modelica.org. [Accessed
21 4 2013].

[22] Modelon, "Modelon," [Online]. Available: www.modelon.com. [Accessed 21 4 2013].

[23] R. Carriveau, Fundemental and Advanced Topics in Wind Power, Rijeka: Intech, 2011.

[24] G. Ofualagba and E. Ubeku, "Intech," [Online]. Available:
www.intechopen.com/download/pdf/16251. [Accessed 28 2 2013].

[25] Møre Trafo, "Nye tekniske data for standard transformatorer 22000 - 415 V," [Online].
Available: http://www.moretrafo.no/uploads/080313-tekn_data_pors-22000-415v.pdf.
[Accessed 15 4 2013].

[26] Cogent, "Electrical Steel," [Online]. Available:
http://www.sura.se/Sura/hp_products.nsf/29a268683cdcefd4c12569ed004229a2/03a8b2
433fae16c4c1256aa8002280e6/$FILE/GO.pdf. [Accessed 2 4 2013].

Appendices

Appendix A, Components created in Dymola

Since some of the components needed for the modeling didn't exist in the Electric Power Library, they had to be created.

The different components are created with usage of blocks from the Modelica Standard Library.

Frequency protection relay:

Protection relay with two levels of over- and underfrequency, and triggering time. Using a value of the type Real as input, and returns an output of the type Boolean.
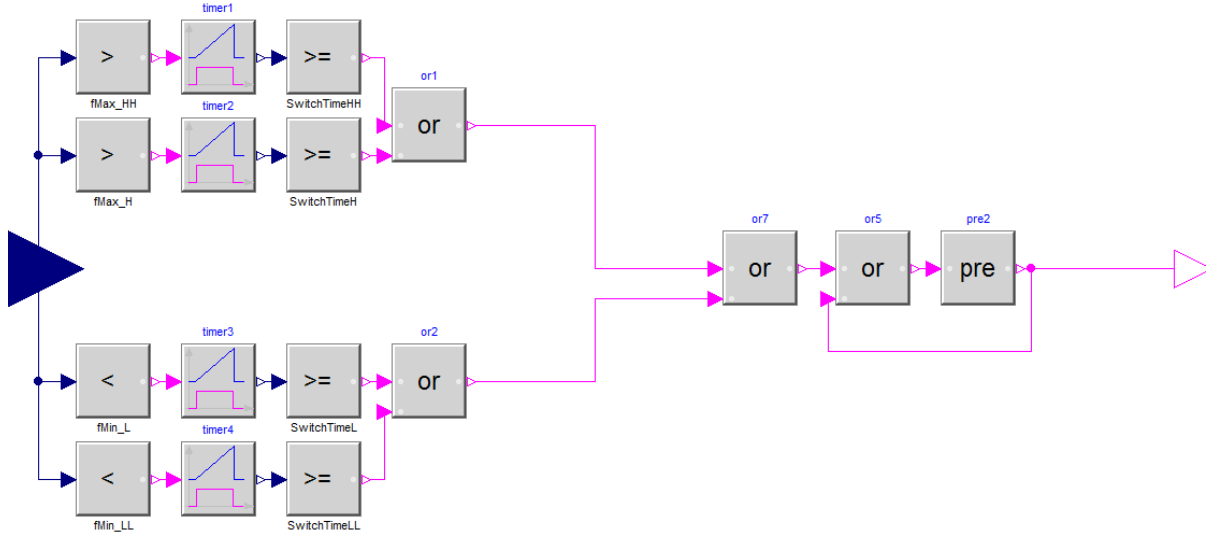
Voltage protection relay:

Protection relay with two levels of over- and undervoltage, and triggering time. Using a value of the type Real as input, and returns an output of the type Boolean. The protection relay does also have logic for avoiding triggering on oscillations during the initialization.
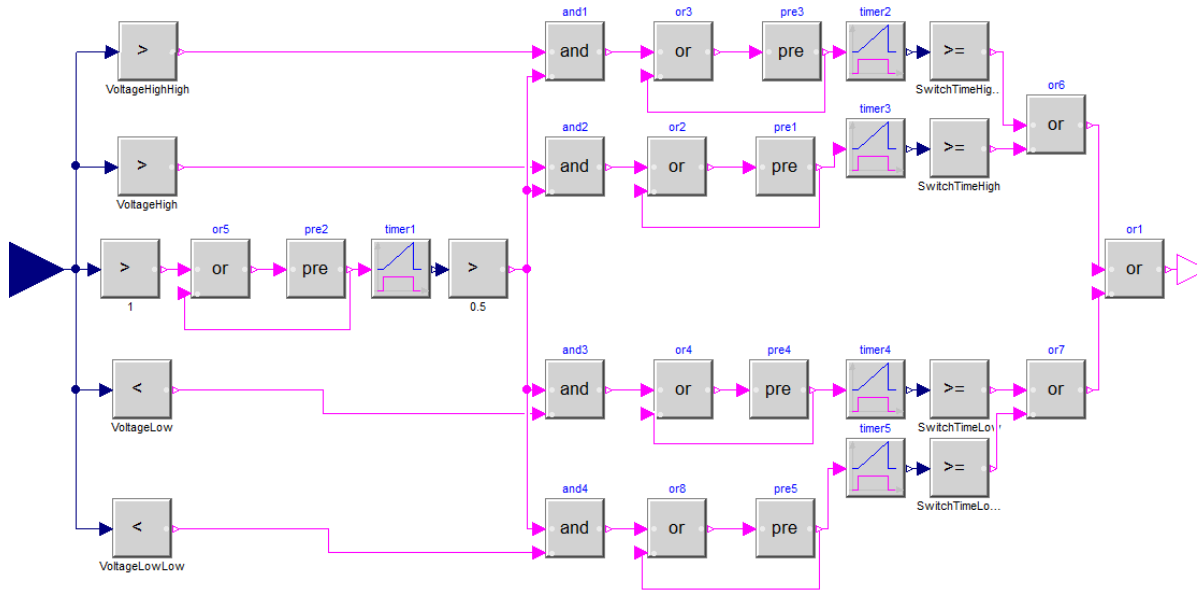
Voltage sensor RMS:

This sensor returns the true RMS value of the voltage. The sensor is based on the RMS sensor from the Modelica Standard Library and customized for *abc* the reference frame in the Electric Power Library.
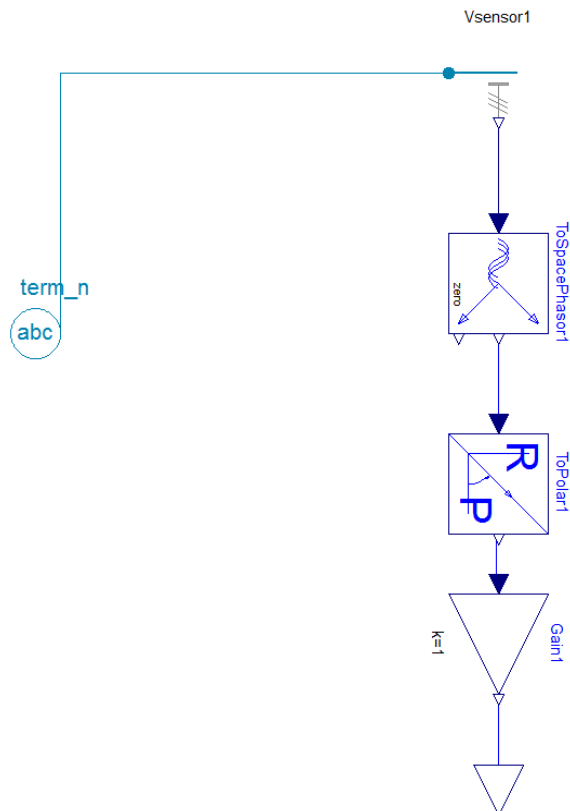
Appendix B, Calculation of cable parameters

In order to model the cables with the Electric Power Library (EPL) in Dymola, the parameters in Table B-1 have to be transformed into per unit values.

Table B-1: Electric parameters for single conductor TSLE cables with a triangular geometry [17]

Type:	TSLE 3x1x400 Al:	TSLE 3x1x95 Al:	TSLE 3x1x50 Al:
Dimension [mm^2]	400	95	50
R per-phase [Ω/km]	0.0778	0.32	0.641
X per phase [Ω/km]	0.11	0.14	0.15
C per-phase [F/km]	0.0000004	0.00000023	0.00000017

The per unit values for the Pi-equivalent model in EPL is calculated from the base values S_nom and V_nom for the cable. Here, the nominal value S_nom was set to the random number 1 MVA, while V_nom was set to 22 kV which is the voltage level in the radial.

The base values where calculated as:

$$R_{base} = \frac{V\_nom^2}{S\_nom} \qquad \text{(B-1)}$$

$$G_{base} = \frac{1}{R\_base} \qquad \text{(B-2)}$$

With the base values known, the p.u./km values for the resistance, r, reactance, x, and shunt capacitance, c, where calculated as follows:

$$r = \frac{R}{R\_base} \qquad \text{(B-3)}$$

$$x = \frac{X}{R\_base} \qquad \text{(B-4)}$$

$$c = \frac{C}{R\_base} \qquad \text{(B-5)}$$

Appendix C, Calculation of power plant parameters, Grunnåi

Turbine and rotor model:

For the turbine model with rotor, the nominal mechanical power of the turbine, P_nom, is 14.75 MW, as calculated Equation C-7.

$$P_{turbine} = S_{generator} * pf * \eta \qquad (C\text{-}6)$$

$$P_{turbine} = 15.853 * 0.95 * 0.98 = 14.75 \; MW \qquad (C\text{-}7)$$

The flywheel effect of the generator is known to be 38 tm^2, by assuming that the flywheel effect of the turbine is 10 % of the flywheel effect of the generator, the total flywheel effect is as follows:

$$GD_{total}^2 = 38 * 1.1 = 41.8 \; tm^2 = 41800 \; kgm^2 \qquad (C\text{-}8)$$

The flywheel effect, GD^2, can be expressed as an H-value in seconds in terms of the apparent power of the generator, S_nom, and the speed, n:

$$H = \frac{1}{2}(\frac{\pi}{60})^2 \frac{GD^2 n^2}{S\_nom} \qquad (C\text{-}9)$$

Appendix D, Calculation of generator parameters, Sagbekken plants

Generator model:

Table D-1 presents the known electrical parameters for the different machines, and results obtained from no-load and locked rotor tests.

Table D-1: Known parameters from data sheets

Brand: Model:	Lönne 14BG 258-4AA60-Z	Lönne 14BG 288-4AA60-Z	Lönne 14BG 317-4AA60-Z	Lönne 14BG 318-4AA60-Z
Known parameters:				
V [V]	400	400	400	400
I_n [A]	134	198	345	430
P_m [W]	**75000**	**110000**	**200000**	**250000**
Coupling$_{stator}$	D	D	D	D
R_1 [Ω]	0.0707	0.0317	0.0192	0.0122
n_s [rpm]	1500	1500	1500	1500
n_n [rpm	1482	1485	1486	1488
pp [-]	2	2	2	2
η [-]	94.4	95.3	95.9	96.1
pf [-]	0.85	0.84	0.87	0.87
J [kgm^2]	0.82	1.81	3.9	-
S_n [VA]	88235	130952	229885	287356
No-load data:				
I_{nl} [A]	49.3	85.6	90.8	127.8
P_{nl} [W]	1946	2991	2800	3973
Pf_{nl} [-]	0.057	0.05	0.045	0.045
S_{nl} [VA]	34140	59820	62222	88289
Q_{nl} [Var]	34085	59745	62159	88199
Locked rotor data:				
I_{lr} [A]	1026	1755	2365	3642
T_{lr} [Nm]	1177	2073	3190	5015
P_{lr} [W]	308300	481300	744100	1148700
Pf_{lr} [-]	0.434	0.396	0.454	0.455
Q_{lr} [Var]	639980	1116045	1460340	2248148
S_{lr} [VA]	710368	1215404	1638987	2524615

By using the parameters known from Table D-1 and the equivalent circuit, the parameters needed for the generator models can be determined.

The no-load resistance, R_m, representing the windage, friction and iron losses can be calculated as [6]:

$$R_m = \frac{V^2}{P_{nl} - 3I_{nl}^2 R_s} \qquad (D\text{-}1)$$

The magnetizing reactance, X_m:

$$X_m = \frac{E_{nl}^2}{Q_{nl}} \qquad (D\text{-}2)$$

The total leakage reactance, $X_{l1} + X_{l2}$, referred to the stator is determined as follows [6]:

$$X_{l1} + X_{l2} = \frac{Q_{lr}}{3I_{lr}^2} \qquad (D\text{-}3)$$

Since the leakage reactance need to be referred to both the stator and rotor, is it normal procedure to the divide the total leakage reactance equally at both sides [6]:

$$X_{l1} = X_{l2} = \frac{1}{2} * \frac{Q_{lr}}{3I_{lr}^2} \qquad (D\text{-}4)$$

By using the already known resistance of the stator, R_1, the rotor resistance, R_2, can be determined:

$$R_1 = \frac{R_{lr}}{3I_{lr}^2} - R_2 \qquad (D\text{-}5)$$

In order to model the transient dynamics of the machines, the transient reactances and time constants had to be calculated. Because of the cylindrical construction of the squirrel cage rotor, the distinction between direct and quadrature axis need not to be maintained for the model [4]. Since there is no damper winding in the squirrel cage rotor, there is only one transient reactance:

$$X' = X_{l1} + \frac{X_m X_{l2}}{X_m + X_{l2}} \qquad (D\text{-}6)$$

94

The open term time constant, T_0, and short-circuit time constant, T', are calculated as follows [4]:

$$X' = X_{l1} + \frac{X_m X_{l2}}{X_m + X_{l2}} \tag{D-7}$$

$$T' = T_0' \frac{X'}{X_{l1} + X_m} \tag{D-8}$$

Table D-2 presents the generator parameters calculated from the no-load and locked rotor tests presented in Table D-1.

Table D-2: Calculated parameters

Brand:	Lönne	Lönne	Lönne	Lönne
Model:	14BG 258-4AA60-Z	14BG 288-4AA60-Z	14BG 317-4AA60-Z	14BG 318-4AA60-Z
P_m [W]	75000	110000	200000	250000
Calculated:				
R_m [Ω]	111.85	69.71	68.84	47.41
X_m [Ω]	4.6942	2.6780	2.5740	1.8141
$X_{l1}+X_{l2}$ [Ω]	0.2027	0.1208	0.0870	0.0565
X_{l1} [Ω]	0.1013	0.0604	0.0435	0.0282
X_{l2} [Ω]	0.1013	0.0604	0.0435	0.0282
R_2 [Ω]	0.0269	0.0204	0.0251	0.0167
X' [Ω]	0.2005	0.1195	0.0863	0.0561
T_0' [s]	0.1564	0.1674	0.1880	0.2032
T' [s]	0.0065	0.0073	0.0062	0.0062

By looking at Table D-1 it can be seen that the inertia, J, is missing for the 250 kW machine. Figure D-1 shows the inertia for different generator ratings plotted with a regression line. It can be seen that the relationship between the inertia and machine rating is approximately linear for the four machines in the plot. The linear regression line has following function:

$$J = 0.00002 * Pm - 0.8225 \tag{D-9}$$

This gives following inertia, J, for the 250 kW machine:

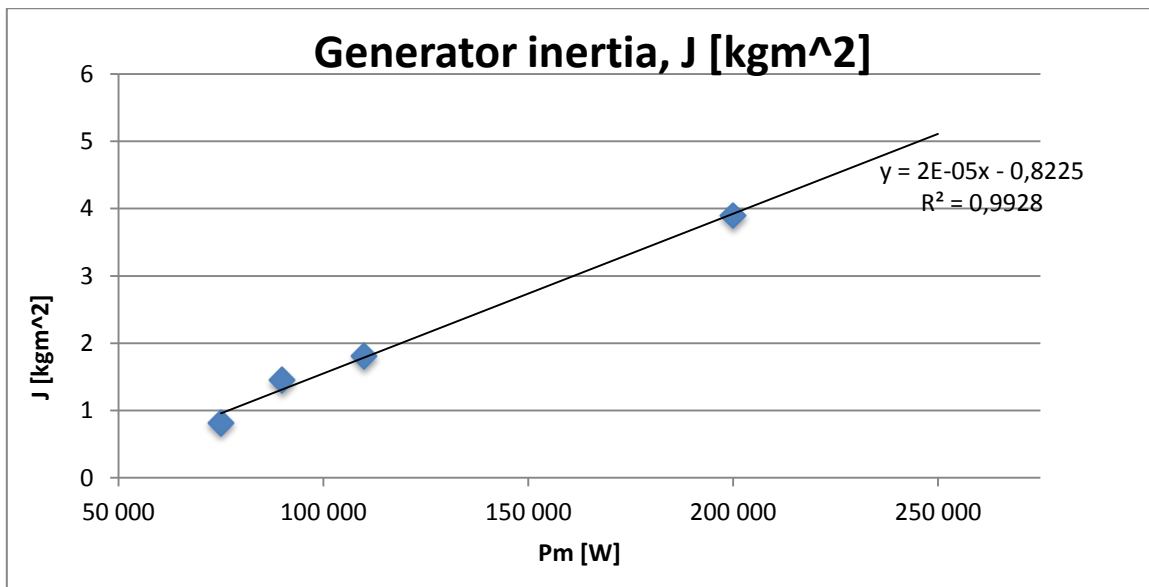$$J = 0.00002 * 250000 - 0.8225 = 4.1775 \; kgm^2 \tag{D-10}$$

Figure D-1: Inertia for different generator ratings with regression line

Appendix E, Calculation of turbine and rotor parameters, Sagbekken 1

The nominal mechanical power of the turbines, P_nom, is set to 100 kW for the two smallest machines, and 200 kW for the largest one.

The inertia, J, or flywheel effect, GD^2, is unknown for the turbines, but the mass, M, and radius, r, of the runners have been obtained from the manufacturer. The inertia of the turbine can be approximated by assuming the turbine to be a homogenous disc with a given mass and radius:

$$J = \frac{1}{2} M r^2 \qquad\qquad (E\text{-}1)$$

For the three turbine runners in Sagbekken 1, the radius and mass is known to be 0.4 m and 48 kg, which gives following inertia, J:

$$J = \frac{1}{2} * 48 * 0.4^2 = 3.84 \ kgm^2 \qquad\qquad (E\text{-}2)$$

The total inertia, J_{total}, for the machines is the sum of the inertia for the rotor, J_{rotor} and turbine, $J_{turbine}$:

$$J_{total} + J_{rotor} + J_{turbine} \qquad\qquad (E\text{-}3)$$

The inertia, J, can be expressed as the flywheel effect, GD^2:

$$GD^2 = J * 4 \qquad\qquad (E\text{-}4)$$

The flywheel effect, GD^2, can be expressed as an H-value in seconds in terms of the apparent power of the generator, S_nom, and the speed, n:

$$H = \frac{1}{2} (\frac{\pi}{60})^2 \frac{GD^2 n^2}{S\_nom} \qquad\qquad (E\text{-}5)$$

By using the calculated inertia of the turbine from Equation E-2, and the inertia of the rotors from Table D-1, the total H-value for each of the machines can be determined.

Appendix F, Calculation of turbine and rotor parameters, Sagbekken 2 and 3

For the turbine and rotor models, the nominal mechanical power of the turbines, P_nom, is set to 75 kW for the three smallest machines, and 250 kW for the largest one.

The turbine runners used in the plant have a radius of 0.45 m and a mass of 52 kg. By approximate the turbine as an homogenous disc, the inertia, J, can be calculated as:

$$J = \frac{1}{2} * 52 * 0.45^2 = 5.265 \; kgm^2 \qquad\qquad (F\text{-}1)$$

The total inertia, J_{total}, for the machines is the sum of the inertias for the rotor, J_{rotor} and turbine, $J_{turbine}$:

$$J_{total} + J_{rotor} + J_{turbine} \qquad\qquad (F\text{-}2)$$

The inertia, J, can be expressed as the flywheel effect, GD^2:

$$GD^2 = J * 4 \qquad\qquad (F\text{-}3)$$

The flywheel effect, GD^2, can be expressed as an H-value in seconds in terms of the apparent power of the generator, S_nom, and the speed, n:

$$H = \frac{1}{2}(\frac{\pi}{60})^2 \frac{GD^2 n^2}{S\_nom} \qquad\qquad F\text{-}4)$$

By using the calculated inertia of the turbine and the inertia of the rotor in Table D-1, the total H-value for each of the machines can be determined.

Appendix G, Calculation of transformer parameters

For modeling purpose, datasheets for the Møre Trafo OTW series transformers are used to obtain transformer parameters, the parameters from the datasheet are shown in Table G-1.

Table G-1: Known parameters for distribution transformers [25]

Brand: Model:	Møre Trafo OTW 3640	Møre Trafo OTW 51170	Møre Trafo OTW 6960
S_n [kVA]	100	630	800
Known Parameters:			
V_1 [kV]	22	22	22
V_2 [kV]	0.415	0.415	0.415
I_{n1} [A]	2.62	16.53	20.99
I_{n2} [A]	139.12	876	1113
P_0 [W]	210	690	850
Q_0 [VAr]	370	510	1040
P_k [W]	1690	5240	6490
Q_k [VAr]	3540	28990	46190

Parameter calculations based on the equivalent circuit:

By using the known the parameters in Table G-1, the resistances and reactances of the equivalent circuit in Figure 2-6 can be determined.

The no-load resistance, R_m, magnetization reactance, X_m, can be calculated by using the active no-load loss, P_0, and the reactive no-load loss, Q_0:

$$R_m = \frac{(V_1)^2}{P_0} \tag{G-1}$$

$$X_m = \frac{(V_1)^2}{Q_0} \tag{G-2}$$

The leakage reactances, X_{l1} and X_{l2} can be calculated by dividing the reactive load loss, Q_k, equally at the primary and secondary side and assuming that the loss is equal at both sides:

$$X_{l1} = \frac{\frac{Q_k}{2*3}}{I_{n1}^2} \qquad\qquad (G\text{-}3)$$

$$X_{l2} = \frac{\frac{Q_k}{2*3}}{I_{n2}^2} \qquad\qquad (G\text{-}4)$$

By assuming that the active load loss, P_k, is equally divided at both sides of the transformer, the series resistances R_1 and R_2 can be calculated as follows:

$$R_1 = \frac{\frac{P_k}{2*3}}{I_{n1}^2} \qquad\qquad (G\text{-}4)$$

$$R_2 = \frac{\frac{P_k}{2*3}}{I_{n2}^2} \qquad\qquad (G\text{-}5)$$

Using Equation G-3 to G-5 to calculate the equivalent resistances and reactances for the Møre Trafo OTW transformers gives the parameters shown in Table G-3.

Table G-3: Calculated parameters for the distribution transformers

Brand:	Møre Trafo	Møre Trafo	Møre Trafo
Model:	OTW 3640	OTW 51170	OTW 6960
S_n [kVA]	100	630	800
Calculated:			
R_m [Ω]	2304761	701449	569411
X_m [Ω]	1308108	949019	465384
R_1 [Ω]	41	3	2
X_{l1} [Ω]	85	17	17
R_2 [Ω]	0.0145	0.0011	0.0008
X_{l2} [Ω]	0.0304	0.0063	0.0062

Saturation parameters calculations:

From Møre Trafo it is is known that the steel used in the core of the OTW series is of the type M103-27P, which is a type of steel with a thickness of 0.27 mm, made for an high flux density, B, with a loss of 0.98 W/kg at 50 Hz [26]. This type of steel saturates at a flux density equals 2.05 T.

From the datasheets of the transformers it is known that the 630 kVA and 800 kVA transformers operates at flux densities equal to 1.64 T and 1.67 T at nominal operations [25].

Figure G-1 shows the saturation curve for the type of steel used in the core of the transformers.
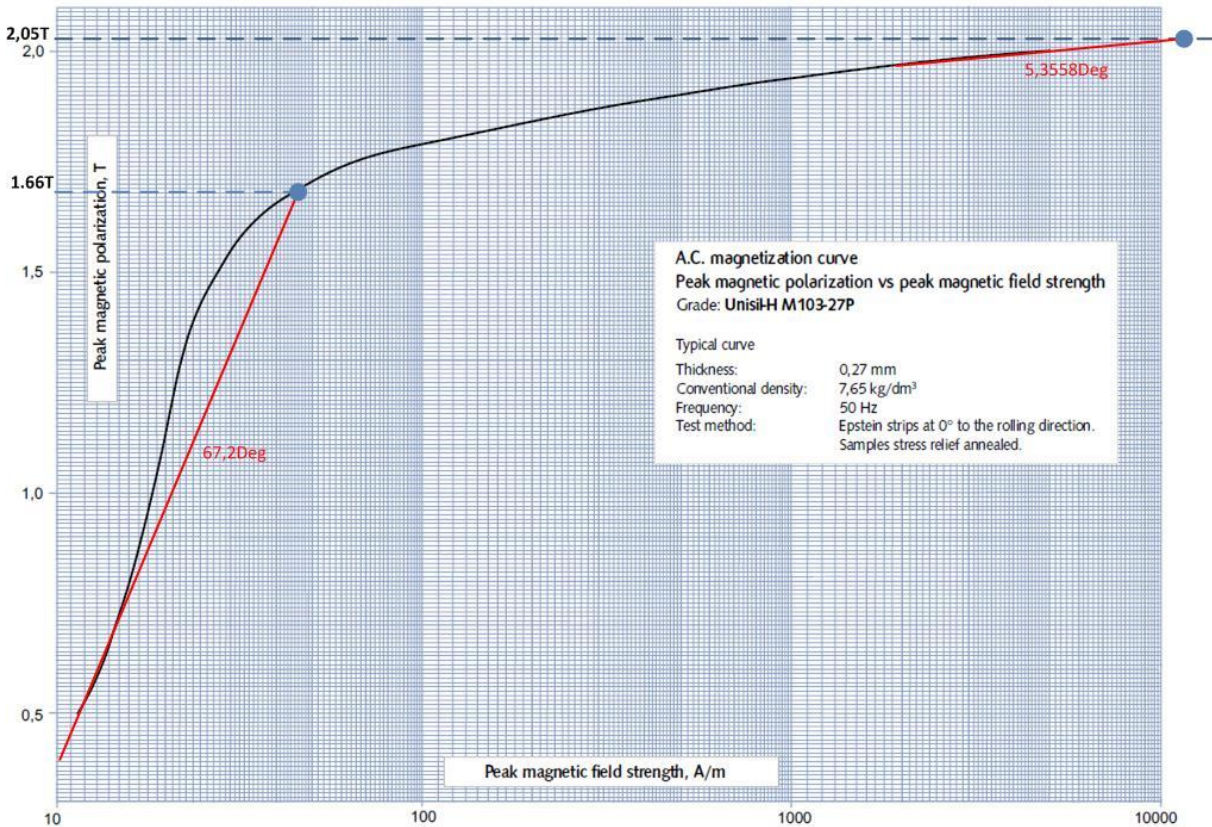

Figure G-1: Saturation curve for M103-27P steel [26]

Since the saturation curve can be expressed in terms of voltage, V, and current, I, instead of flux density, B, and magnetic field strength, H, the ratio between the axis can be expressed as the magnetization reactance, X_m:

$$X_m = \frac{V}{I_m} \qquad \qquad G\text{-}6)$$

It is desirable to determine the fully saturated magnetization reactance for the transformers. The saturated reactance is approximated by using the gradient of the two different operating points to determine the ratio. The steel is simplified to be in a fully linear region up to nominal flux density, a straight line with 67.2 degrees slope is therefore drawn in Figure G-1 to present the linear region. For the saturated value, a line with 5.35 degree slope is drawn.

By using the magnetization reactance, X_m, for the linear region calculated in Table G-3 and the and the slopes determined in Figure G-1, the saturated magnetization reactance, X_{mSat}, can be determined as follows:

$$X_{mSat} = \frac{X_m}{67.2\ Deg} * 5.35\ Deg \qquad\qquad (G\text{-}7)$$

This approximation leads to some uncertainties, and both the transformers are therefore assumed to operate at a flux density equal to 1.67 T in nominal operations. The ratio between the saturated and unsaturated flux density is therefore:

$$B_{sat} = \frac{2.05T}{1.67T} = 122\ \% \qquad\qquad (G\text{-}8)$$

Table G-4 shows the calculated saturation parameters for the 630 kVA and 800 kVA transformers.

Table G-4: Calculated saturation parameters

Brand:	Møre Trafo	Møre Trafo
Model:	OTW 51170	OTW 6960
Sn [kVA]	630	800
Calculated:		
X_m [Ω]	949019	465384
X_{mSat} [Ω]	55905	37091
B_{sat} [%]	122	122

Appendix H, Project description

Høgskolen i Telemark

Skagerak Energi

FMH606 Master's Thesis

System dynamics of asynchronous generators at islanded grid operation

TUC supervisor: Dietmar Winkler
TUC co-supervisor: Bernt Lie
External partner: Skagerak Kraft AS
External censor: Ingvar Andreassen w/Skagerak Kraft AS
Student: Håkon Evardsen

Task description: The following tasks should be carried out:

1. Give an overview of the system dynamics theory of an electric grid with both asynchronous and synchronous generators in an islanded grid operation.
2. Develop a model of the dynamics between asynchronous and synchronous generators, connected with loads and power cables, that can be disconnected from a stiff grid and then be running in an islanded grid.
3. Adapt this model to the power system at Grunnåi, running on an islanded grid from the main transformer in Seljord. This system must contain a model of Grunnåi hydro power plant together with power cables and several smaller power plants using asynchronous generators.
4. Discuss available data from the grid and power plants around Grunnåi, and consider calibration and validation of the model.
5. Analyse the system dynamics. Simulate the model of the Grunnåi grid area at the time around disconnection from the main grid.
6. Consider the protection relays in the system and analyse the settings of the relays on the background of the simulations.
7. Document the work in a report.

Task background: Skagerak Kraft is the main owner of Grunnåi hydro power plant in Seljord, build in 2006. It has a synchronous generator and a Pelton turbine with an installed capacity of 14.9 MW. The challenge is that there have been some problems with unstable voltage in this area. The generator was damaged in 2010 and is now replaced. In 2011 there was an earth circuit incident at Grunnåi that was an indication of an unstable voltage that occurred.

There is a need of investigating the system dynamics in this area of the grid, to prevent further damage on the power equipment in the system.

The Grunnåi area grid is connected to the main transformer in Seljord by an eight kilometre long cable. Connected to this cable is also some load and seven smaller asynchronous generators at several mini hydro power plants. The problem occurs when the grid around Grunnåi suddenly disconnects from the main grid in Seljord. What happens then is that the asynchronous generators are supplied with reactive power from the long cable, which then functions as a large capacitor. The frequency and the voltage in the islanded grid will then suddenly rise, due to the asynchronous generators which have no control of speed and voltage.

Hence, there is a need to further investigate this dynamics. Firstly to be able to choose god parameters for the protection relays to protect the generators and the other power system components. Secondly to learn more about the dynamics in such a system for better planning of new hydropower plants and their grid connections.

Prerequisites:

- Successful completed course SCEV3210 (implies good knowledge in Modelica®, Hydro Power Systems, and Energy Systems)
- Comfortable with the usage of modern software tools (version control systems, code editors, mathematical analysis tools (e.g., Dymola, MATLAB, SciPy)
- Knowledge of Norwegian is needed since most of the current documentation of the Norwegian energy system is available in Norwegian only.

Student category: SCE students

Practical arrangements: Student needs to have own laptop and may be working partly at the Skagerak premises for the literature research.

Supervisor/co-supervisor: Dietmar Winkler
Email: Dietmar.Winkler@hit.no
Phone: 3557 5165
Room: B-252

Bernt Lie
Email: bern.lie@hit.no
Phone: 3557 5169
Room: B-256

External censor: Ingvar Andreassen
Skagerak Kraft AS
Email: ingvar.andreassen@skagerakenergi.no
Phone: 35 90 21 73

Signatures

Student (date and signature):

30/1-2013   Håkon Molland Edvardsen

Supervisor (date and signature):

30.1.2013   D. Winkler